Rebeka Amanatidou
Mälardalen University
April 2008

CFD Measurements of the Cooling Air in a DC-Motor

Supervisors: Stefan Israelsson
Peter Löfgren

Examiner: Jan Sandberg

Abstract

The cooling system of a DC-motor is examined in this thesis. A change of direction of the cooling air is desired to prevent the generated coal dust from entering into the windings of the machine. Ultimately this will have a negative effect on the cooling in the machine and the loss of cooling needs to be compensated through other ways. The purpose of this thesis is to work for an improved operational safety and performance of the DC-motor and to make it more competitive in the market. By modelling the interior geometry of the machine and defining the boundaries in the software programs Gambit and FLUENT respectively, the motion and the heat transfer of the airflow could be simulated. The simulation results would give us an understanding of the flow pattern which later could be used to develop design modifications on the cooling system of a DC-motor. In this thesis the main focus lies on creating a simulation model with a sufficiently fine mesh size.

Keywords: CFD, DC-Motor, Mesh Modelling, Flow Simulation

Summary

The cooling system in a certain rotating machine of the type direct current (DC-) motor is examined in this thesis. In a DC-motor there is coal dust generated at the connecting surfaces between a stationary part where the electric current is inserted to the rotor (the Brushes) and the adjoining rotating surface (the Commutator). This dust is sucked in through the windings of the machine when the airflow is going from the non-drive side of the machine, which is the most common nowadays, and this dust is causing a lot of damage. The idea investigated in this thesis is to drive the airflow through the machine from the opposite side, the drive side, and by doing so also avoid getting the dust into the machine. From a thermodynamic point of view though this is less efficient and the deterioration of the cooling should be counteracted by improving the cooling in other ways. The purpose is to work for an improvement of the operational safety and the performance of the DC-motor and to make it more competitive in the market.

The first and main goal with this thesis work was to create a simplified model of the DC-motor that simulates the flow and heat transfer of the cooling air through the system. This model could then be used to analyze the airflow through the machine. By examining different properties of the cooling air it would eventually lead to a better understanding of the general motion and heat-transfer pattern of the air in the system. The final objective would have been to use the simulation model and the knowledge of the patterns in the fluid to develop design modifications in the machine that would improve the cooling. Unfortunately this goal was never reached because of the complexity of the task and time limitation of the thesis.

For the building up and the simulation of the created models the software programs Gambit and FLUENT were used. First of all a simple 2D model version was made to give us an overview of what kind of problems that could occur during modelling and simulation. A cross section segment of the Commutator was modelled and simulation results of the velocity and temperature in the airflow were generated from it. From those results it was noted that there was a short cutting airflow along the outer wall where cold air went directly from the inlet to the outlet passage, and another flow closer to the Commutator wall that was circulating in a vortex formation distributing the heat from the surface to a larger area.

The main modelling work was put on a 3D-model of the DC-motor with sizes of geometry and mesh parametrisized. Since the modelling was rather complex it was delimited to include just the Commutator part of the machine. Further it was necessary to systemize the geometry building to get a higher level of control and this was accomplished by defining the whole geometry in Python script which would generate a Gambit journal file when compiled. In the Python script the geometry was divided into three separate sections, each projected onto a general radial plane, and there after extruded stepwise in the axial direction. The formed volumes could then be activated or deactivated from its mesh according to the conditions in the machine which is reproduced. Because of the structure in the axial direction it is possible to use prism-shaped mesh cells in each section and thereby decrease the number of mesh cells needed. All the volumes containing air were meshed and simulated as well as one solid volume, the copper layer on the Commutator surface where axial heat conduction occurs. Further the turbulence model used here was the k-omega model. It was chosen because it was more convenient since you are able to use both a near wall function and a function for the wall roughness for the same surface.

For the 3D-simulations made the boundary conditions are based on very roughly set or assumed values and can therefore only be used for studies of relative effects. The influence of the mesh size on the results was studied by generating and simulating meshes with different sizes and then comparing the results. Data used for this comparison were the average heat transfer coefficient on the Commutator surface and the net heat transfer rate of the cooling air through the boundaries. The data fluctuation within each mesh was studied as well to examine their time dependence. It was found that all the simulated mesh sizes gave rather similar results when compared to each other and when compared throughout the fluctuation in time within each mesh. Therefore the differences in mesh size could be neglected. Visual comparisons were also made of the simulation results between the meshes, and the monitored results were the temperature and the velocity patterns of the cooling air. The fluctuation of the flow of each mesh was visually examined as well, by creating a movie out of a bunch of velocity pictures.

A steady state solution could not be reached for the simulations because the quick oscillation in the flow the solutions are prevented from being stabilized. On the other hand it would have been too time-consuming to look for a transient solution at once, since the oscillating flow needs small time steps to be resolved while the solid heat conduction needs a long time to stabilize. So therefore it was necessary to divide the whole simulation process into two steps, first a transient simulation where the heat transfer was neglected and thereafter a steady state simulation of the heat transfer with the flow fixed at its current position. Through this way the simulation could be made within reasonable time and the result would be accurate enough since the heat transfer in the model is not likely to influence the fluid motion noticeably.

Table of Content

CFD MEASUREMENTS....1

of the Cooling Air in a DC-Motor....1

Abstract....1

Summary....2

Table of Content....4

1 Introduction....6

1.1 PROBLEM DESCRIPTION....7

1.2 Purpose....8

1.3 Objectives....8

1.4 Scope....9

1.5 Structure....10

2) Brief Theory....12

2.1 INTRODUCTION TO DC MOTORS 12

2.2 Theory of Computational Fluid Dynamics....13

2.3 Heat Transfer Theory....16

2.3.1 Heat Transfer Coefficient....17

2.3.2 Net Heat Rate....18

3) THE 2D MODEL....20

3.1 Geometry and Mesh....20

3.2 Simulation Settings....21

3.3 Simulation Results....22

3.4 Conclusions for the 2D Model....24

4 The 3D-Model....25

4.1 The Geometry....26

4.1.1 Modelling Process....26

4.1.2 File Structure....27

4.1.3 Model Result....28

4.1.3.1 The Planes....32

4.1.3.2 The Meshes....43

4.2 Simulations....47

4.2.1 Boundary Conditions and Settings....47

4.2.2 SENSITIVITY ANALYSIS.....49

4.2.3 Simulation Results.....51

4.2.3.1 Figures.....53

4.2.3.2 PICTURES.....58

4.3 CONCLUSIONS FOR THE 3D MODEL.....63

1 Introduction

In general it can be said that all electrical equipments has a production of heat due to the electrical losses in the system. This heat is increasing the temperature of the surrounding materials and it can damage some sensitive parts of the unit. To insure a secure operation the temperature needs to be kept down by leading the heat away, either naturally or by a special design.

In electrical rotating machines electrical power is used to create mechanical power through electromagnetic forces. The mechanical and electrical power losses in the system are transformed into heat and to avoid overheating some kind of cooling system is needed. An effective way to cool down the motor is to lead a fluid, either water or air, to flow over the hot parts of the machine and transfer the heat out of the system.

A highly efficient machine is a machine that for a minimum material cost can generate a high level of mechanical power output. This means that for a certain machine a maximum of mechanical power output is desired. When increasing the power for the motor you need to deal with the additional heat generated from this. Therefore the cooling plays a key role in the improvement of the machine.

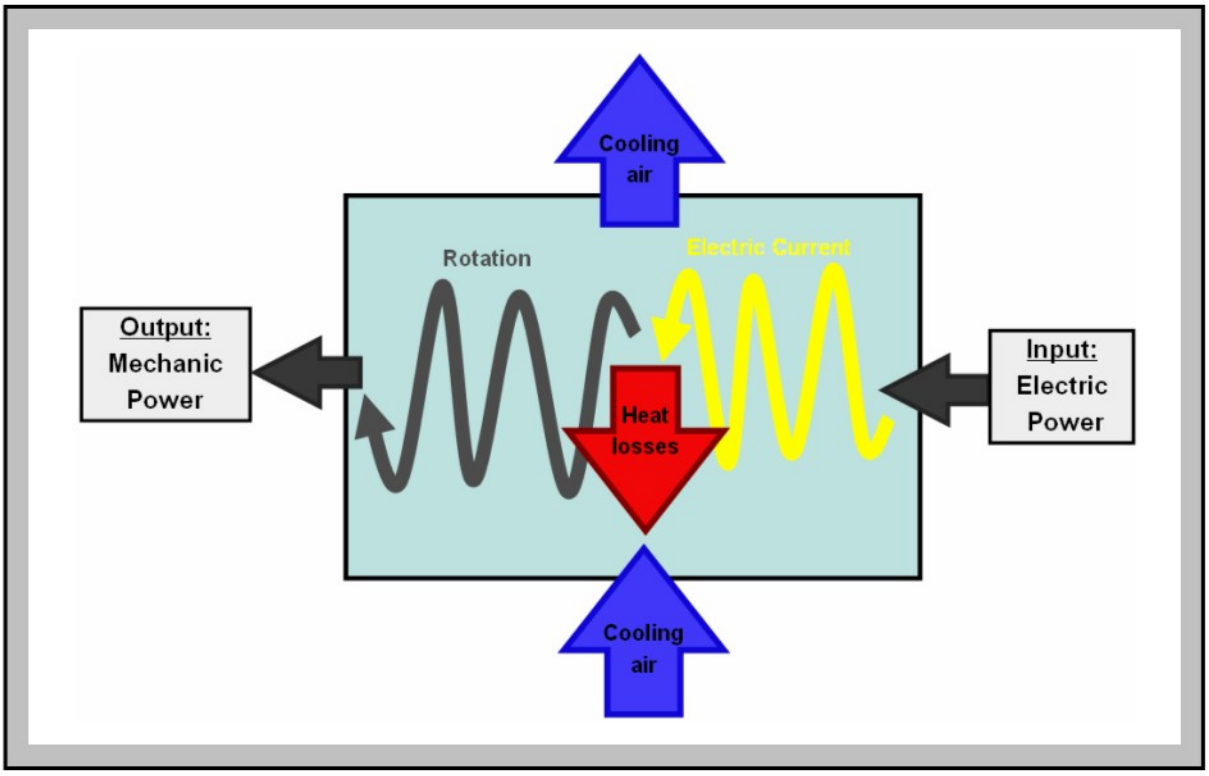

Figure 1: The principle outline of an electrical machine and its cooling system

1.1 Problem Description

The particular motor examined in this thesis is a DC-motor with air cooling driven by an external fan. There are three important factors that need to be considered when designing the cooling system of a DC-motor. First of all there is a delimited part of the Rotor in a DC-motor where electrical current is transferred, called the Commutator. This part of the machine is exposed to a high level of heat generation. In addition to that the Commutator is also very sensitive to high temperatures and requires more cooling compared to the other parts. The stator windings are another part of the DC-motor where heat is generated and where cooling is needed. But since the material of the windings is less sensitive it can endure higher temperatures then the Commutator. Finally there are a number of stationary graphite blocks through which the transfer of current to the rotating Commutator occurs, called the Brushes. They are exposed to a lot of friction which results in a certain amount of coal dust production. This coal dust can damage the machine, and it is preferred to keep the dust away from the Stator windings to prevent short circuit between the windings.

For the ABB produced DC-motors the cooling air is currently added from the non-drive side, also called N-side. The advantage of N-side cooling is that cold air is supplied directly to the Commutator where the ultimate restriction of the maximum operating power for the DC-motor is made. By effective cooling of the Commutator a high maximum operating power can be obtained. The downside of this cooling though is that the produced coal dust is transported in through the stator windings together with the cooling air and can eventually cause damage.

For a safer operation it is suggested that the cooling air should be inserted from the drive side, here called the D-side. The coal dust would then be blown out with the cooling air from the Commutator without passing the Stator windings. On the other hand this implies that the cooling air that reaches the Commutator already is heated up by the stator windings. Because of the decreased cooling effect there is a risk of overheating the Commutator and this is something that should be avoided above everything. The response to that is to decrease the operating power and therefore also the performance of the machine. Another way to deal with this problem would be to improve the cooling in the Commutator which is also the topic of this thesis. The task is to find a way to improve the cooling of the DC-motor when it is cooled from the D-side.

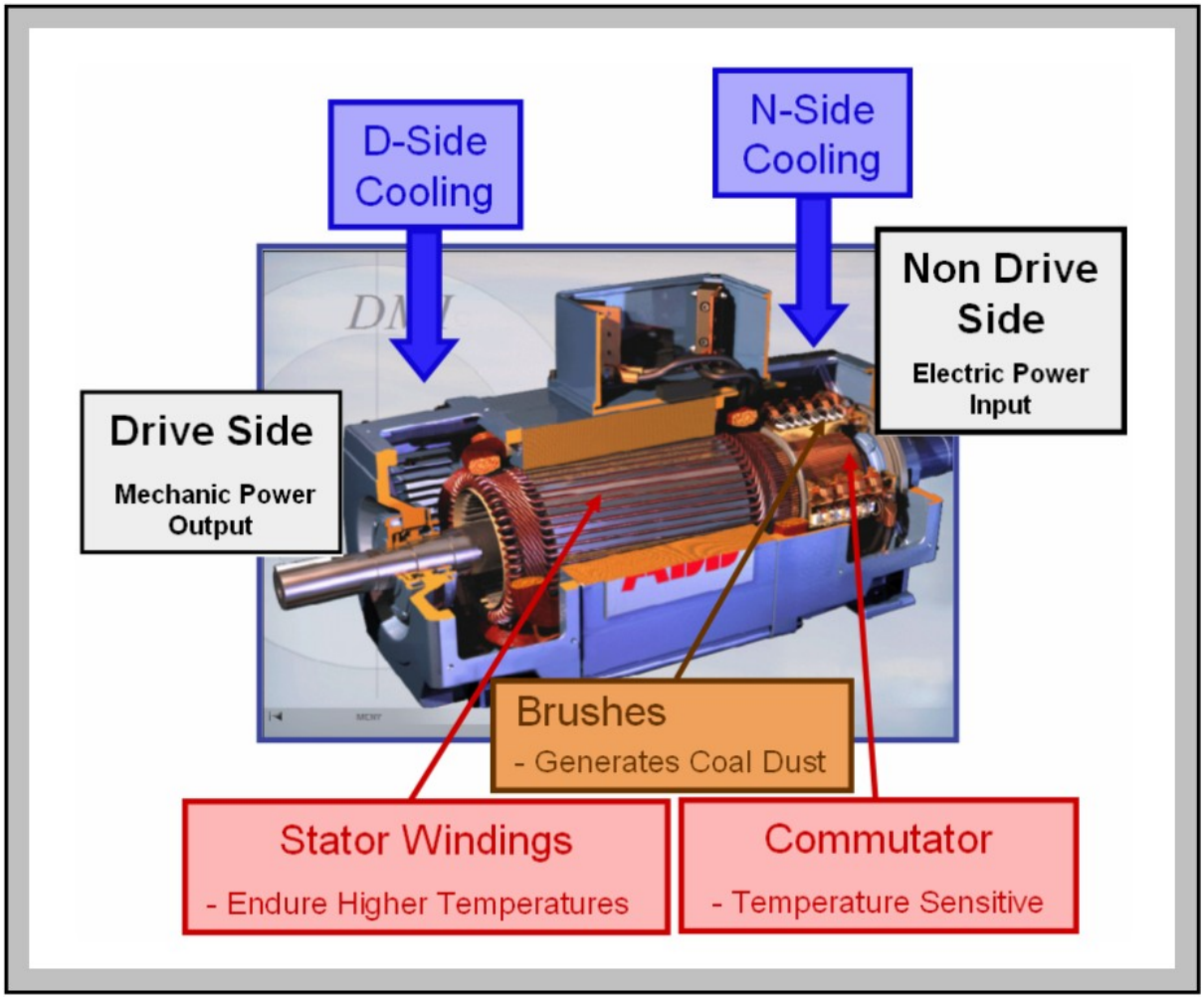

Figure 2: A picture of a DC-motor marking out the essential factors affecting the choice of cooling system. The picture is originally taken from the product catalogue over ABB's DC-motor products.

1.2 Purpose

The purpose of this thesis is to work for an improvement of the operational safety and the performance of the DC motor. The idea is that this eventually could make the DC motor more competitive in the market against other comparable alternatives.

1.3 Objectives

The main goal with this thesis work was to create a simplified model of the DC-motor that simulates the flow and heat transfer of the cooling air through the system. The intension was to make the model geometry parametrical and easy to modify so it can be used for describing the cooling system of different types and sizes of DC-motors.

The following goal was to analyze the results simulated from the created model of a specific DC-motor. By examining different properties of the cooling air it would eventually lead to a better understanding of the general motion and heat-transfer pattern of the air in the system.

Finally the main goal would have been to use the simulation model and the knowledge of the patterns in the fluid to develop design modifications in the machine that would improve the cooling. Unfortunately this goal was never reached because of lack of time.

1.4 Scope

The main task for the thesis was to build a mesh model of a DC-motor with the software program Gambit and then import it into the program FLUENT to make simulations of the airflow. A certain type of motor was chosen for the study, the DMI 280P-komp TTR248. This is a DC-motor with 4-poles, short gear brush and an output power of 178-658 HP.

To get an overview of the problems that could occur during the modelling a simplified version in 2D was firstly made. From the 2D simulations it was possible to get an understanding of what types of problems that could occur later for the 3D model.

The modelling process of the DC-motor in 3D was much more complicated and time consuming. Therefore the geometry had to be simplified as much as possible. One of the choices made to delimit the geometry was to just model the air gap in the Commutator part and skip the rest of the motor. This was decided because the Commutator is the most critical part when it comes to cooling and therefore also the part that should mainly be focused on. Additionally to that the other parts of the motor, such as the stator windings, have a very complex geometry which would complicate the modelling significantly and still fail to give a correct representation of the reality. Another simplification made to the geometry was to consider the brushes at each brush arm as merged units. There are a lot of wires surrounding the brushes that were also neglected, though they could interfere with the flow, so the level of geometrical accuracy is not too high. Another important thing that could be said about the geometry is that all the sizes of the model had to be defined with parameters from a separately implemented parameter list. This was a necessity if it should be possible to modify the geometry of the model in a later stage.

The closeness of the mesh was also parameterisized so that the mesh size easily could be changed. The intention was to create an as coarse mesh as possible which at the same time also would generate accurate enough simulation results. In general it can be said that a coarser mesh is preferable because it shortens the simulation time. To make the mesh coarser a combination of prism shaped and tetrahedral cells were used.

Most part of the meshed volume in the model is made for the fluid flow occurring in the air gap between the Commutator and the motor casing. Though there is one solid that also has been meshed, namely the copper layer on the Commutator surface. There is a heat flux from the rotor that is transferred to the Commutator flowing in axial direction through the copper layer. Thanks to the solid mesh this axial effect will be considered as well.

For the simulations made, all boundary conditions are based on assumed values. The settings of the cases are set very roughly and can only be approved when used for studies of the relative effects, for instance between simulations with different meshes. The electrical and mechanical losses for the Commutator are defined as a heat flux coming from the interface wall between the brushes and the Commutator. For the stator the heat losses are given by a certain fixed surface temperature. Further more the equations considered in the simulations are for the velocity, the heat and the k-omega turbulence equations.
Finally a sensitivity analysis was made where the influence of the mesh size was studied. The mesh size in the outer main regions of the model was varied, as well as the mesh size at the boundary layer directly above the Commutator surface and five mesh models with different combinations of those variables were created and simulated. The simulation results from the different mesh models where compared to each other, both visually as well as from calculated data. In the visual comparison pictures of the velocity and temperature distribution of the air were used. For the data comparison the average heat transfer coefficient in the Commutator and the net heat rate of the cooling air were used. In addition to that, the influence of time fluctuation on the result was analysed within each mesh, to find out if the flow could be considered as transient or in steady state. From the analysis of the different mesh models one single mesh size could be selected as most suitable for future use.

1.5 Structure

The report starts with a short introduction of the task that has been studied, including the problem description, the purpose, the objective and the scope of thesis.

Next there is a survey section that contains a short introduction to the DC-motor and its operational principles. The survey is continued with an overview of the fluid dynamics theory and the heat transfer theory.

The 2D modelling of the DC-motor is described in the next section. It starts with the geometry and mesh building and settings of boundary conditions, to the final simulation results and the conclusions.

Later the 3D-model of the DC-motor is presented. The modelling process and file structure of the geometry program is firstly described and pictures of the resulting model are shown. The process of generating and simulating different model cases with varying mesh size is described here as well and the simulation results are presented in figures and pictures. The results are analysed and thereafter compared with each other in a so called sensitivity analysis of the mesh size. Conclusions are then drawn about the model from the gained simulation results.

In the final section about the future work an overarching plan for the continued work is presented. A collection of different ideas of how to improve the cooling of the DC-motor is laid out as well.

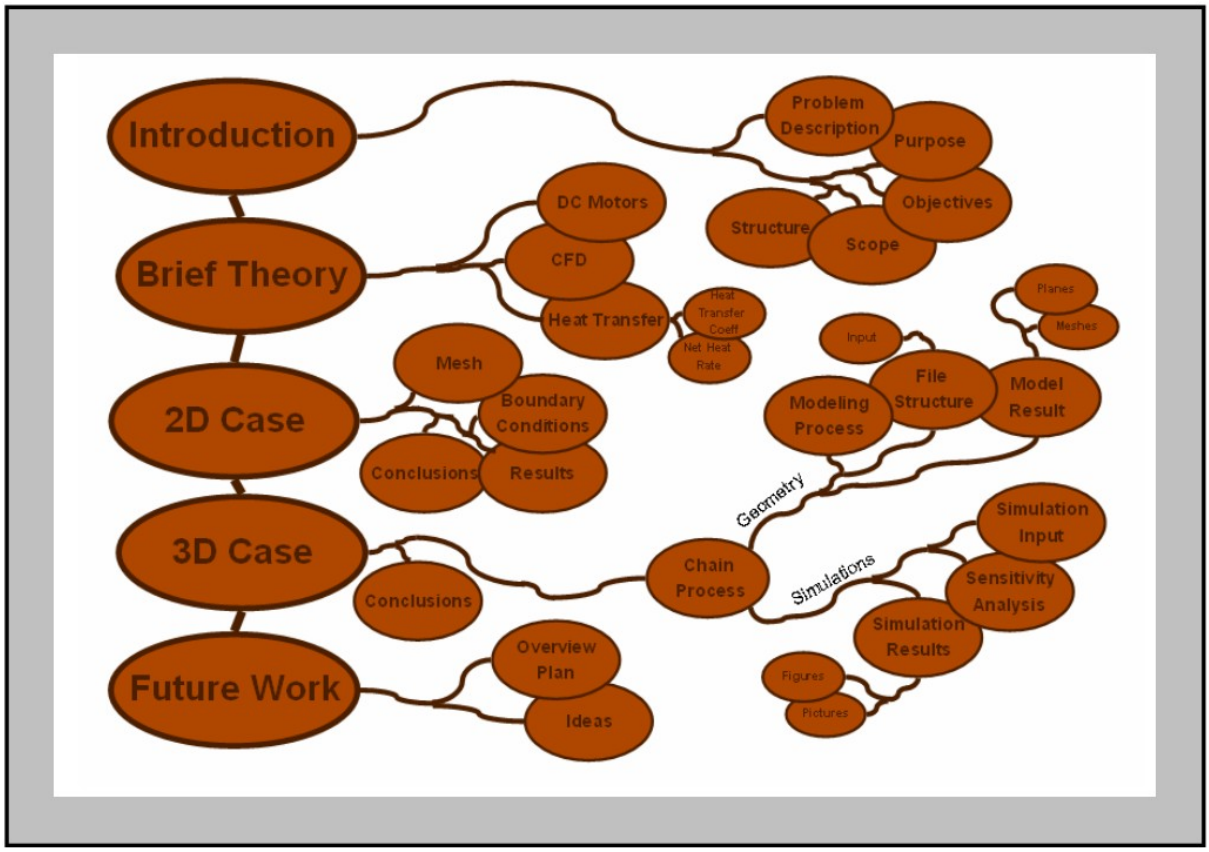

Figure 3: A schedule showing the structure in this report

2) Brief Theory

A brief theory has been included in the report concerning subjects toughed upon in this thesis. First there is a simplified description of the working principles of a DC-motor and further there is a chapter with a short introduction to CFD- theory and what it is based on. The final chapter is about heat transfer in general as well as a more detailed definition of some coefficients used in this report to measure the heat transfer.

2.1 Introduction to DC Motors

A DC-motor works by converting electric power onto mechanical work through electromagnetic forces. This is accomplished by forcing current through a coil and producing a magnetic field that spins the motor. The rotation occurs through counteraction between the inner magnetic field in the rotor and the external magnetic field in the stator. [4]

The electrical rotating machines can be divided into two main groups, the direct current motors and the alternating current motors. And each of them can further be divided into smaller groups due to the machines different construction and working principles. [1]

Every DC-motor has six basic parts: the axle, the rotor, the stator, the commutator, the field magnets and the brushes. The external magnet field is produced by high-strength permanent magnets or through electromagnetic forces in the stator windings. The stator is the stationary part of the motor together with the windings wrapped around it and the motor casing. The rotor consists of windings on a core that rotates with respect to the stator surrounding it. As for the commutator it is also a rotating part that is attached to the rotor and is electrically connected to the rotor windings. The brushes are stationary graphite blocks that are in contact with the commutator surface and lead over the electrical current to the rotating part of the motor. [5]

When power is applied to the DC-motor, current flows through the brushes and over to the Commutator. Through the brushes the current is then inserted to the commutator with different polarity, where it runs in a number of axial passages insulated from each other, all the way to the rotor windings. The differently polarised current reaches the rotor windings from different ends and forms a circuit, and due to the formation of the winding a magnetic polarization of the rotor is formed. This polarity of the rotor will be the same as the polarity of the outer magnetic field generated by the stator. There is then a repelling force between the rotor and the stator due to this same magnetic polarity, which generates a rotation. Though when the commutator rotates and therefore changes position compared to the stationary brushes the direction of the current through the axial passages in the commutator become reversed. This leads to a flip of the magnetic field, driving it to continue the rotation. In real life, DC-motors will always have more than two poles to avoid “dead spots” in the commutator. [5]

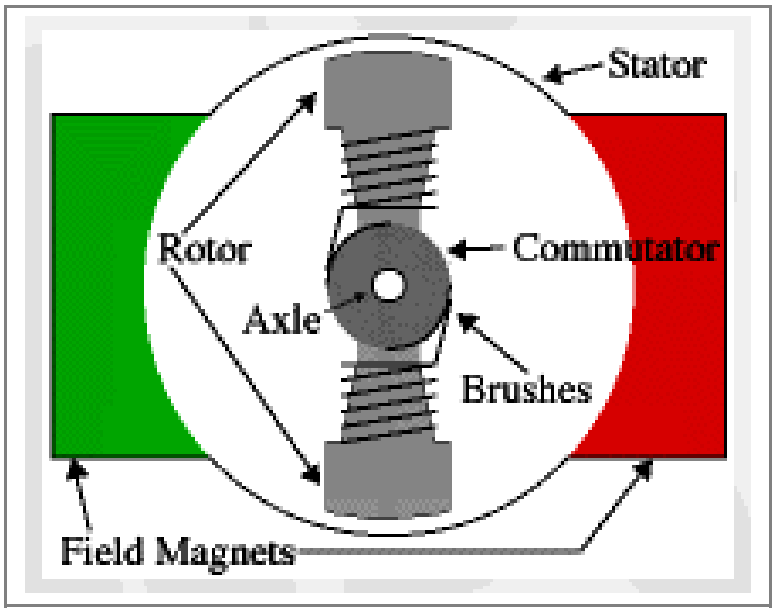

Figure 4: A simplified motor layout of a DC-motor with the rotor inside the field magnets (or the magnetic field caused by the stator) [5]

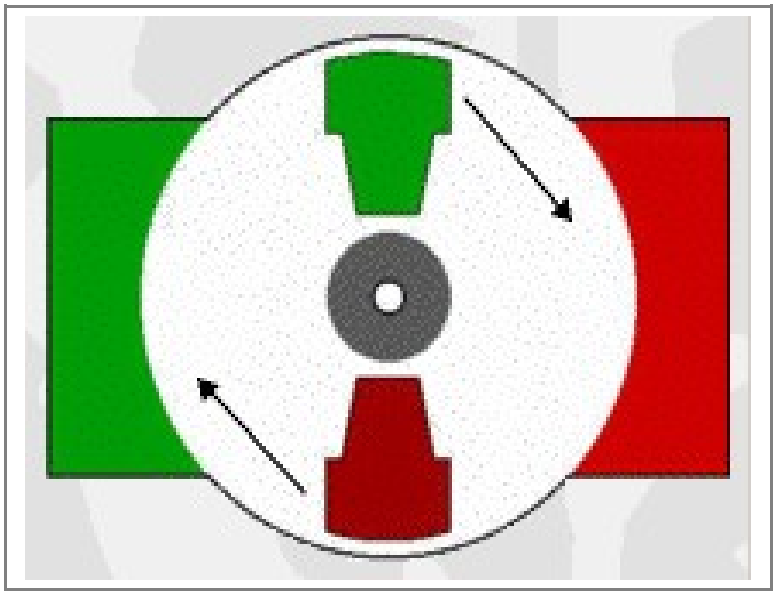

Figure 5: The figure shows a sketch of the working principle of a DC-motor. The red parts represents magnets or windings with a "North" polarization, while the green represents "South" polarization [5]

2.2 Theory of Computational Fluid Dynamics

Computational Fluid Dynamics or CFD is the analysis of systems involving fluid flow, heat transfer and associated phenomena such as chemical reactions, by means of computer-based simulation. This technique is widely used in different industrial applications, such as for example within electrical engineering and cooling of equipments. [2]

The CFD code is structured around the numerical algorithms that can tackle fluid flow problems. There are three main stages in the CFD-processing: the pre-processing, the equation solving and the post-processing.

In the post-processing the following things are done:

- The computational domain containing the geometry of the region at interest, here called the Volume, is defined. The time span for the simulation is also decided for those cases where the simulation results are transient.
- The domain is thereafter divided into sub-domains that form a mesh of cells. As for the simulation time span, it is also divided into smaller time steps.
- Then the physical and chemical phenomena of interest are selected for the model.
- The properties of the fluids and solids in the model are defined. A turbulence model also needs to be selected that will be appropriate for the type of flow that is examined. Some examples of turbulence models are the Reynolds stress model, the k-omega model and the k-epsilon model.
- Finally the boundary conditions are set for the cells at the domain boundaries, and thereafter the initial conditions are set for the whole domain.

The flow variables are calculated through an energy balance in each cell. For the variable examined, its rate of change with respect to time (for example Q_{stored}) is defined as its net flux through conduction and convection (radiation could also be included), as well as its creation inside the element (for example Q_{gen}). Since the underlying physical phenomena are complex and non-linear the solution needs to be obtained through iterations. [2]

In the post-processing stage the simulated results are processed. Flow variables such as temperature and velocity can be displayed through vector plots and contour plots on 3D as well as 2D surfaces. Other things that can be monitored are particle tracking and the property changes with time.

CFD is a powerful tool that can calculate complex flows, and through the use of it it's possible to concretise and visualize complicated flows that would have been very complicated through measurements and experiments.

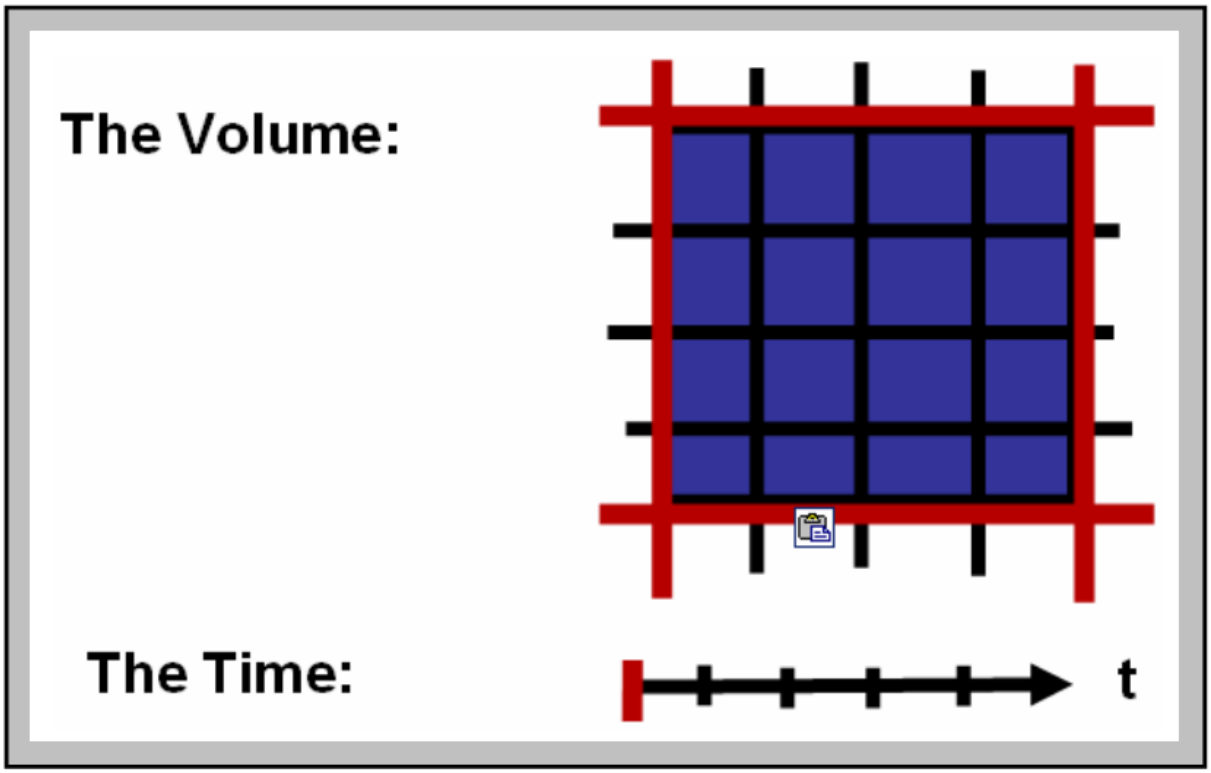

Figure 6: The sketch is showing the pre-processing work for CFD-simulations. The total volume is divided into smaller units and the total simulated time is divided into smaller time steps. Before the calculation process is engaged the conditions at the boundaries of the volume and the initial conditions have to be set.

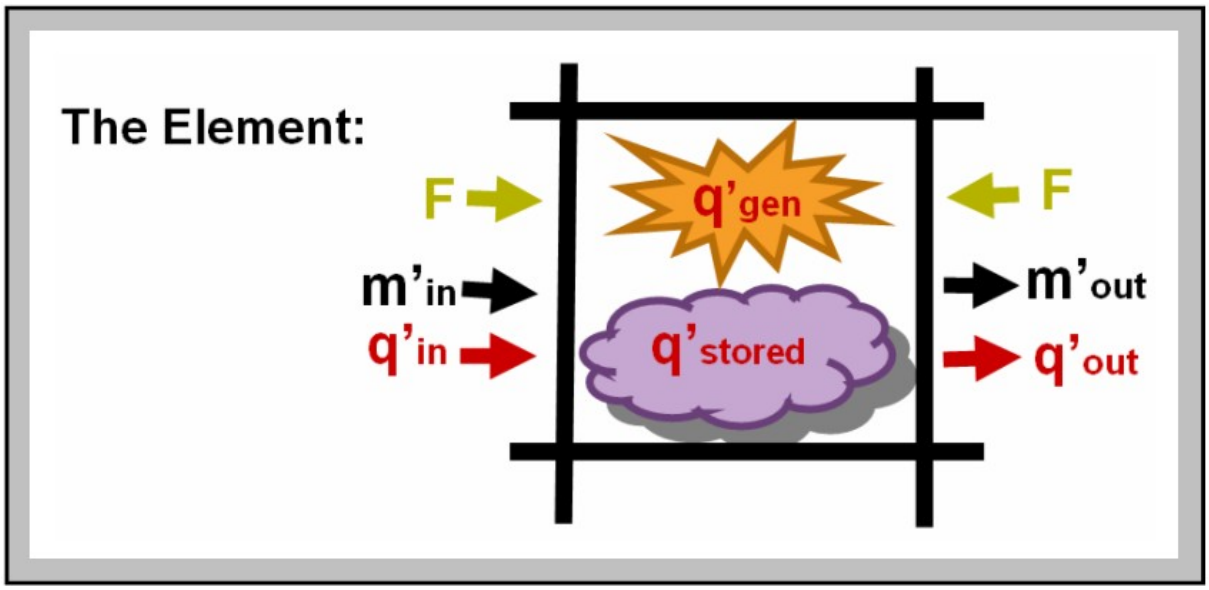

Figure 7: The sketch is showing the energy and mass balance in a particular mesh cell (or element)

2.3 Heat Transfer Theory

A simple way to define heat transfer is as thermal energy in transit due to a temperature difference. Whenever there is a temperature difference in a medium or between media, heat transfer must occur. The heat transfer can be divided into three types: conduction, convection and radiation. [3]

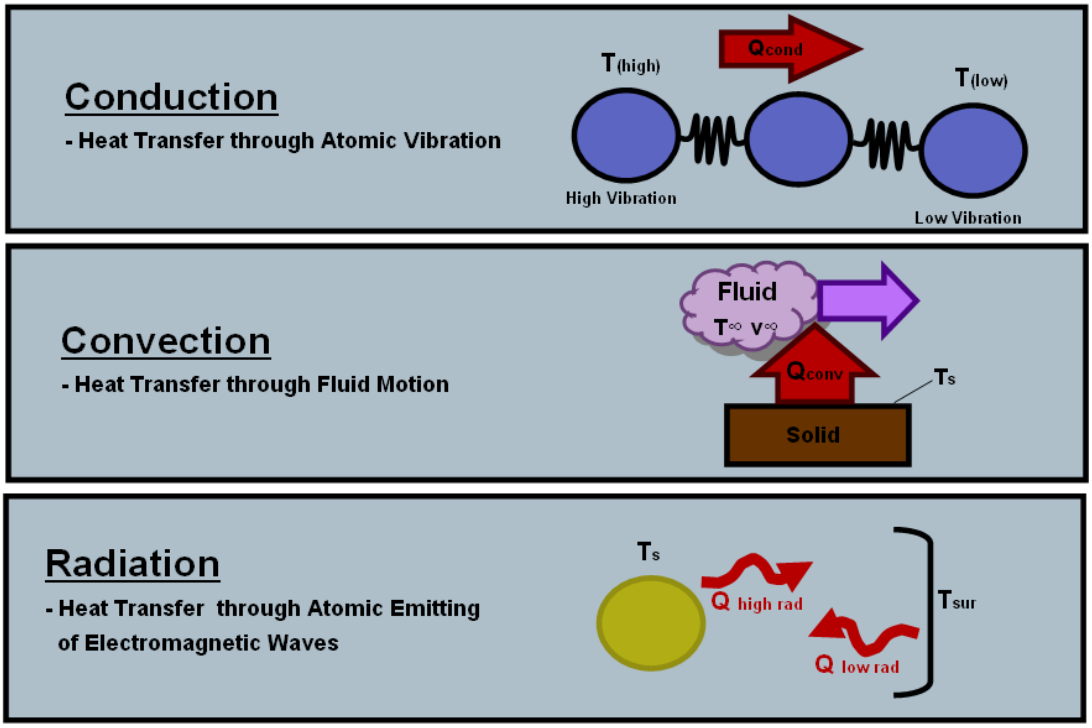

Figure 8: Three different types of heat transfer

We use the term conduction to refer to heat transfer that occurs across a stationary medium, which could be a solid or a fluid. This type of heat transfer occurs on the atomic level, where the particles with higher temperature also have a larger random motion or vibration due to their higher energy containment. The vibration is spreading along the adjacent particles causing a flux of energy, also called diffusion.

Convection on the other hand refers to heat transfer that will occur between a surface and a moving fluid when they are at different temperatures. The heat transfer then occurs due to transportation of energy due to the fluid motion.

The third form of heat transfer is termed thermal radiation. All surfaces emit energy in the form of electromagnetic waves due to changes in the electron configurations of the constituent atoms. The higher the surface temperature is the more energy is emitted and therefore there is a net heat transfer between surfaces with different temperatures. [3]

2.3.1 Heat Transfer Coefficient

A way to measure the heat transfer from a surface due to convection is through a coefficient called the convection heat transfer coefficient. This coefficient is defined from the expression for the convection heat transfer, called Newton's law of cooling: [3]

$q'' = h * (T_s - T_\infty)$,

where q'' = heat flux in W/m2
T_s = surface temperature in K
T_∞ = fluid temperature in K
h = heat transfer coefficient in W/m2,K

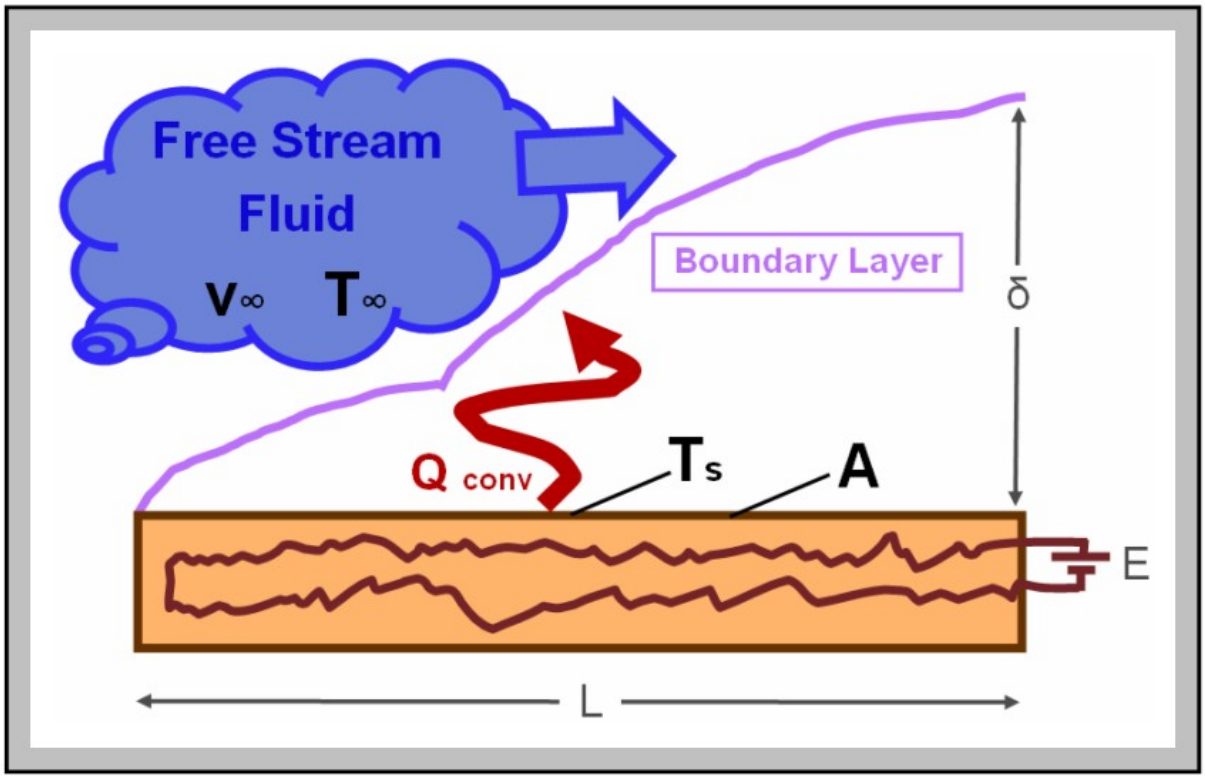

Figure 9: A sketch showing the development of the laminar and turbulent boundary layer for a fluid flow over a flat plate and the parameters affecting the heat transfer

The average heat transfer coefficient between a surface and a fluid can be estimated through experiments. By knowing the amount of heat that is generated and transferred from a certain surface, and by also knowing the surface temperature and the free stream temperature that is not affected by the surface, the heat transfer coefficient can be found through Newton's law of cooling. [3]

Another way to calculate the heat transfer is through the use of empirical equations. The input needed for those equations are some properties of the fluid derived from the velocity of the free stream fluid as well as the approximate temperatures of the free stream fluid and the surface temperature. [3] Those empirical equations simplify the heat transfer analysis substantially.

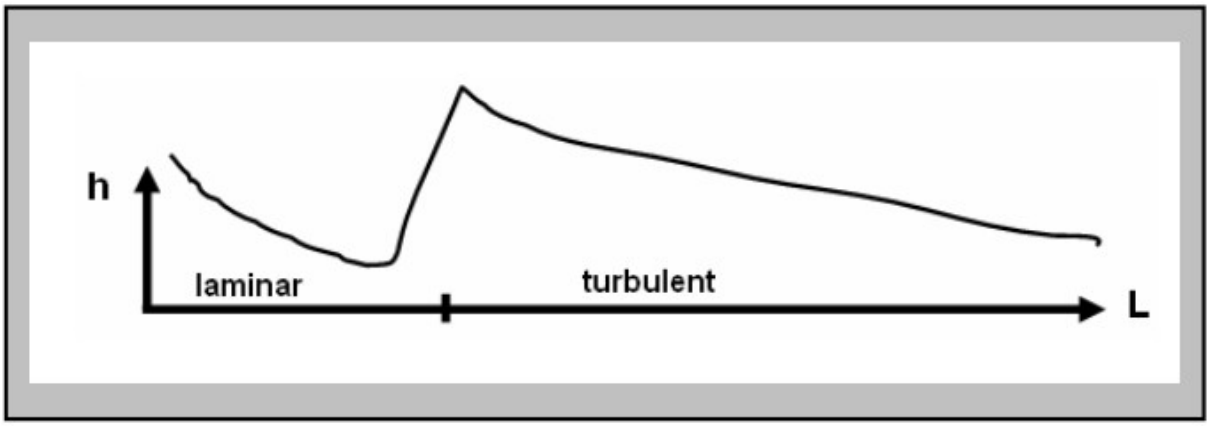

Figure 10: A diagram showing how the heat transfer coefficient is depending on the development of the boundary layer (when compared to figure 9)

The heat transfer coefficient could vary over a surface, since the efficiency of the heat transfer is dependent on the boundary layer formed between the free stream and the surface. A thicker boundary layer would ultimately result in decreased heat transfer and therefore also a lower heat transfer coefficient. In general it can be said that the heat transfer coefficient is at its highest at the beginning of the surface where the boundary layer is not yet built up, and then it slowly decreases with the building up of the boundary layer. If the flow is initially laminar it eventually turns into turbulent and since the mixing is better at turbulent flow the heat transfer increases at that point. [3]

The heat transfer coefficient is used as a way to measure the ability for a specific surface to transfer heat to a free fluid stream above it.

2.3.2 Net Heat Rate

A method to evaluate the efficiency of a cooling system is to measure the amount of energy that is transported out of the system through this specified cooling system and compare it with the total amount of heat that is generated. The additional heat that is not transported through the air cooling system is finding other ways to exit through the solid, but this heat flow is not a part of the cooling system examined. If we consider a system with air as cooling medium flowing through its boundaries the increase of heat in the air, the net heat rate, would be of great interest. By comparing the net heat rate for different setups it would be possible to grade their cooling efficiency relatively between each other.

The drawing on figure 11 is showing a system and its boundaries, where the heat flow and fluid flow moving through the boundaries are marked with arrows. When the system reached a steady state the heat generated (Q_{gen}) should be equal to the net heat transported out with the fluid and the heat that leaves the system through other ways such as through radiation ($Q_{other\ cooling}$).

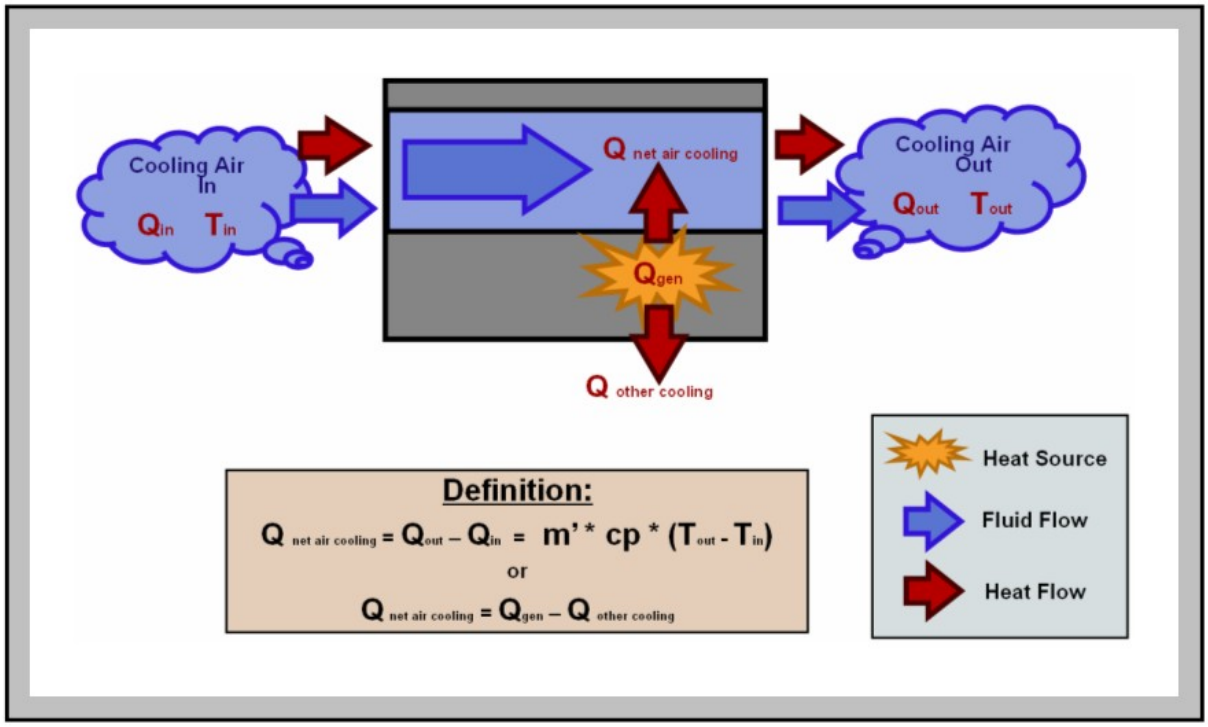

Figure 11: A sketch showing the definition of the net heat rate for the cooling air through a certain boundary

3) The 2D Model

Since building of the 3D-model needs a lot of time and effort a simplified 2D version was done previously from the main modelling. This model could give us a clue of what kind of problems that would occur during the simulation process of the larger 3D model.

3.1 Geometry and Mesh

For the reproduction of the motor into a 2D model it had to be decided what kind of simplifications that should be made to the geometry. First of all a radial cross-section plane of the motor was chosen. In this plane just one quarter was selected, due to an assumed symmetry. The two ends of this section were then connected periodically to each other which mean that the flow leaving one end side is directly entering the other end side. Further more the outer bearing-shield wall was made in a cylindrical shape and the cross section of a brush was placed above the Commutator wall. It should be noted that the brush is stationary while the Commutator wall is moving according to the rotational speed of the machine.

The first model that was made had no inlet or outlet, which resulted in that the same air was assumed to flow around only driven by the rotation of the Commutator wall. In the second model the constant injection of new air in the system was taken into consideration. For that purpose two straight pipes were added on the bearing shield wall, one that represented the inlet of the air and one for the outlet. Later though this model met some problems during simulation. The large width of the pipe ends resulted in back flows as well as circulation flow within the pipes. To avoid those phenomena a new version of the model was made where the inlet and outlet pipes had the form of a cone with the larger ends attached to the shield wall. Through this way the flow in and out from the model was forced into a beam normal to the bearing shield wall and the circulation within the pipes was suppressed. In a final 2D model the effect of an obstacle object disturbing the flow was examined. This obstacle was shaped as a rectangle and placed in an upright position leaving just a small air gap between its bottom wall and the Commutator wall. The occurrence of this obstacle would give us an understanding of how the air flow reacts to a flow obstacle and also how the heat transfer from the Commutator wall is affected.

The geometry of each model was built up in a Gambit journal file. Each point used in the model was defined and named individually. Thereafter the points were connected to lines and the lines into surfaces. Finally the whole surfaces representing the air space between the Commutator surface and the bearing shield wall was meshed with quadrilateral cells. The mesh size was subordinated to a size function set on the delimiting edges of the model, which made the mesh smoother closer to those edges and a bit coarser further away.

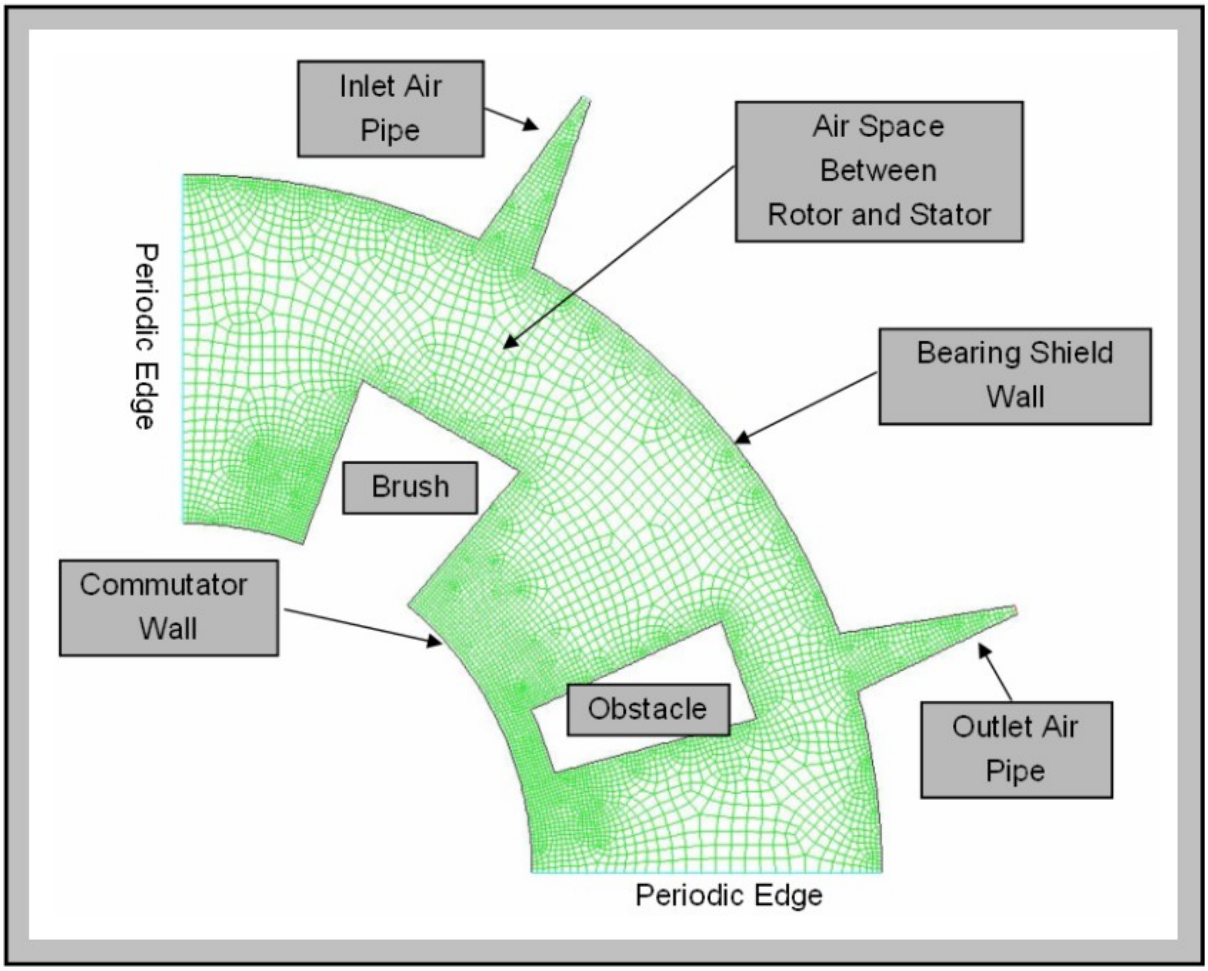

Figure 12: A 2D mesh model showing a 90 degrees periodic segment of a 4-pole DC-motor seen from a radial cross section. This particular model has a cone shaped inlet/outlet and an obstacle object close to the Commutator surface disturbing the flow.

3.2 Simulation Settings

The completed mesh was exported into FLUENT where the flow and heat transfer simulation was done. The first thing that had to be set was the boundary conditions of the model. It was set according to table 1 below and figure 13. The rotation of the Commutator surface is set to go counter clockwise.

Table 1: The boundary conditions of the 2D mesh model

Commutator wall:	Temperature	400 K
	Rotational Speed	1500 rpm
Bearing shield wall:	Temperature	300 K
Air inlet:	Temperature	300 K
	Velocity (into pipe)	5 m/s *
Air outlet:	Pressure	0 Pa
Obstacle, Brush and Pipe walls:	Heat Flux	adiabatic

**The velocity out of the cone shaped inlet pipe is approximately 1 m/s due to five times larger opening.*

The turbulence model used for the simulation was the k-epsilon model, which is usually used as a standard model in the initial stage when the advantages of other models are not yet examined for the particular case studied. Moreover the heat transfer equation and the flow equations are considered as well. The model was set up to find a steady state solution using the upwind differencing scheme method in the discretized equations.

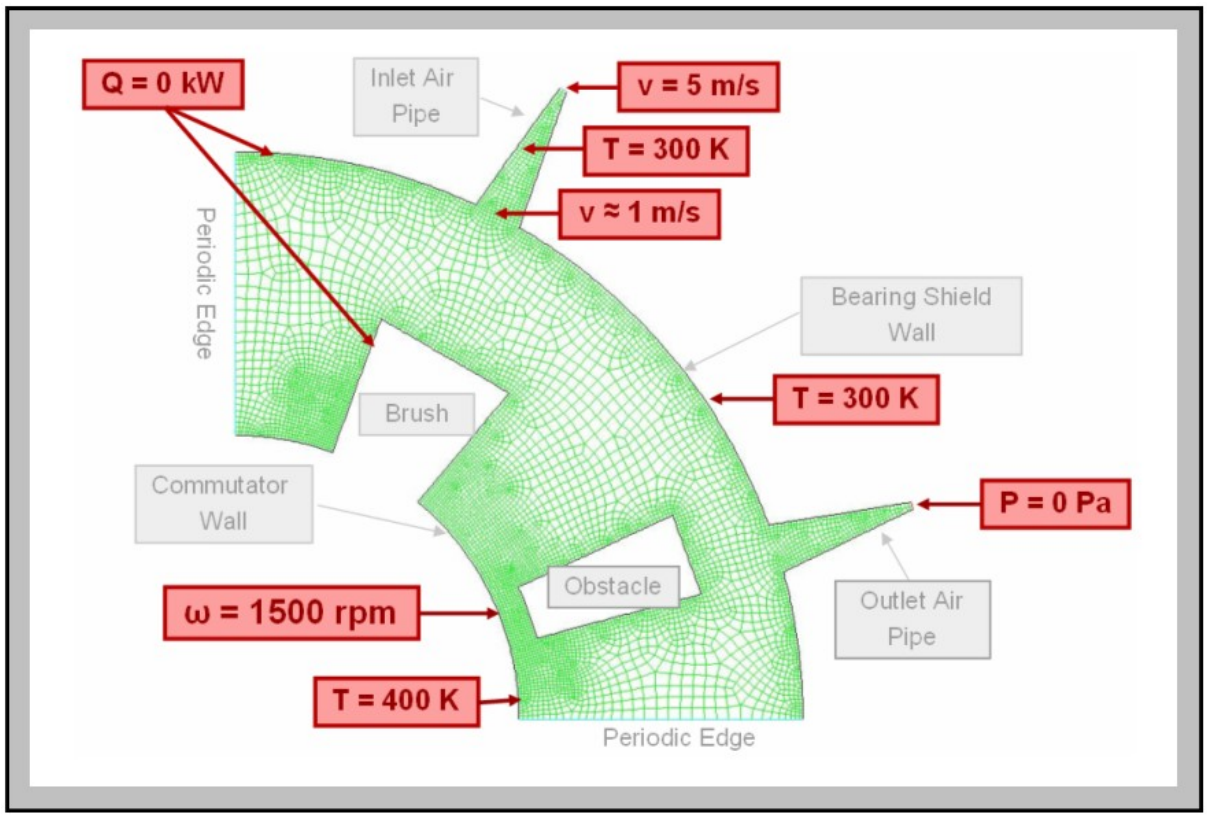

Figure 13: A 2D mesh model showing a 90 degrees periodic segment of a 4-pole DC-motor seen from a radial cross section. This particular model has a cone shaped inlet/outlet and an obstacle object close to the Commutator surface disturbing the flow. The boundary settings are stated in the picture and the rotation is set clockwise motion.

3.3 Simulation Results

When simulating the 2D model with the above mentioned settings a steady state solution was reached. The result is presented in figures 14 and 15.

In Figure 14 the velocity vector field is shown. The circulation of the flow is mainly driven by the velocity difference between the moving Commutator wall and the stationary outer wall. A clearly distinguished velocity boundary layer is formed near the Commutator surface where the velocity is decreasing rapidly. Because of this velocity difference there are vortex formations appearing, one on each side of the obstacle object. This is resulting in a mixing between the hot and cold areas. The obstacle is suppressing the global circulation of the flow, dividing one vortex formation into two separate ones. Another effect that the object has on the flow is that it increases the turbulence and therefore also the mixing of the fluid. If the object

is placed near the moving Commutator wall the velocity boundary layer is forced to be narrower which results in an increased velocity gradient and better heat transfer.

The flow is entering the inlet pipe with a high velocity and the velocity is thereafter decreasing due to increased pipe cross section area. Thanks to the cone shape of the pipe the flow is forced to move straight forward and circulation inside the pipe is avoided. The injection flow to the machine has a relatively high velocity and can therefore supply cold air to the lower regions of the machine. Some of the inlet flow is taking a shortcut directly towards the outlet pipe, passing above the vortex instead of circulating in it firstly.

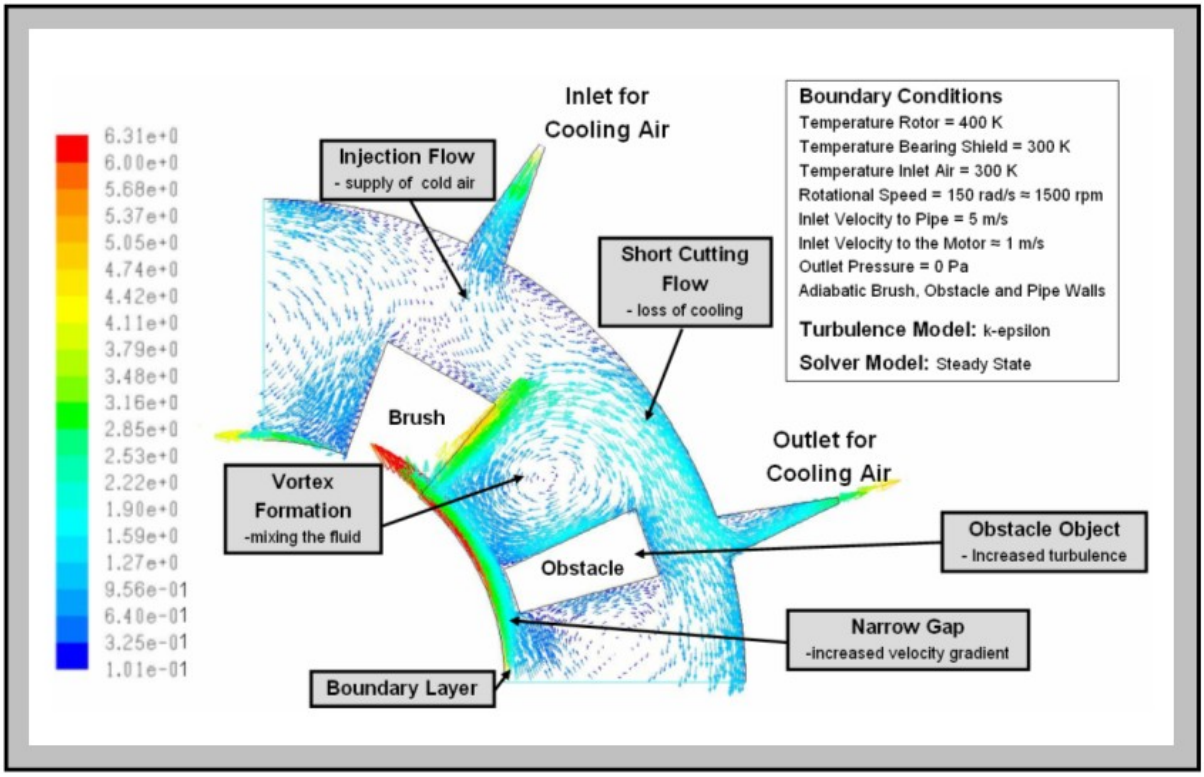

Figure 14: The velocity vectors of the simulated air flow for the 2D mesh model coloured by the velocity magnitude [m/s]. A small interval range is chosen for the colour chart bar to visualize the small differences of velocity in the major parts of the model.

The temperature distribution of the model is schematically described in Figure 15. In the vortex formation between the brush and the obstacle it can be seen that the temperature is evenly distributed as a result of the circulating flow. This circulation allows the flow heated up by the Commutator surface to reach higher, colder regions and thereby increase the heat transfer. The heat transfer is also increased by the obstacle object, due to increased turbulence and increased velocity gradient near the Commutator surface.

About the inlet air it can be seen that it creates a colder region just beneath the inlet pipe. There is high heat flux perpendicular to the flow going from the vortex formation to the air inlet region and it is caused by the large temperature difference between them. As mentioned above some of the inlet flow has a tendency to take a shortcut to the outlet by flowing next to the bearing shield wall and never interact with the circulating flow. This is of cause a loss for the cooling system.

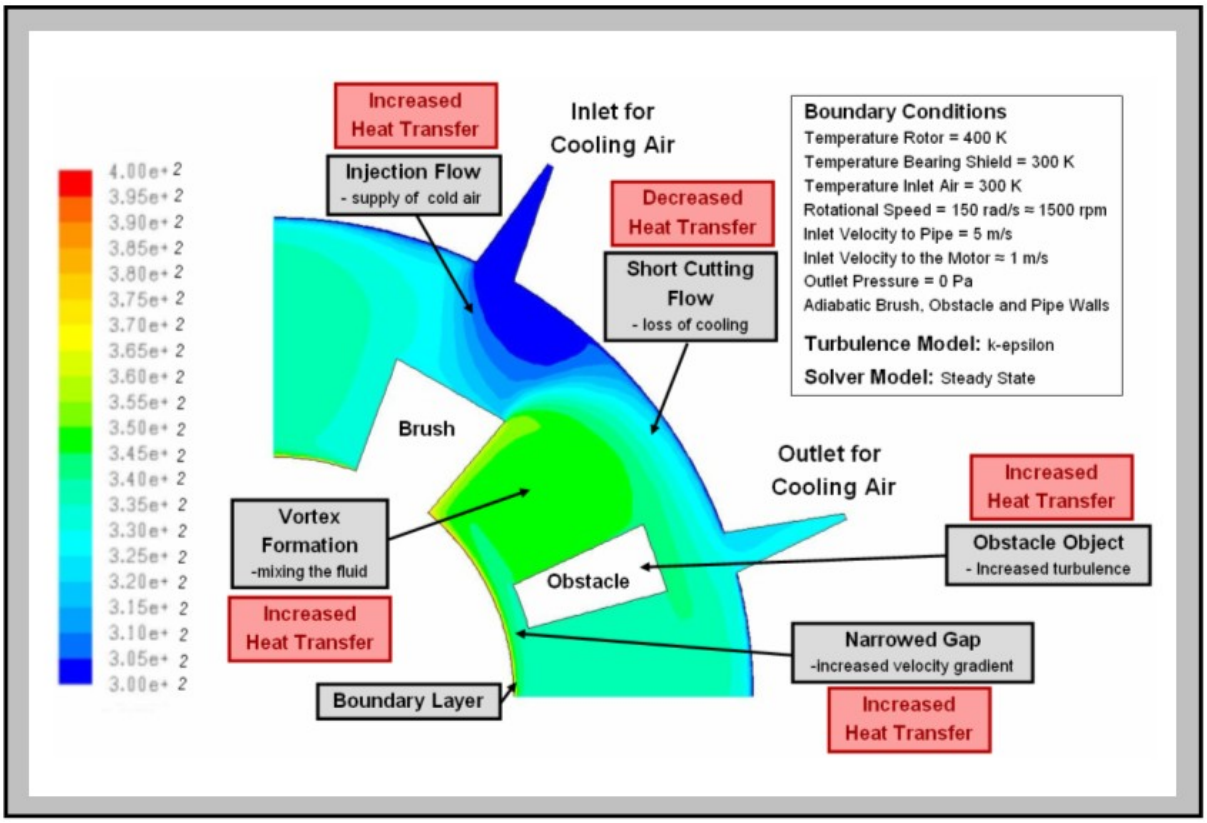

Figure 15: Temperature contours of the simulated air flow for the 2D mesh model [K]

3.4 Conclusions for the 2D Model

The 2D models can give us a better understanding of the basic flow and heat transfer phenomena which occur in the cooling system of the machine. It has its advantages compared to the 3D modelling because it is less time consuming to create and to simulate. You can easily try out new ideas by making simple modifications on the 2D model and study their influence. Later the ideas could be applied on the 3D model where the complexity of the geometry and the three dimensional effect of the flow also are taken into consideration.

There are two driving forces for the airflow in the machine. One of them is the shear stress in the fluid made by the moving wall of the Commutator on one side and the stationary outer wall on the other. The second force observed is the constant injection of air from the inlet pipe that globally drives the airflow through the machine and out through the outlet pipe.

One tendency of the airflow seen in the 2D model is the appearance of vortex formations due to the rotation. Basically the machine is functioning as a fan mixing up the air inside it and resulting in an enhanced cooling of the Commutator surface. It is also seen that some of the injected airflow is shortcutting directly to the outlet pipe. This is a loss of cooling energy and should be suppressed as much as possible. Finally, the appearance of an obstacle object is seen to have an impact on the airflow since vortexes are formed on both sides of it. It seems like the obstacle is disturbing the global circulation of the air which might have an effect on the cooling. In the meantime the local circulation increases which results in increased

turbulence and therefore also increased heat transfer. Both of those influences have to be taken into consideration when placing air obstacles in the machine.

4 The 3D-Model

The building up of a 3D model of a DC motor is rather complex and time consuming. To make the process more structured and surveyable the work was divided into different levels.

Firstly, the geometry of the model was defined in a computer programming language called Python. All the geometrical sizes as well as the mesh sizes were made parametrical to make the program more user-friendly and to simplify the modification process of the model sizes later on. The modelling of the geometry was definitively the most challenging part of the whole work with the 3D model and also the most time consuming.

When running the geometry script in Python a Gambit journal file is generated according to the script. The process time is about 10 seconds. There are a lot of advantages with letting a program create a journal file instead of creating the journal file directly. First of all the written code is significantly compressed. A 300 kB python script is made to create a 2 MB journal file, which implies in less coding. Another advantage of using this method is that you can control and regulate the structure of the mesh and therefore also the number of cells in the mesh, in a way that is not possible directly from the journal file. From the script, both the geometry and the mesh is made to be extruded in the axial direction which results in prism shaped mesh cells instead of pyramid shaped once. Through this way the total amount of cells can be brought down perhaps about 10 times, to less than 1 million cells. Another advantage with dividing the process in different levels is that you can activate certain parts that you wish to work with for the moment and deactivate the rest of the geometry and thereby further decrease the amount of active cells.

When running the gambit journal file in Gambit it takes about half an hour to complete and it will then generate a visual version of the model (dbs-file) as well as the mesh of the model. The mesh is then imported into the program FLUENT for simulation of the airflow and heat transfer. This simulation takes about 1-4 days according to the size of the mesh and the final data file with all the simulated results around 200-400 MB. From this file the results can be extracted in the form of pictures or data.

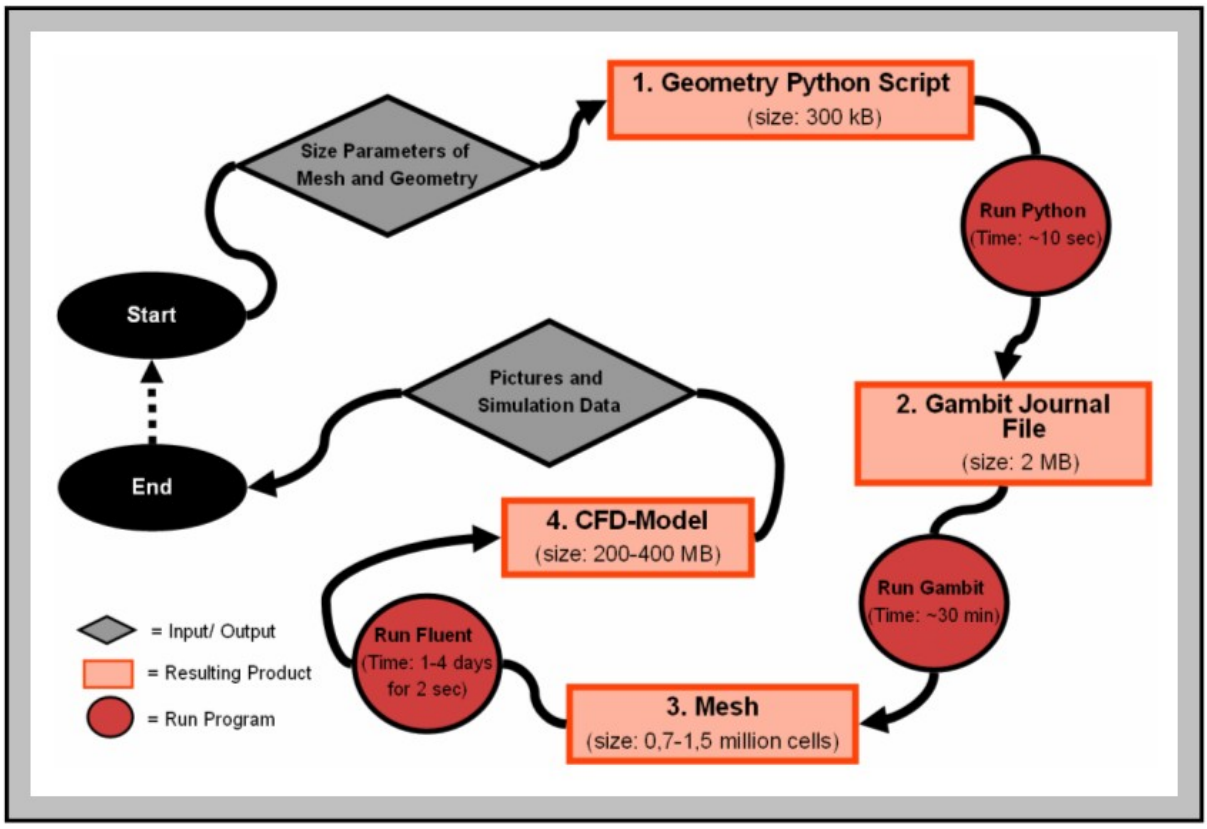

Figure 16: Scheme of the working chain process for building the CFD model, all the way from the modelling of the geometry to the final simulation results

4.1 The Geometry

The geometry of the DC motor is defined in a python script that is set to generate a gambit journal file from which the final mesh is generated. The modelling process of this script as well as the file structure of the script will be described below. Finally the resulting geometry and mesh model will be presented.

4.1.1 Modelling Process

To model the air gap in a DC-motor is a very complicated matter because of the complexity of its geometry. In an attempt to delimit the work only the Commutator part of the motor was chosen for modelling leaving out the stator package. The model had to be in 3D since it doesn't have axis-symmetrical shape. One example of that is the inlet air to the Commutator part from the gap in the stator windings as well as from the rotor axis which both are directed in the axial direction. Another example is the gear brush with the brushes that covers just a part of the Commutator section of the motor. The idea to select just a segment in the radial plane was also examined. But since the cross section of the bearing shield has a rectangular shape and the cover of the outlet air is on the sides of the motor this was also not possible. The inclinations of the ventilation cover openings are directed downwards and when the machine is rotating the generated flow would look differently at the both sides. So that left us

with no other choice than to build up the whole 3D geometry of the air gap in the Commutator part.

The modelling process for the 3D model was as follows:

1. The modelled Commutator part of the machine was divided in three sections: the section next to the stator box, the middle section with the actual Commutator and the section next to the N-Side Bearing Shield Wall.
2. Each of the sections was projected onto a general radial plane, here called an XY-plane. In those planes the vertices, edges and faces of the geometry were set. All the coordinates of the vertices were defined with parameters and collected in a parameter list.
3. The general XY-planes where then extruded in the axial direction and became volumes. In the volumes some separate XY-planes were defined where the geometry changes in the axial (Z) direction.
4. The active faces of each of the separate XY-planes were meshed with triangular cells. The mesh was controlled by size functions and the variables in those functions were collected in a parameter list.
5. The mesh was then extruded between the separate XY-planes in the Z-direction creating prism shaped mesh cells forming a structured mesh in the Z-direction.
6. Between the three separate geometry sections two middle sections were created to connect the sections. Those volumes were created with tetrahedral mesh cells forming an unstructured mesh.
7. Now when the whole geometry and mesh were created the boundary types of the faces at the boundaries of the model were set. Those surfaces were grouped in an intuitive way and defined as inlets, outlets or plane walls. The volumes were also grouped after their continuum type; the meshed solid volume, the meshed air volume and the volume that is not active in the simulation.
8. Finally the completed mesh was extracted.

4.1.2 File Structure

The geometry program created to generate a Gambit journal file was made with Python script. The main file holding track of all the subordinated files was called “dcgenTot.py”. From this main file the help file “layout.py” was called which is made as a tool to translate the python script into gambit script. All the parameters of the geometrical sizes and the mesh sizes were set in the files “dcgenSize.py” and “dcgenMesh.py” respectively. The parametrical geometries and mesh for the different sections were then defined in the files “dcgenDel1.py”, “dcgenDel2.py” and “dcgenDel3.py” and the connecting geometry between the sections were made in “dcgenConABC.py”. Finally the physical settings for the model such as the boundary and the continuum settings were set in the file “dcgenBC.py”.

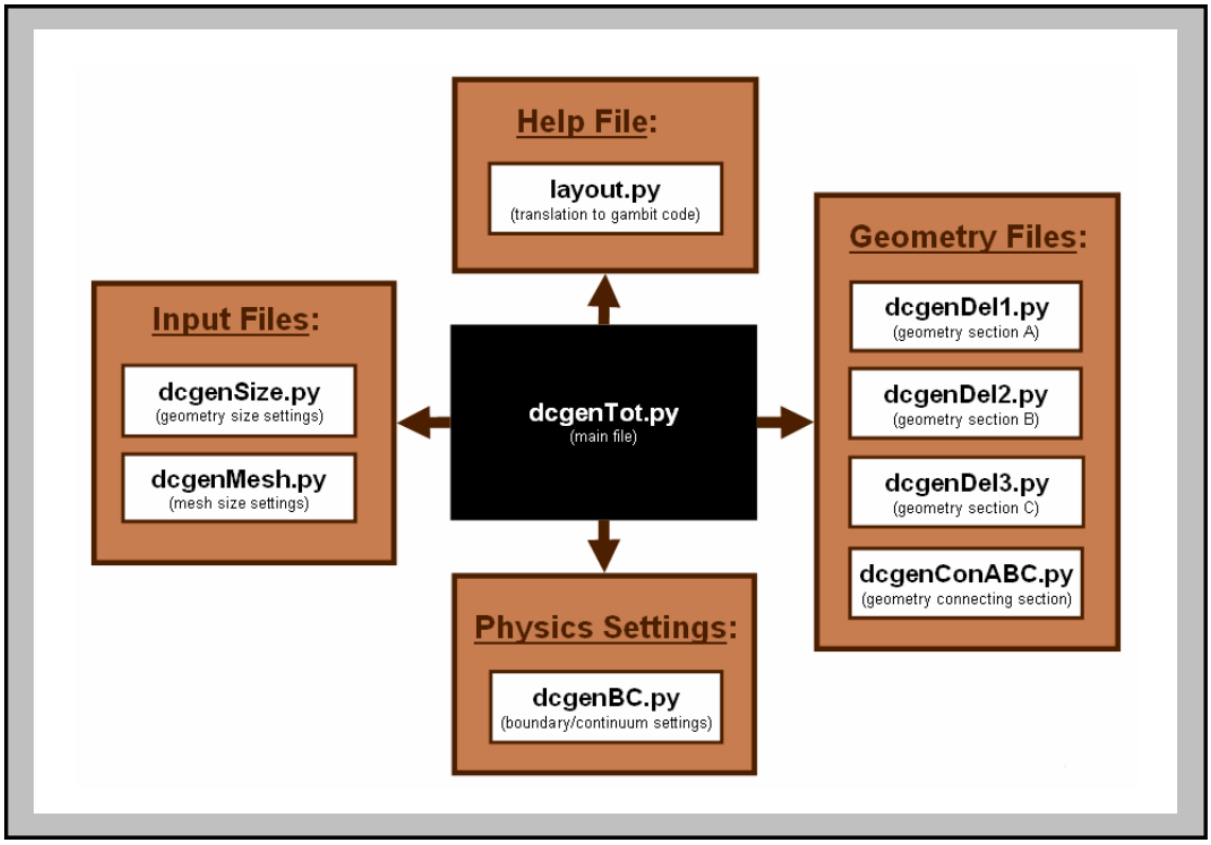

Figure 17: File structure of the 3D model geometry script

Because of the parameterisation of the geometrical sizes it is easy to enlarge or reduce the model to be able to simulate the airflow of machines with different sizes. The input parameters for the model are collected in Figure 59 found in the Appendix.

4.1.3 Model Result

In this chapter the resulting model of the Commutator part of the DC-motor will be presented. The side view of the model can be seen in Figure 18. From there it is possible to see how the different sections of the model and the planes that they are divided into. There are three main sections namely section A, B and C and there are transition sections in-between that connect the sections, namely A-B and B-C. Another fact that can be mentioned is that the total amount of planes is 18.

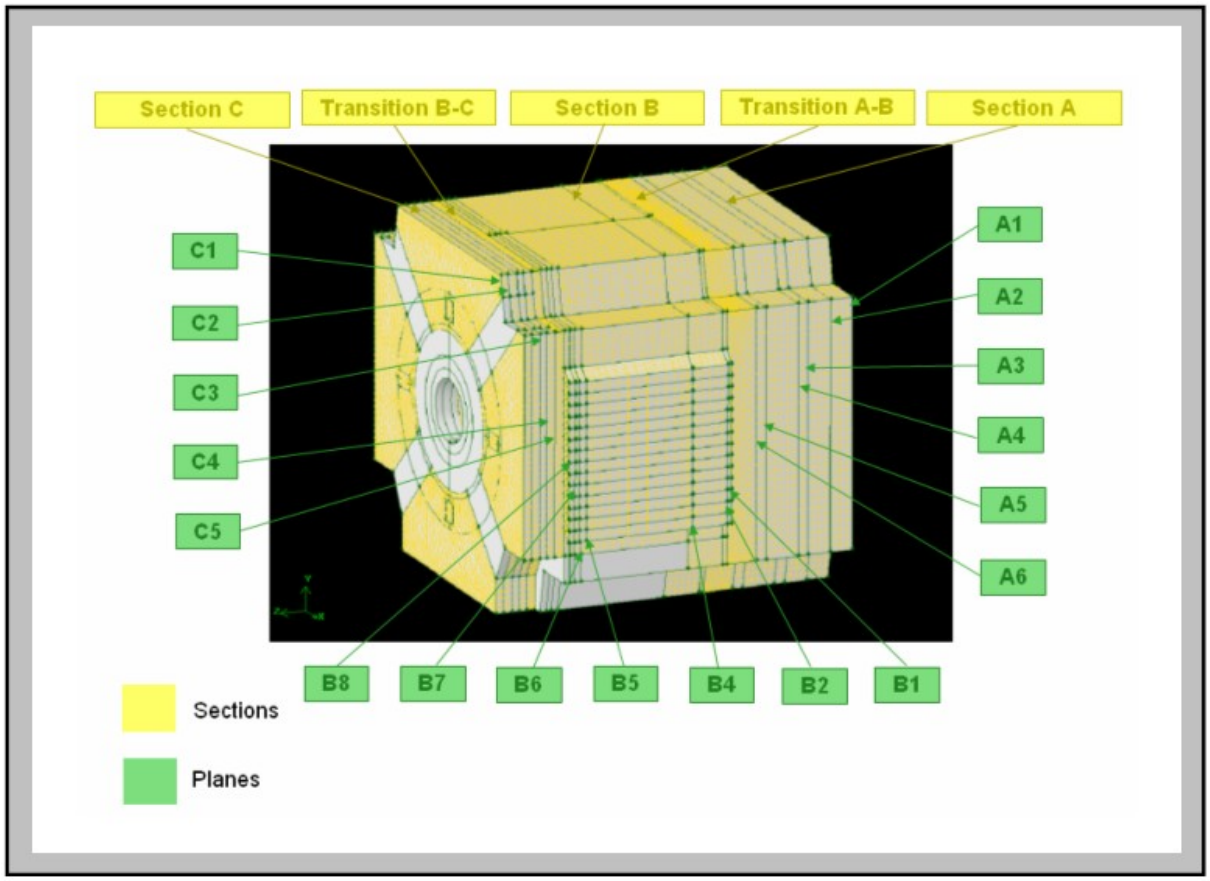

Figure 18: A side view of the mesh model, presenting the Commutator part of a DC motor, where the sections and the planes are marked.

The geometry of the model with excluded mesh will also be shown. First in Figure 19 the side view of the model is shown together with labels of the most important parts of the model. After that the geometry of the separate sections are shown as they will look if the cover of the machine was taken away, as well as the volume of the air void. Some solids are also taken away just to make the geometry more easy to grasp.

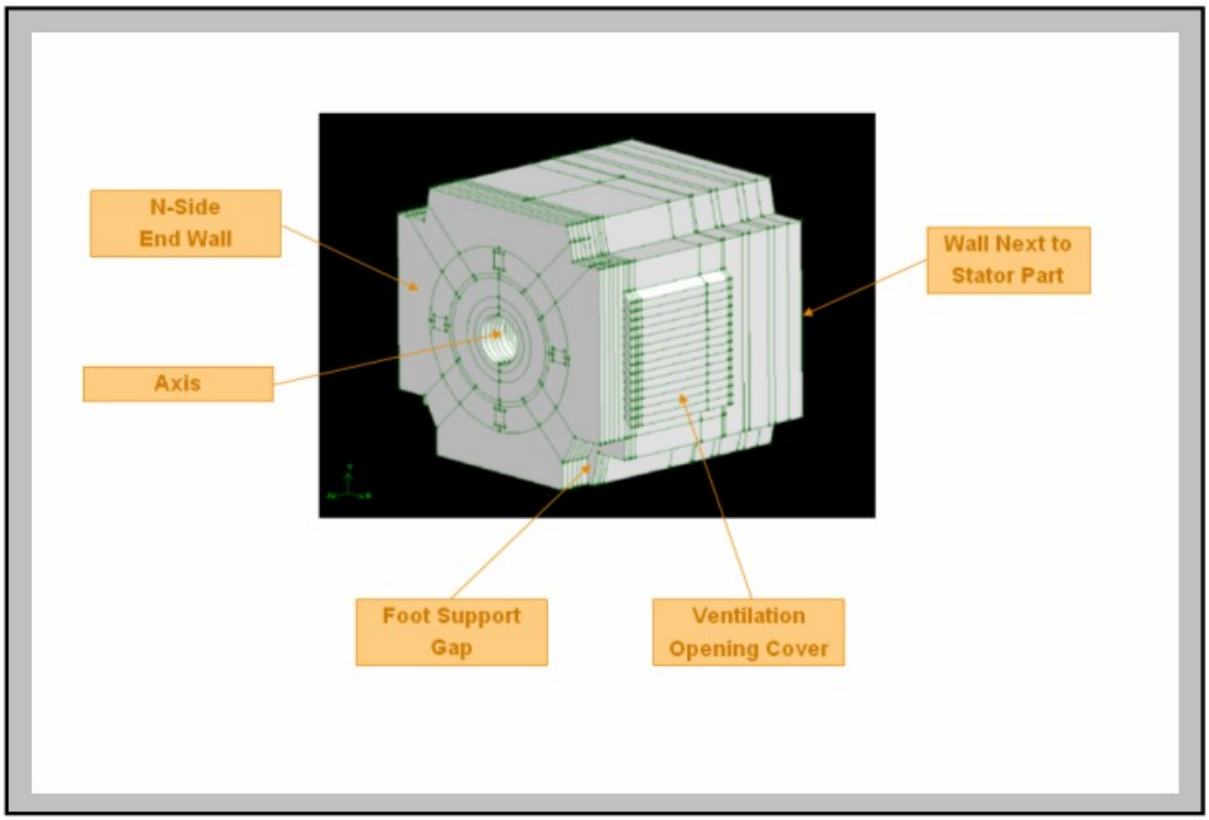

Figure 19: Side view of the model with labels showing some important details

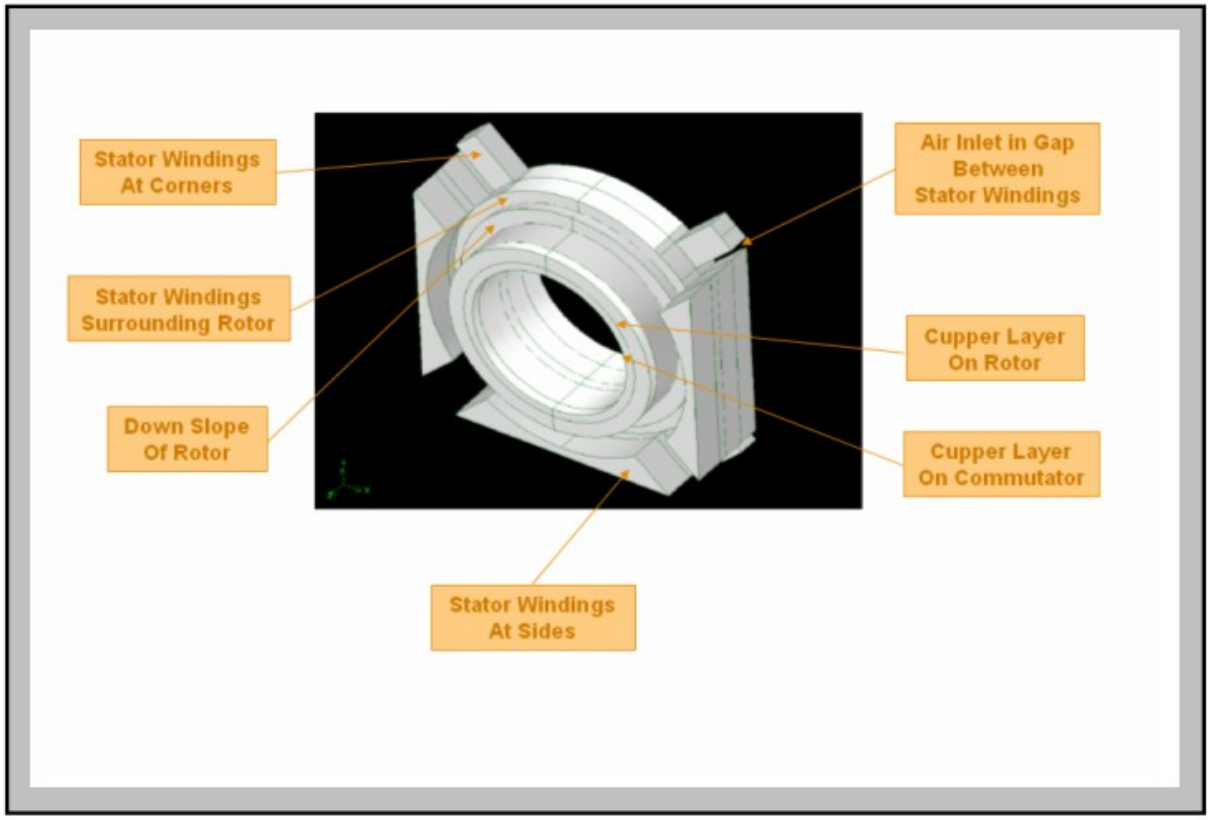

Figure 20: A side view of the solid of section A when the cover of the motor is taken away

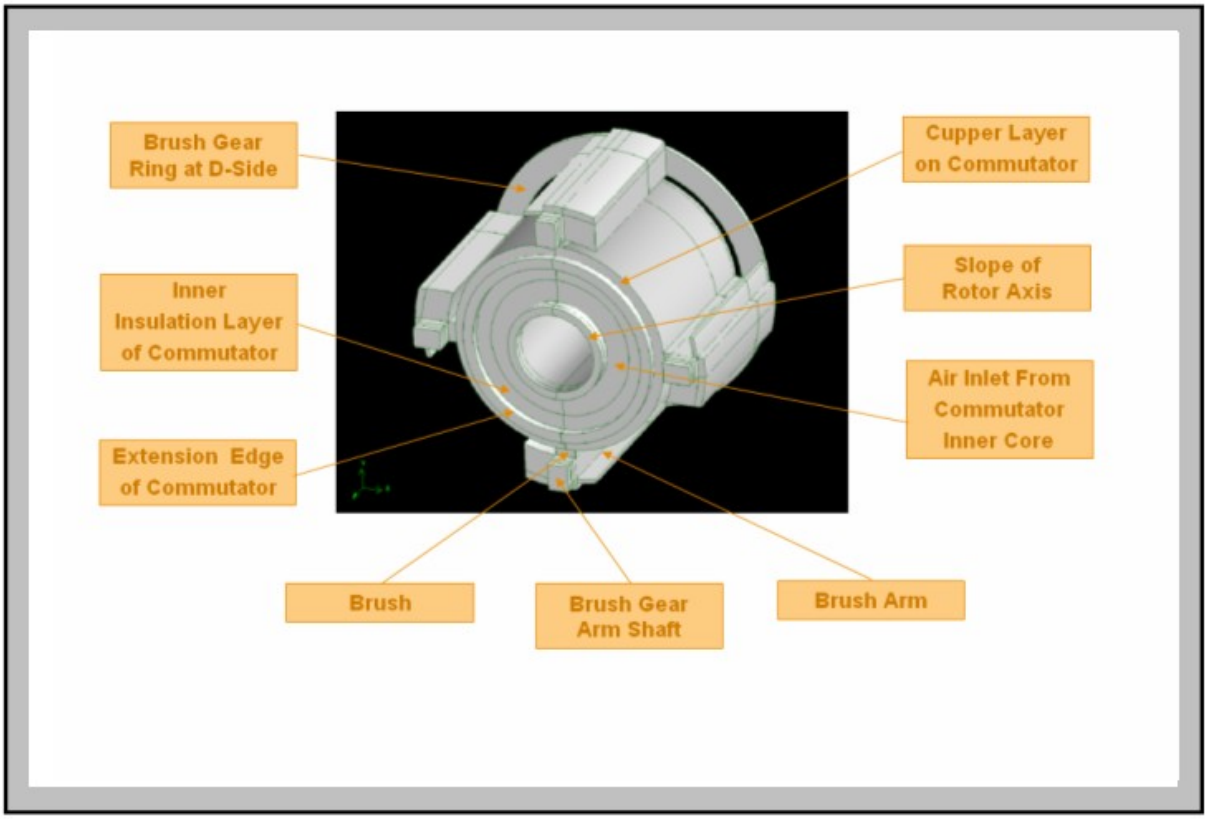

Figure 21: A side view of the solid of section B when the cover of the motor is taken away

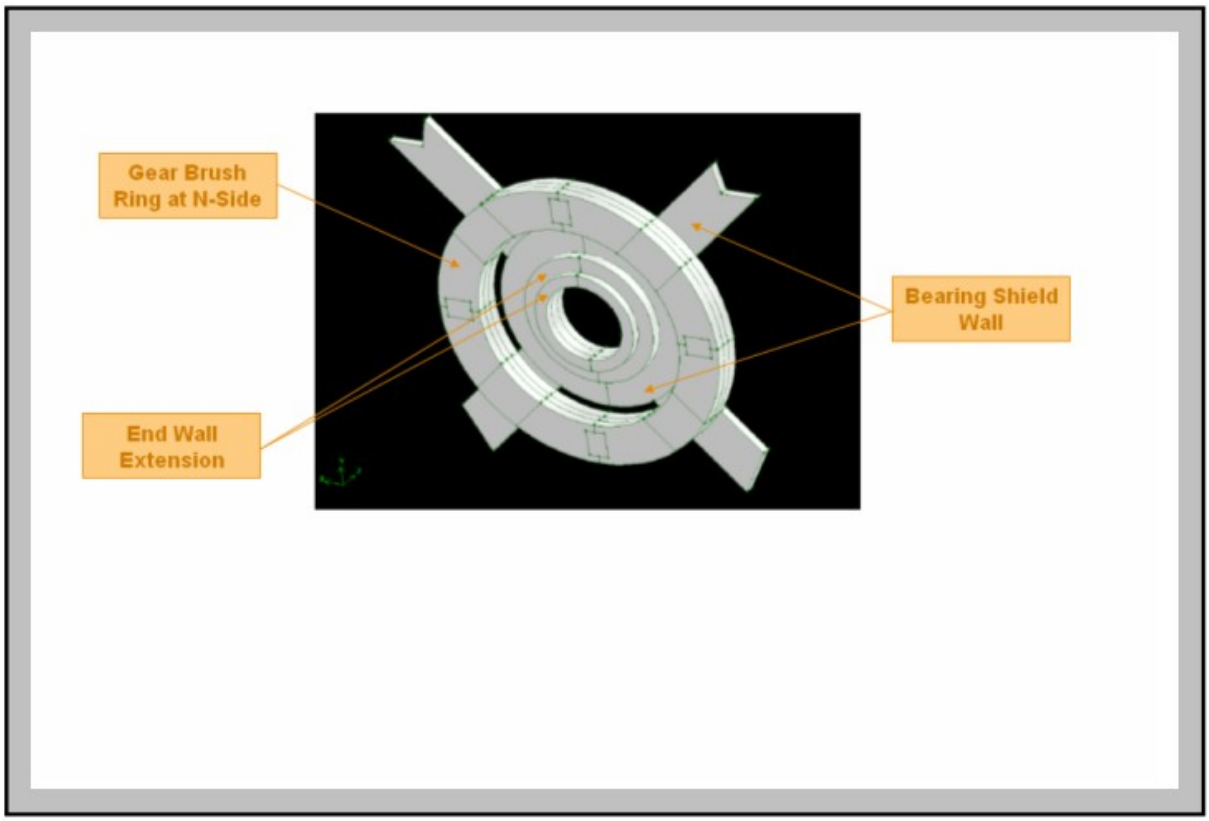

Figure 22: A side view of the solid of section C when the cover of the motor is taken away

4.1.3.1 The Planes

In this chapter each of the XY-planes for the different sections will be pictured one by one. The highlighted surfaces on the planes are the surfaces that are active and will be meshed either as solids or fluids. From those surfaces the volume mesh is extruded towards the next XY-plane in the Z-direction. The planes are ordered so that they start from the stator shield wall and goes until the end wall of the Bearing Shield. Labels are shown for the surfaces in the planes where the mesh will be turned off or activated in the next coming volume. It should be noted that for section C, since the geometry building was done in the opposite direction the surfaces that will be active in the next coming volume are not yet highlighted. But the newly activated or deactivated surfaces are labelled in the same way as in the previous sections.

The geometry of section A starts from the end of the stator shield and goes all the way to the beginning of the Commutator surface. In Figure 23-28 the faces with active mesh are pictured for the planes A1-A6. The faces active in plane A1 are the faces on the D-sides outer boundary of the model representing the meshed volumes in the forward direction. In plane A6 the active faces are the once representing the mesh volume in the transition section A-B.

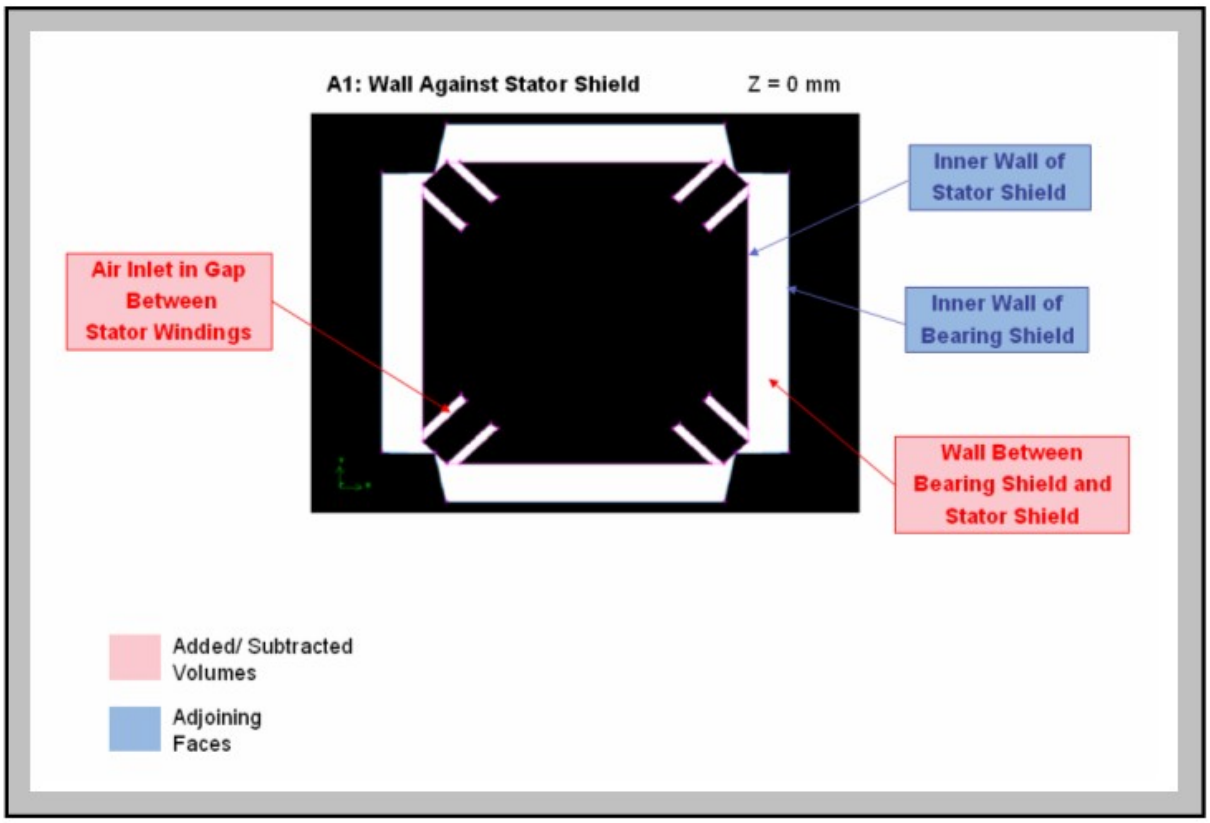

Figure 23: The surfaces with active mesh, in forward direction, at the cross section plane A1 of the modelled DC-Motor

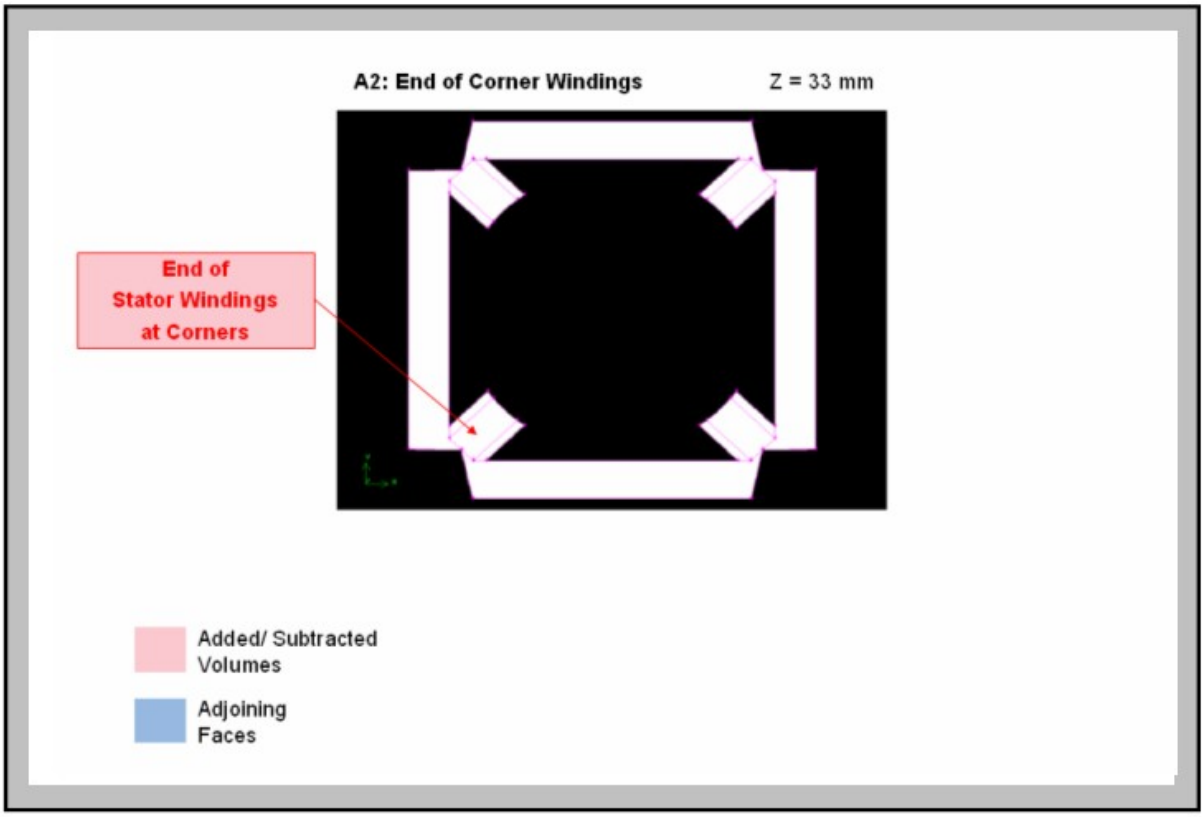

Figure 24: The surfaces with active mesh, in forward direction, at the cross section plane A2 of the modelled DC-Motor

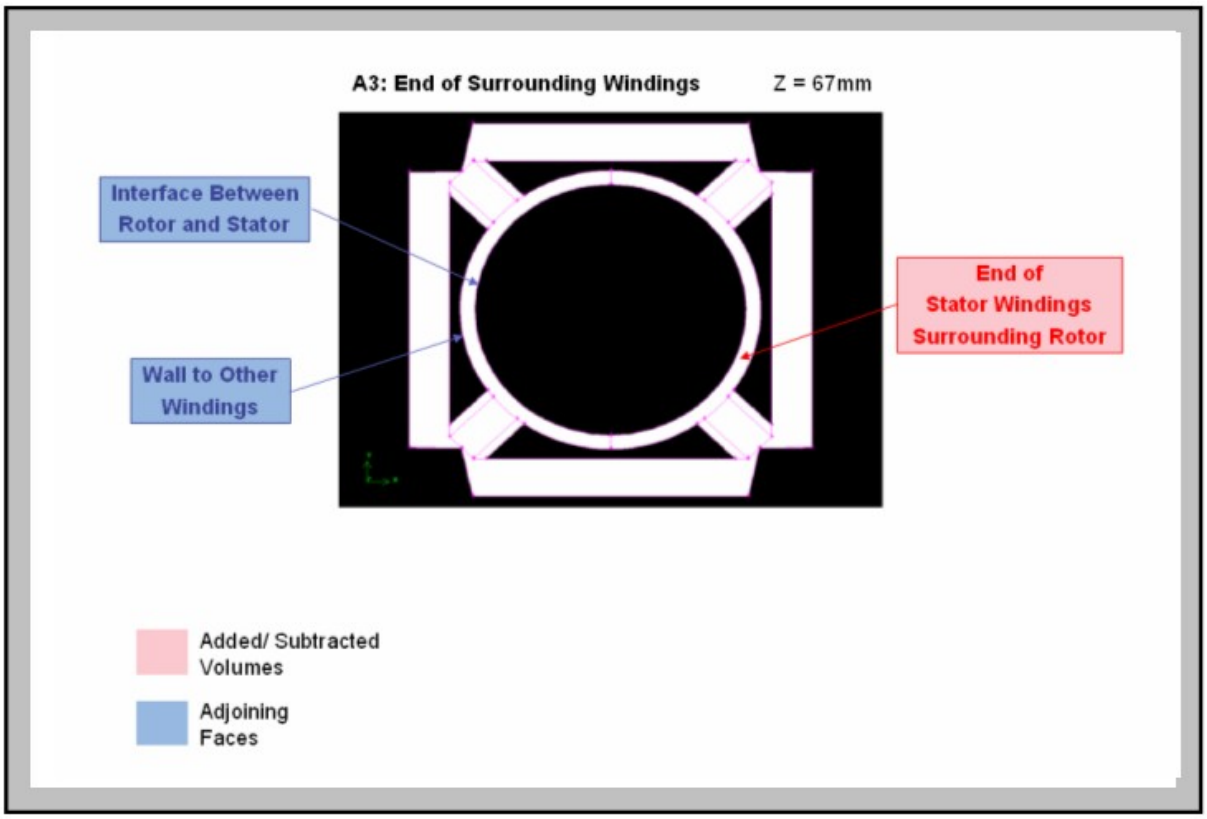

Figure 25: The surfaces with active mesh, in forward direction, at the cross section plane A3 of the modelled DC-Motor

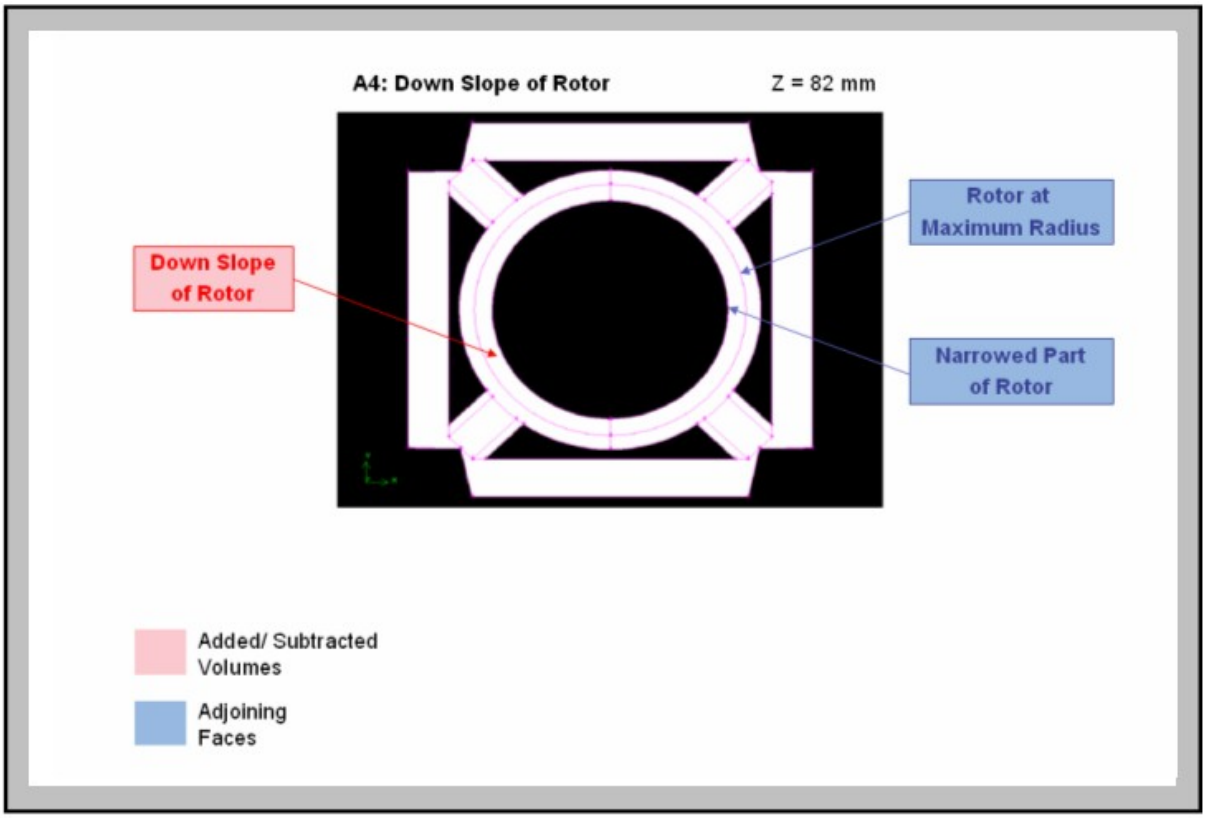

Figure 26: The surfaces with active mesh, in forward direction, at the cross section plane A4 of the modelled DC-Motor

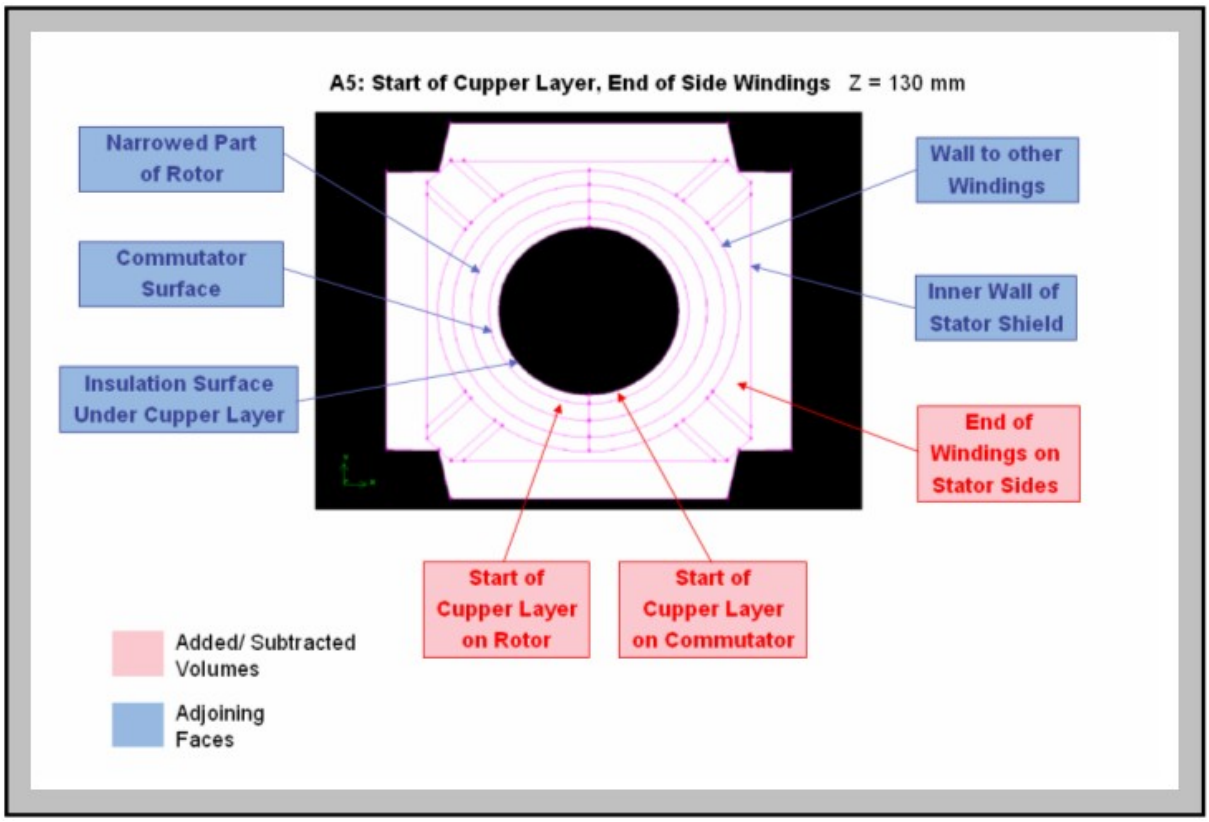

Figure 27: The surfaces with active mesh, in forward direction, at the cross section plane A5 of the modelled DC-Motor

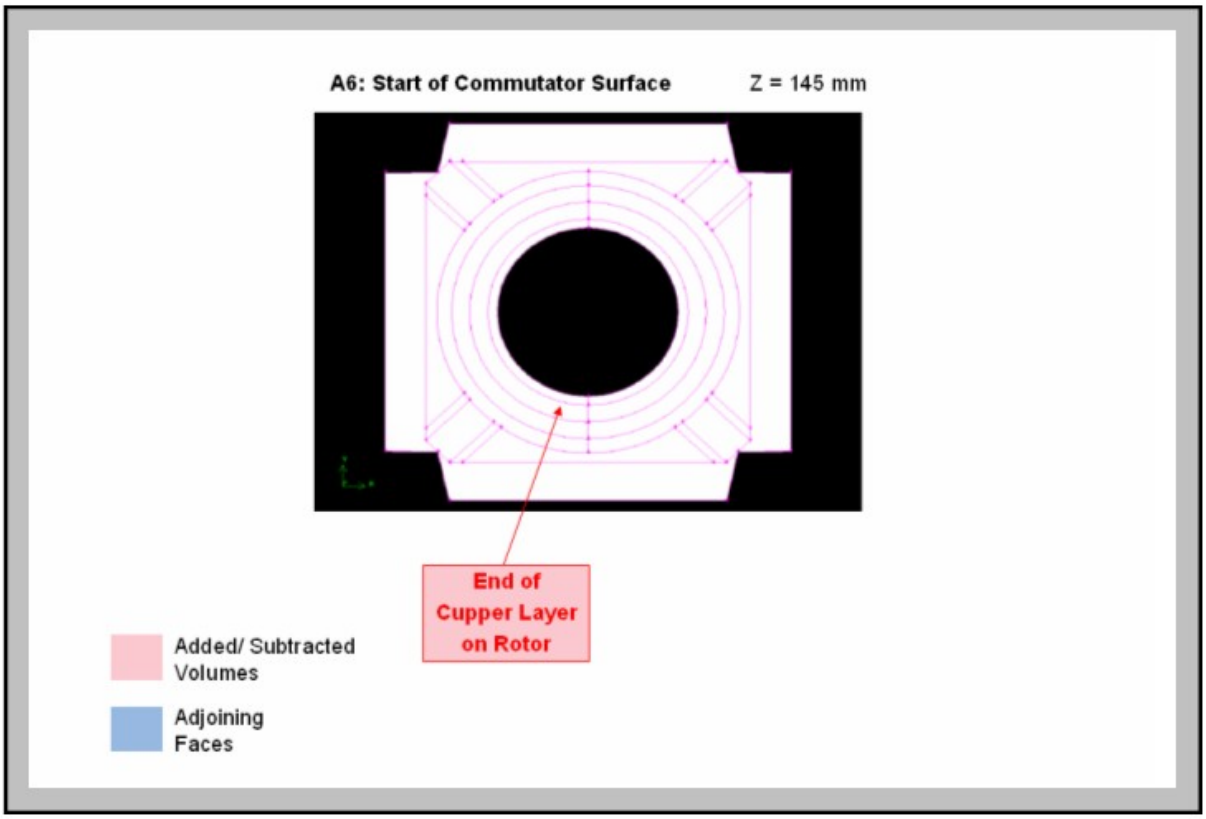

Figure 28: The surfaces with active mesh, in forward direction, at the cross section plane A6 of the modelled DC-Motor

The geometry of section B starts from the beginning of the Commutator surface and goes all the way to where the ventilation cover ends. In Figure 29-36 the faces with active mesh are pictured for the planes B0-B8. The active faces in plane B0 shows the meshed volumes in backward direction (transition section A-B). In plane B8 the active faces are the once representing the mesh volume in the transition section B-C.

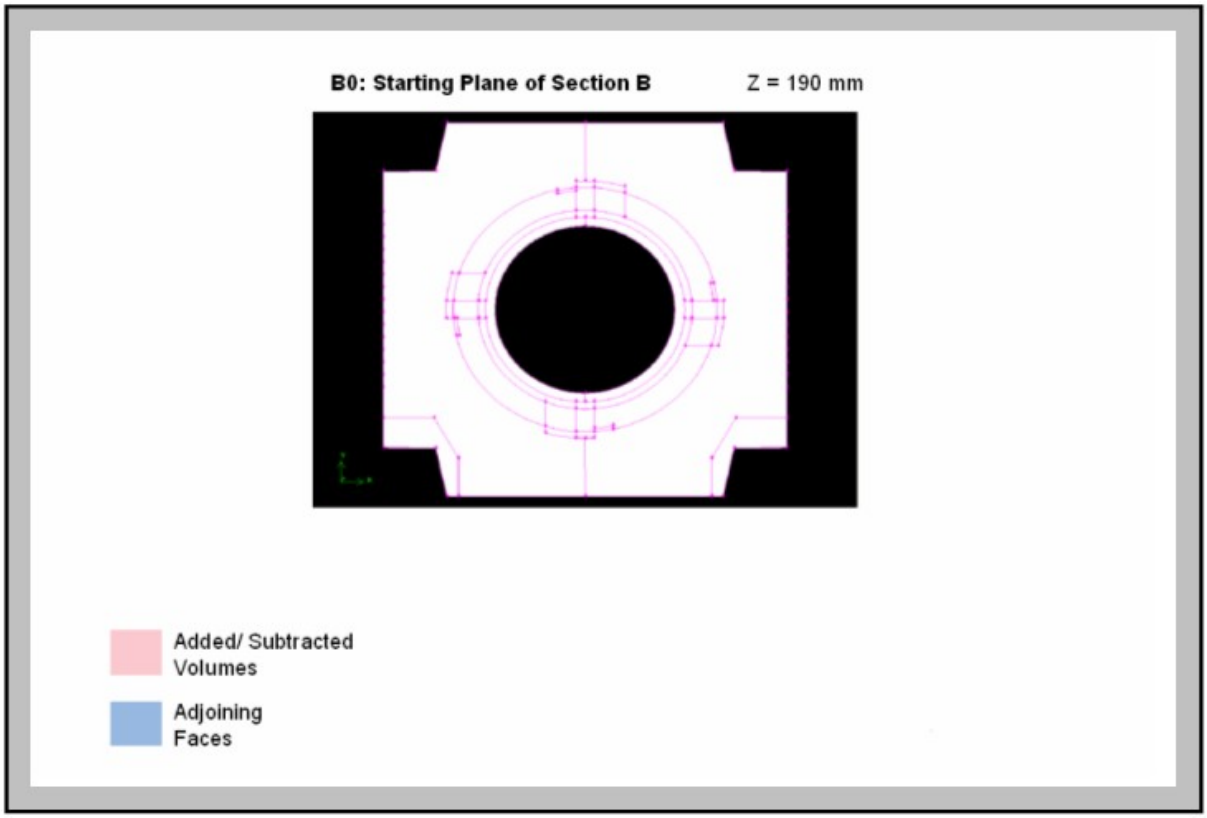

Figure 29: The surfaces with active mesh, in backward direction, at the cross section plane B1 of the modelled DC-Motor, here called plane B0.

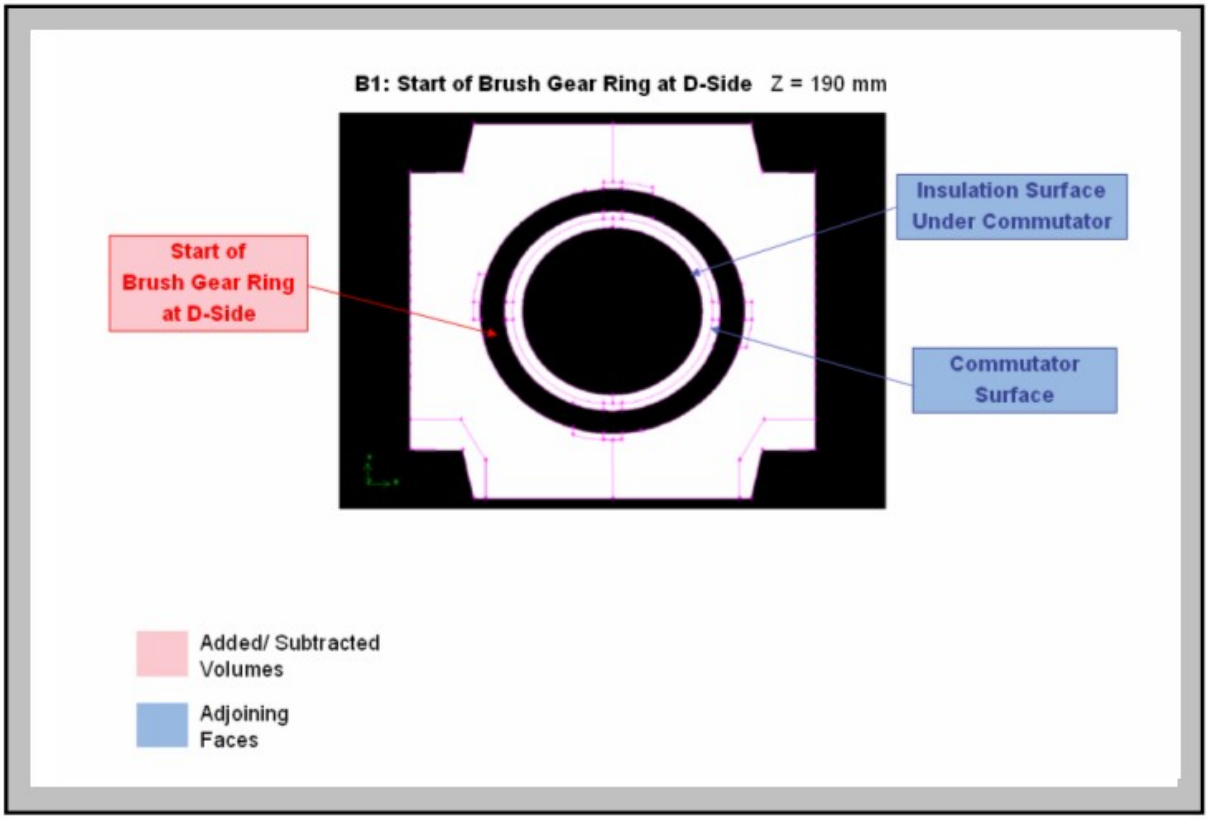

Figure 30: The surfaces with active mesh, in forward direction, at the cross section plane B1 of the modelled DC-Motor

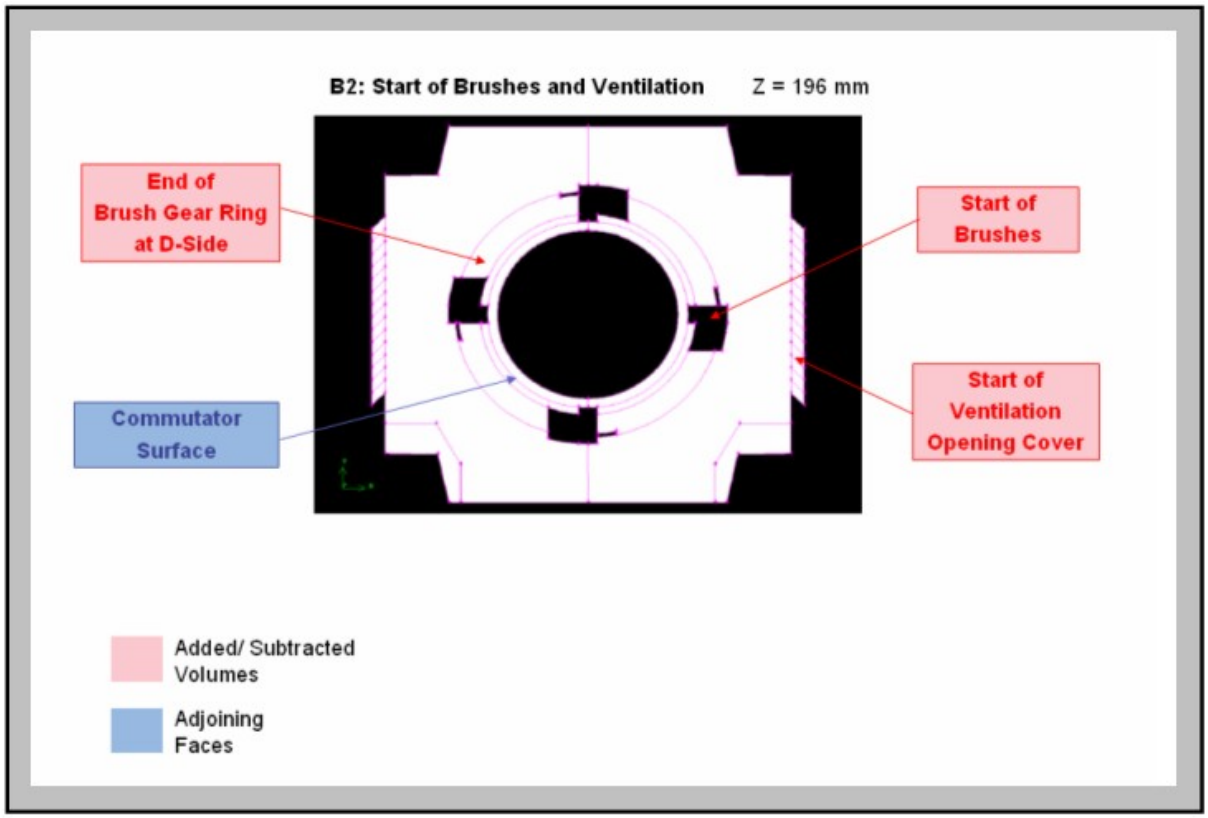

Figure 31: The surfaces with active mesh, in forward direction, at the cross section plane B2 of the modelled DC-Motor

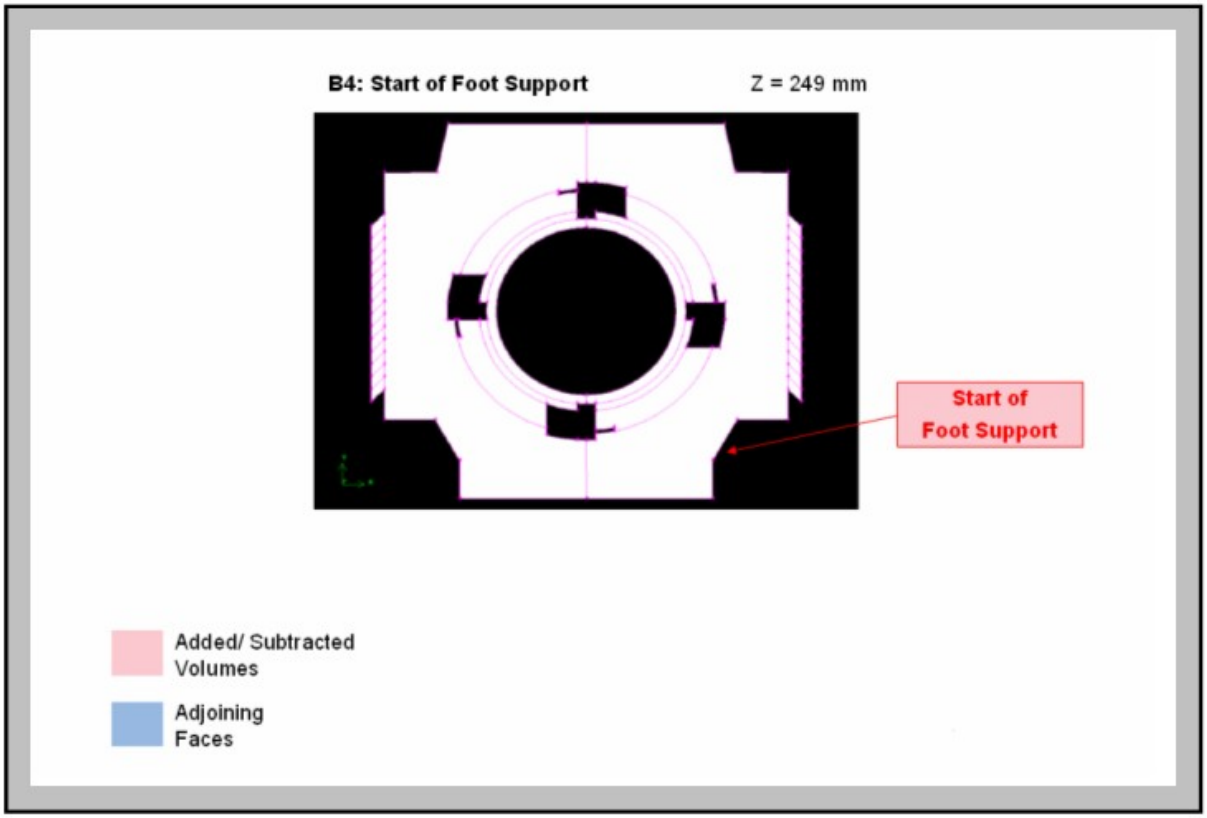

Figure 32: The surfaces with active mesh, in forward direction, at the cross section plane B4 of the modelled DC-Motor

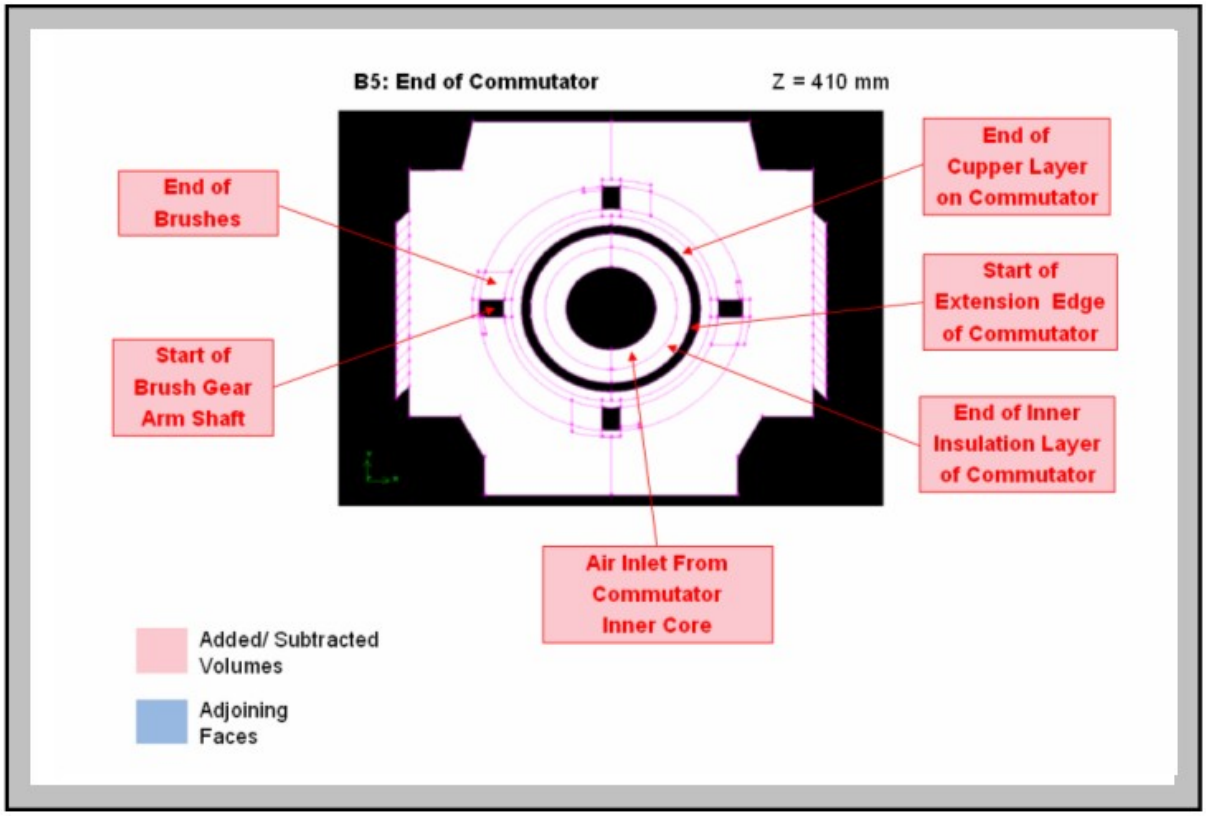

Figure 33: The surfaces with active mesh, in forward direction, at the cross section plane B5 of the modelled DC-Motor

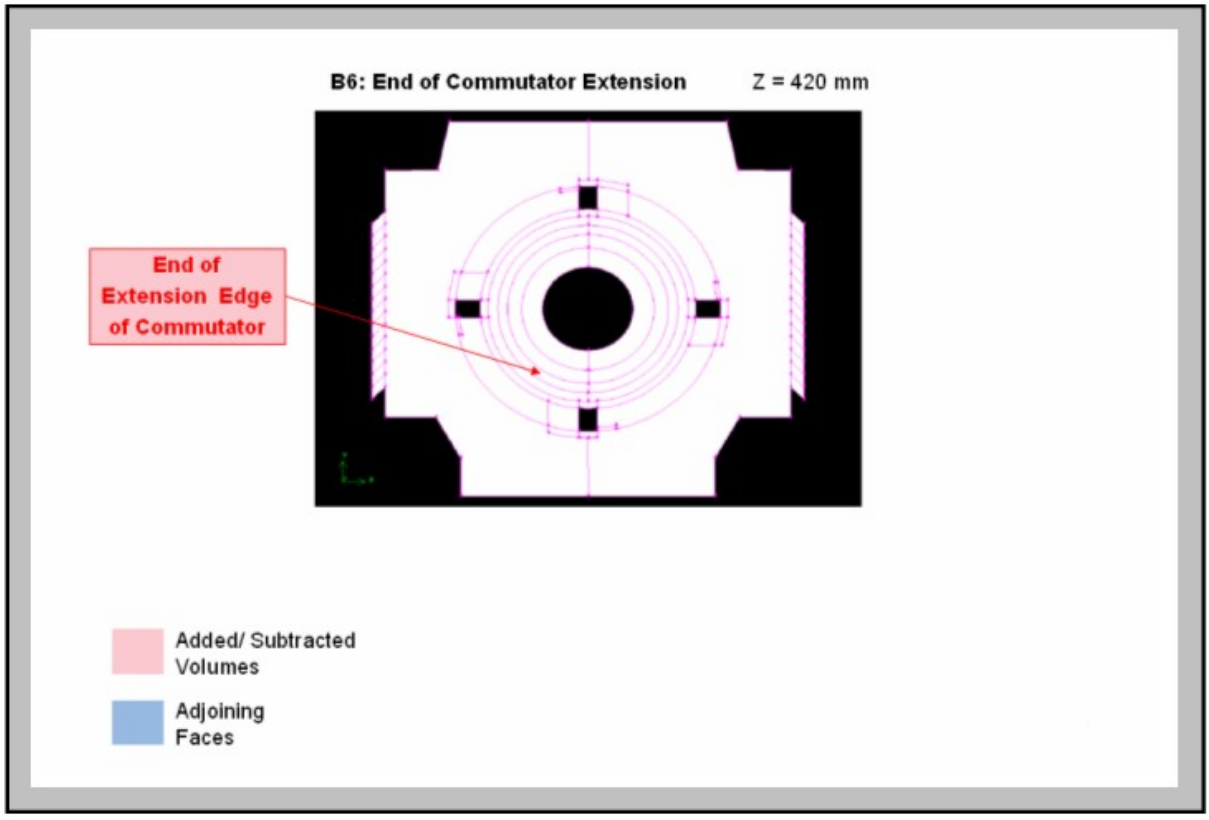

Figure 34: The surfaces with active mesh, in forward direction, at the cross section plane B6 of the modelled DC-Motor

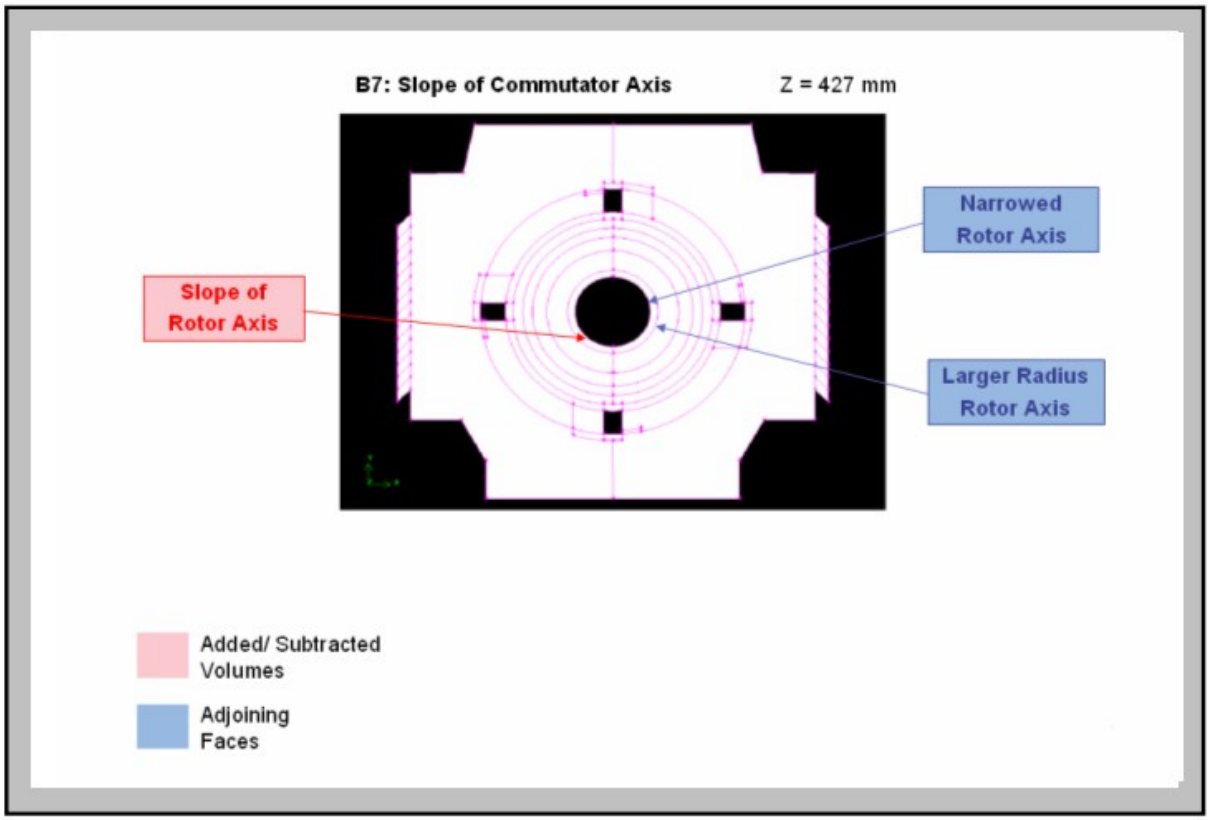

Figure 35: The surfaces with active mesh, in forward direction, at the cross section plane B7 of the modelled DC-Motor

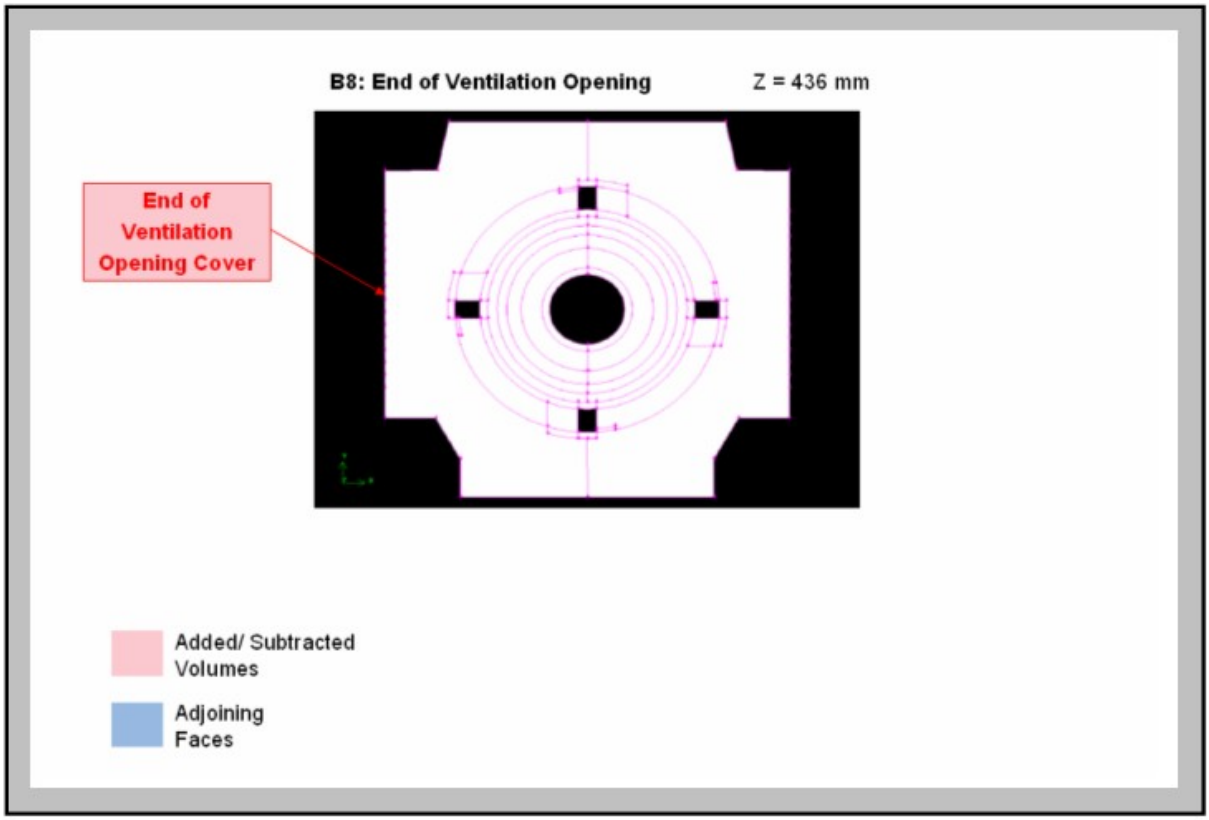

Figure 36: The surfaces with active mesh, in forward direction, at the cross section plane B8 of the modelled DC-Motor

The geometry of section C starts from where the brush gear ring at N-side starts and goes all the way to the Bearing Shield end wall. In Figure 37-41 the faces with active mesh are pictured for the planes C1-C5 in opposite direction. The faces active in plane C1 are the faces on the N-sides outer boundary of the model representing the meshed volumes in the backward direction. In plane C5 the active faces are the once representing the mesh volume in the backward direction (transition section B-C).

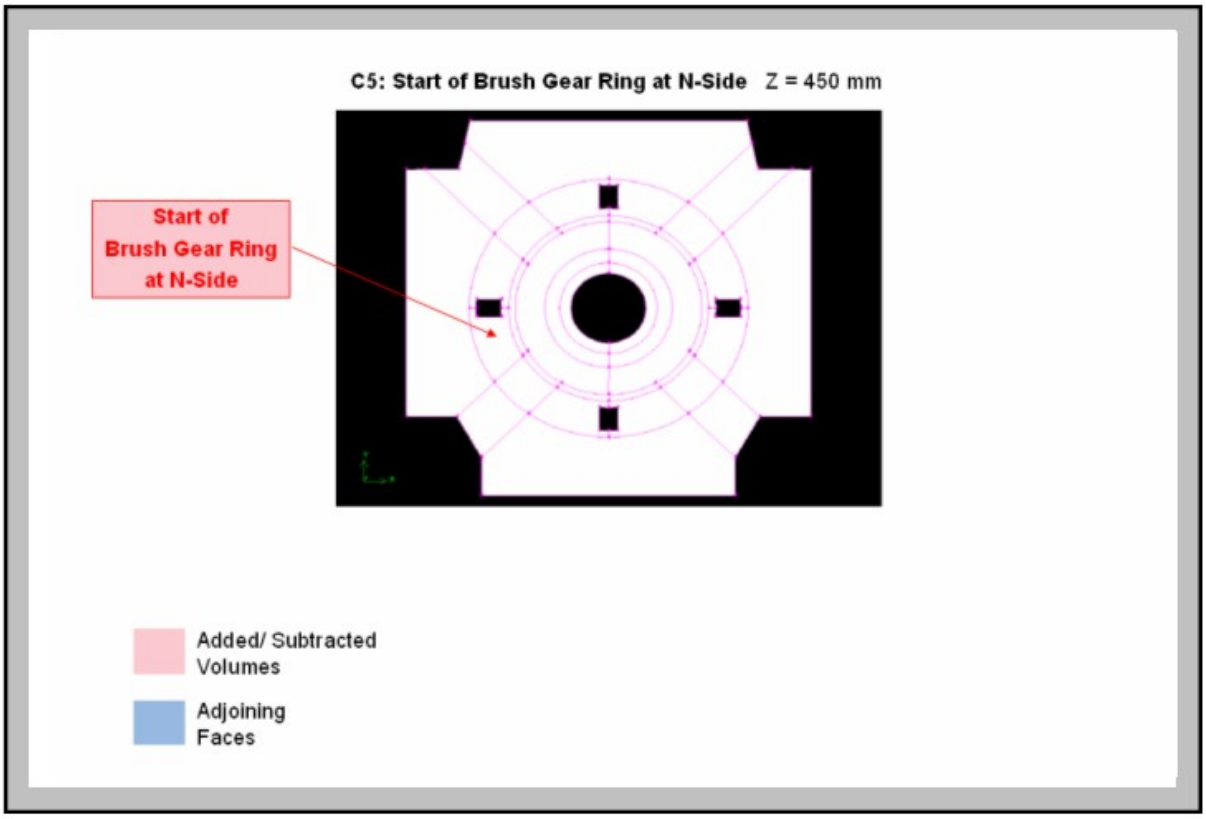

Figure 37: The surfaces with active mesh, in backward direction, at the cross section plane C5 of the modelled DC-Motor

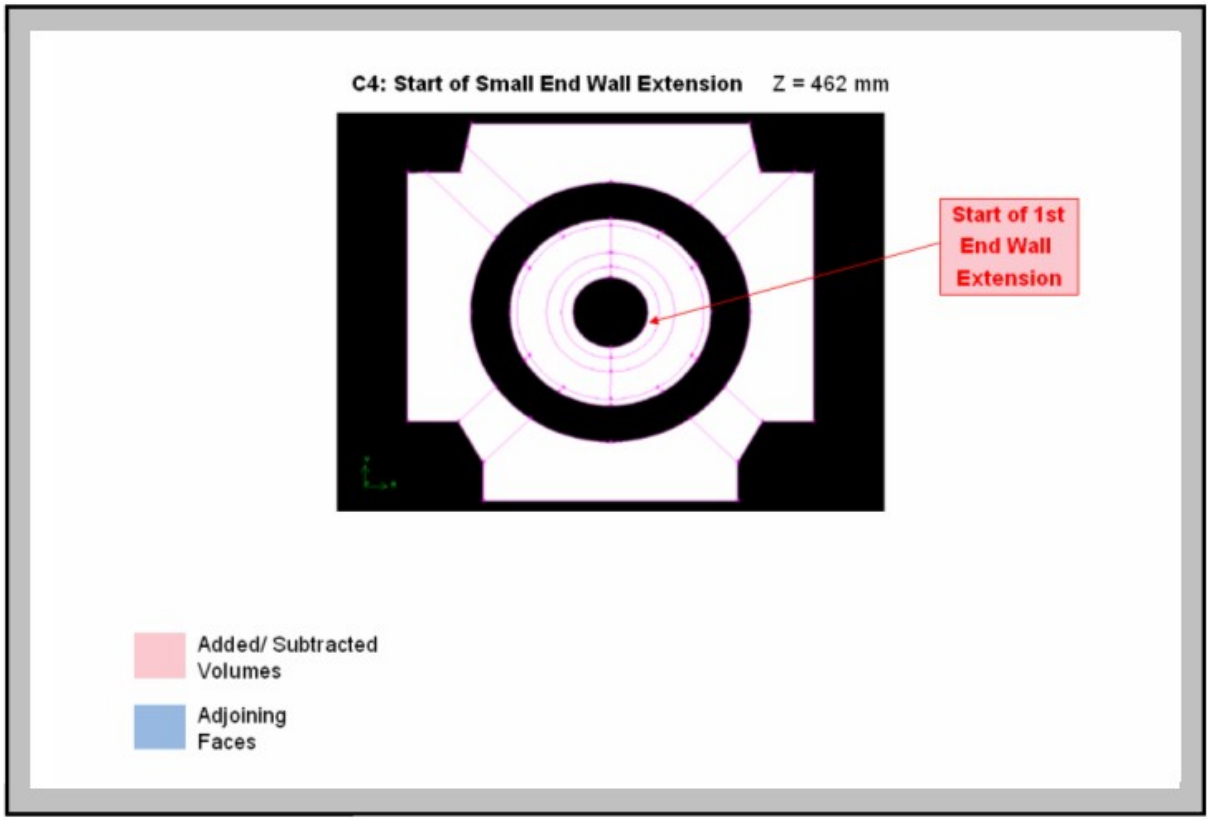

Figure 38: The surfaces with active mesh, in backward direction, at the cross section plane C4 of the modelled DC-Motor

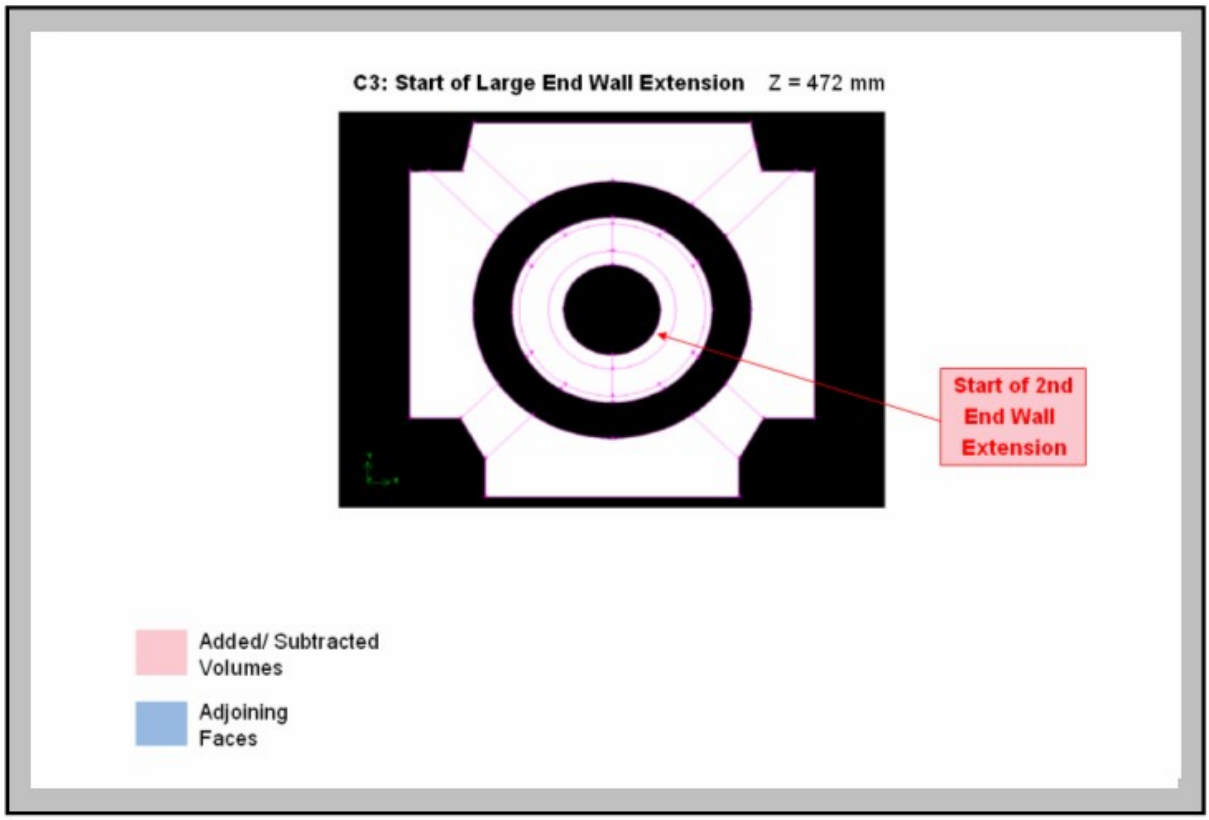

Figure 39: The surfaces with active mesh, in backward direction, at the cross section plane C3 of the modelled DC-Motor

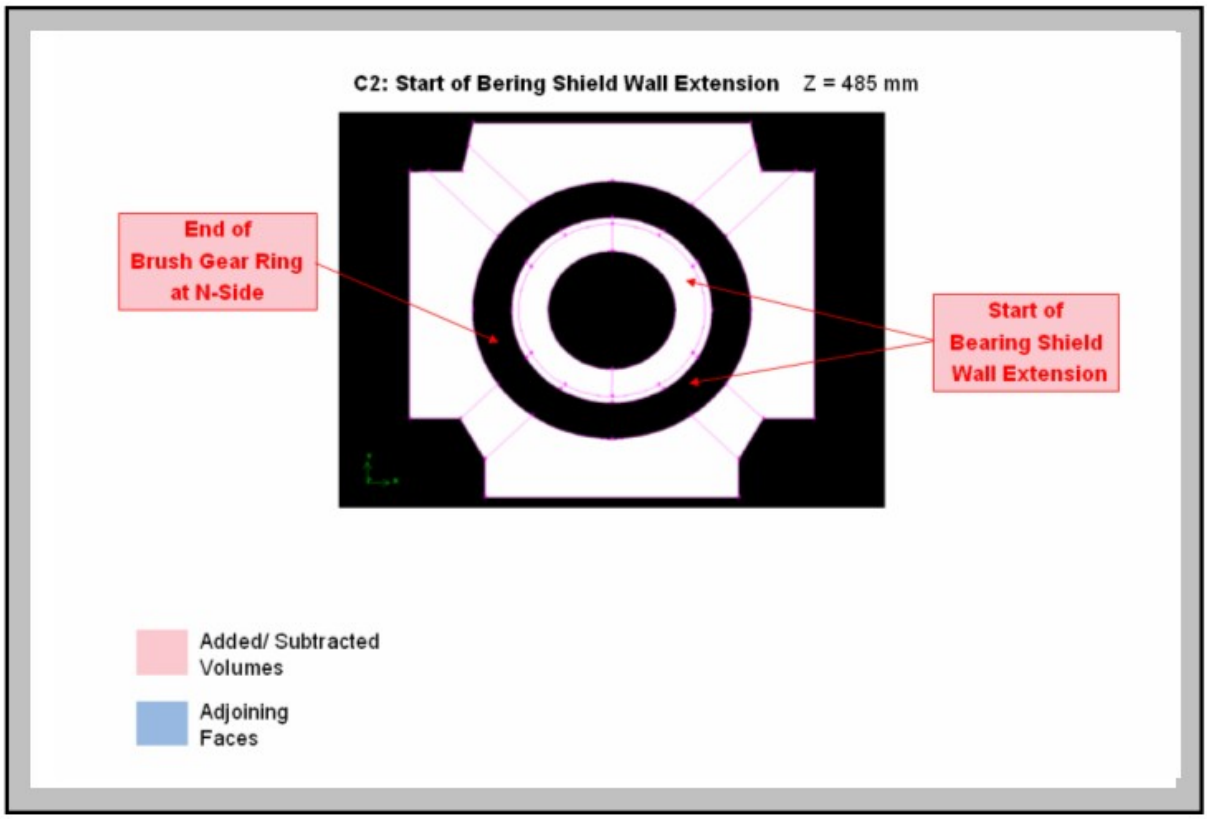

Figure 40: The surfaces with active mesh, in backward direction, at the cross section plane C2 of the modelled DC-Motor

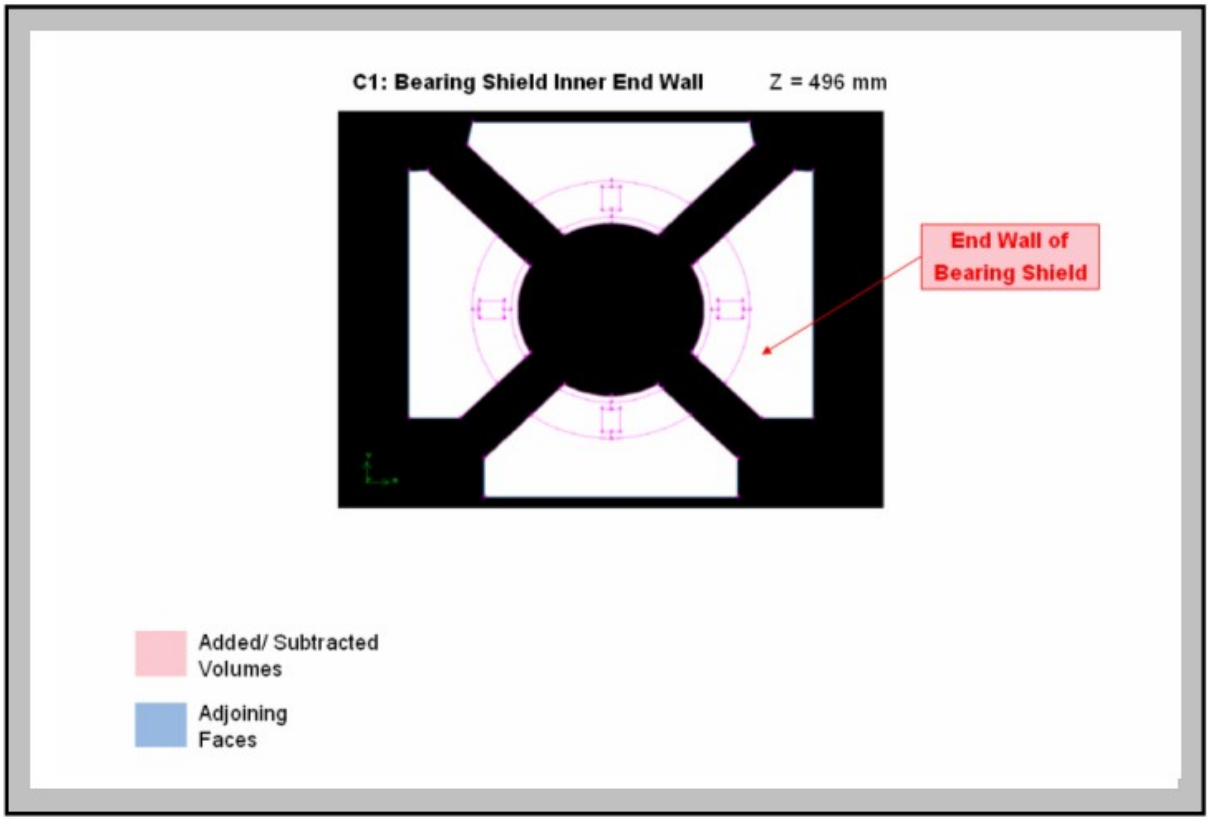

Figure 41: The surfaces with active mesh, in backward direction, at the cross section plane C1 of the modelled DC-Motor

4.1.3.2 The Meshes

When the mesh of the model was created the mesh size was made to be controlled by different scalar parameters. The idea with this was that the mesh size of the model easily would be changeable. One of the scalars, named scalar I, controls the mesh size in the radial direction near the Commutator surface. This is where the thermal boundary layer would occur during the simulation and it is referred to as inner mesh. The other scalar, scalar Y, controls all the other mesh sizes in both radial and axial direction and is referred to as scalar I.

By varying the two scalars five different meshes were generated. The scalar Y was given three different values and depending on the chosen value the generated mesh would have a finer, a normal or a coarse size relatively to the others. For scalar I only two values were given, one for a fine inner mesh and one for a coarse inner mesh. Information about the five different mesh models can be found in Figure 42 bellow. The total amount of cells is about 0.6-1.5 million, depending on the scalars chosen.

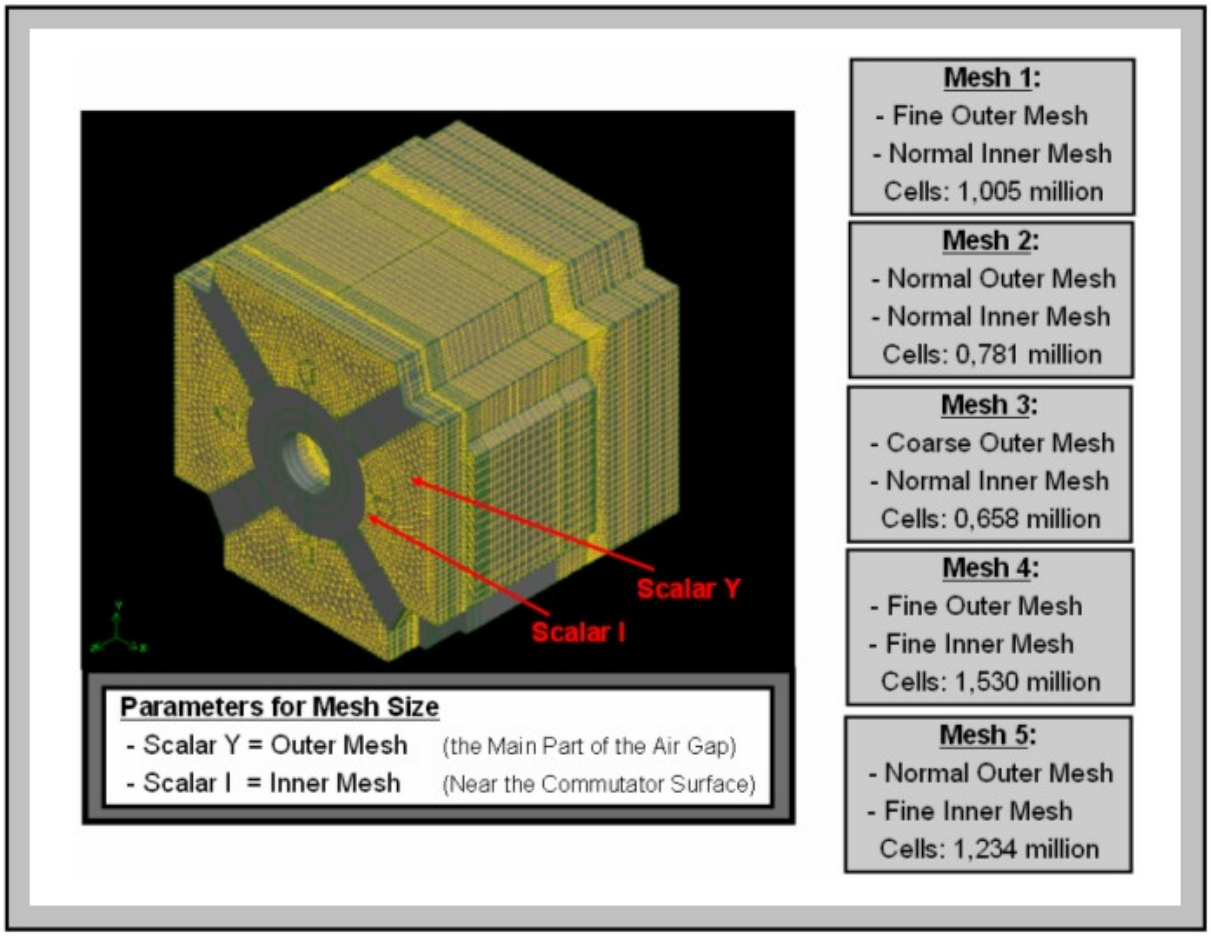

Figure 42: Information about the different mesh sizes used in the simulation of the fluid flow in the DC-motor

The quality of the mesh plays a significant role for the stability and accuracy of the numerical computation. A good mesh consists of cells with high quality. One way to measure the quality of the cells is by their skewness, how much the cells differ from equilateral cells with the same volume. The skewness of the mesh should be as low as possible. At the same time it is important to keep down the number of cells in the mesh to get a shorter simulation time. By using cells that are prism shaped both of the criteria, low skewness and short simulation time, could be accomplished.

The prism shaped mesh cells were used as much as possible in the model. For the three sections were the geometry made from a projection in on a radial plane and then extruded into a volume, the prism shaped cells were easily used. Though in the two transition sections connecting those three main sections, the geometry was less structured in the axial direction and therefore the prism shape could not be used for the mesh cells. In those sections the mesh was made with tetrahedral cells.

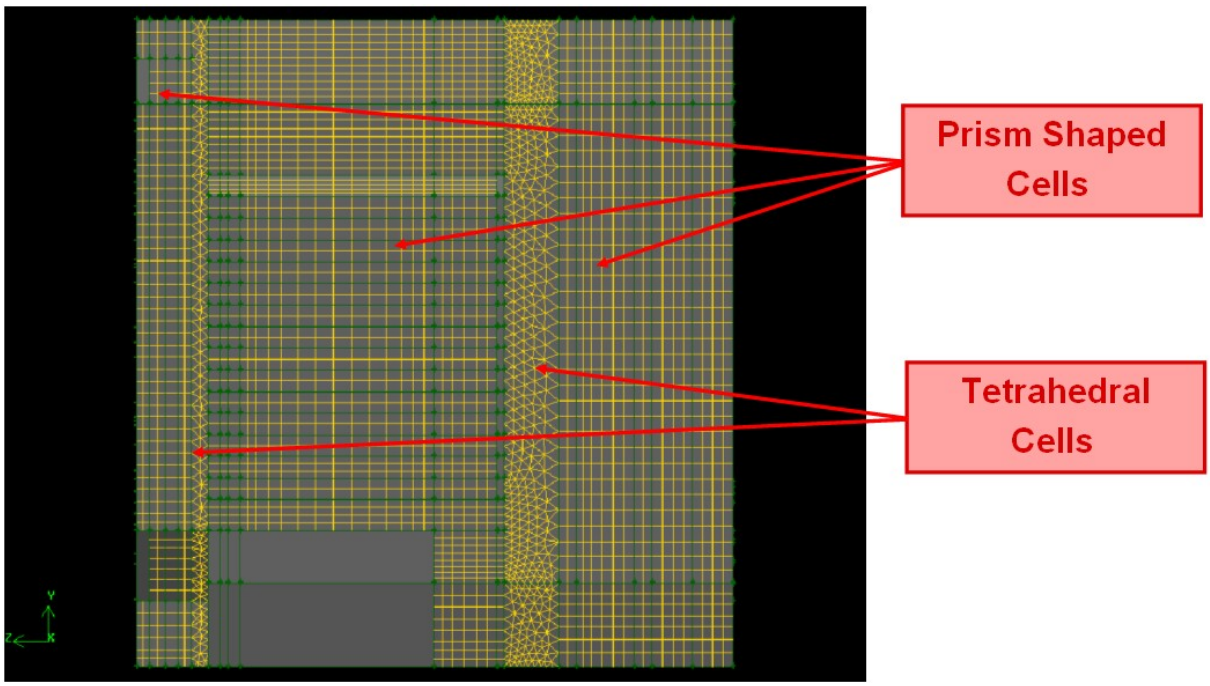

Figure 43: Side view of the mesh of model 2

Most part of the meshed volume in the model is made for the fluid flow occurring in the air gap between the Commutator and the motor casing. Though there is one solid that also has been meshed, namely the copper layer on the Commutator surface, see Figure 44. There is a heat flux from the rotor that is transferred to the Commutator and it is flowing in axial direction through the copper layer of the Commutator. Thanks to the solid mesh this axial effect will be considered as well.

In section A there is an inlet for the air that comes from the air gaps in the stator windings. When meshing section A, see Figure 44, it was important to mesh the faces for the inlet of the air with smaller cells in order to get a more stable simulation. The finer mesh was accomplished by using size functions that controlled the mesh in those areas.

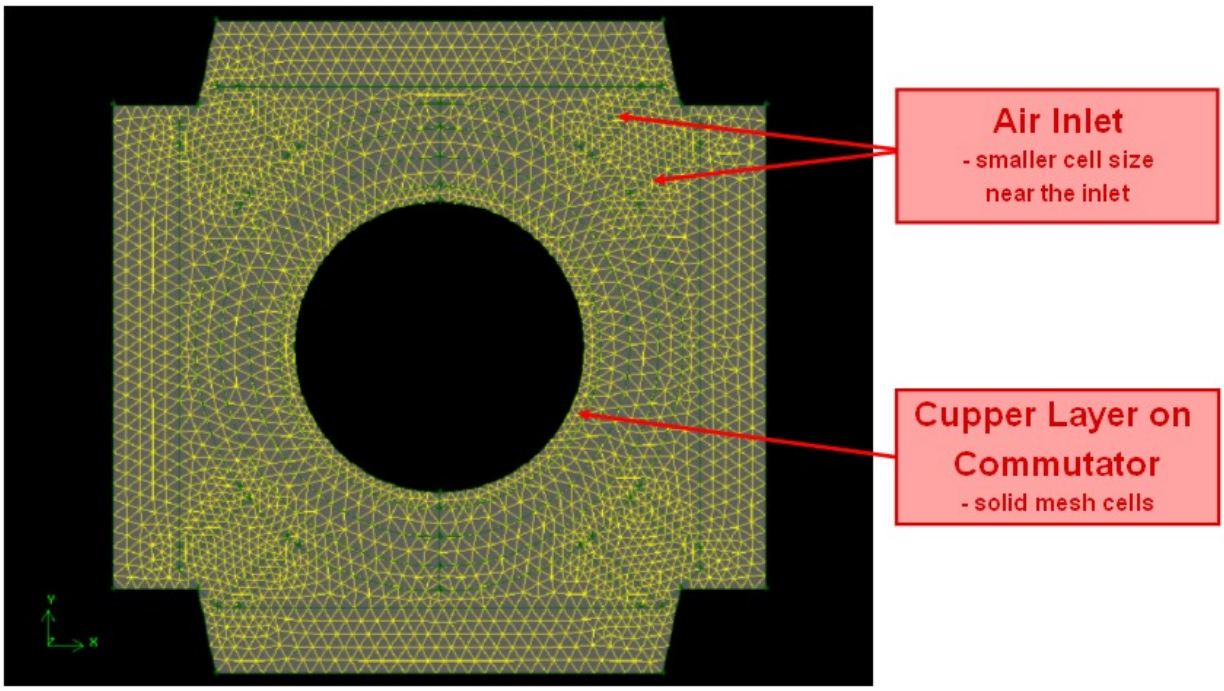

Figure 44: Front view of the mesh of section A in model 2

The section B was made with a relatively fine mesh, especially in the area of the Commutator. Those parts where inactive between most of the planes in section B. They become active first at the axial position where the Commutator ends. Since the inlet air of the rotor is entering in that same axial position and since the actual meshed volume after the Commutator ends is low the mesh was made rather fine without causing an extreme increase of the total cell number. For the same reason as above the mesh of the brush parts can also be made very fine and this is necessary since a lot of things will happened around the brushes that need to be considered.

When it comes to the ventilation opening the mesh was made slightly finer match the requirements of outlet boundary mesh. Perhaps the mesh should have been made even finer in this area; this would be a suggestion for later simulations.

The cells near the outer Commutator surface are very important because they will simulate the heat transfer in the thermal boundary layer between the Commutator and the cooling air that flows above it. In the numerical calculations of the mesh cells near those active boundary surfaces the near wall effect has to be considered since the heat transfer is affected by the boundary layer. It is important to make sure that the boundary layer doesn't contain more than one layer of mesh cells because additional cells in the boundary layer would cause inaccurate heat transfer calculations. Another way to avoid those calculation errors is to enable near wall functions that takes the effects of the boundary layer into consideration automatically. To avoid unnecessary iterative work this near wall function was used.

In both section B and C the cells near the surfaces of the outer wall was made smaller by using a mesh size function. The refining of the cells in outer surfaces of section A was neglected because it was found unnecessary since the stator windings is partly blocking the flow activity in those areas.

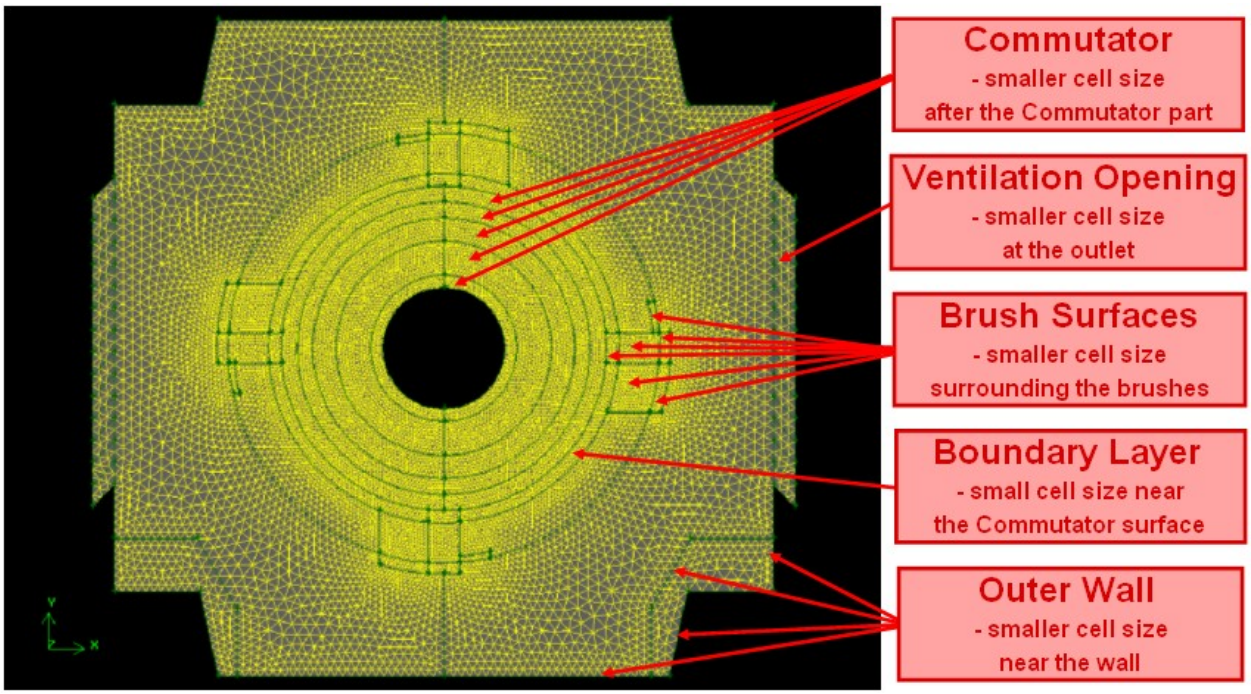

Figure 45: Front view of the mesh of section B in model 2

Some surfaces in section C were made with slightly finer mesh since it was supposed that a lot of flow activities would occur there. Those surfaces are all situated close to the axis along which the inlet air, coming from the Commutator core, is flowing.

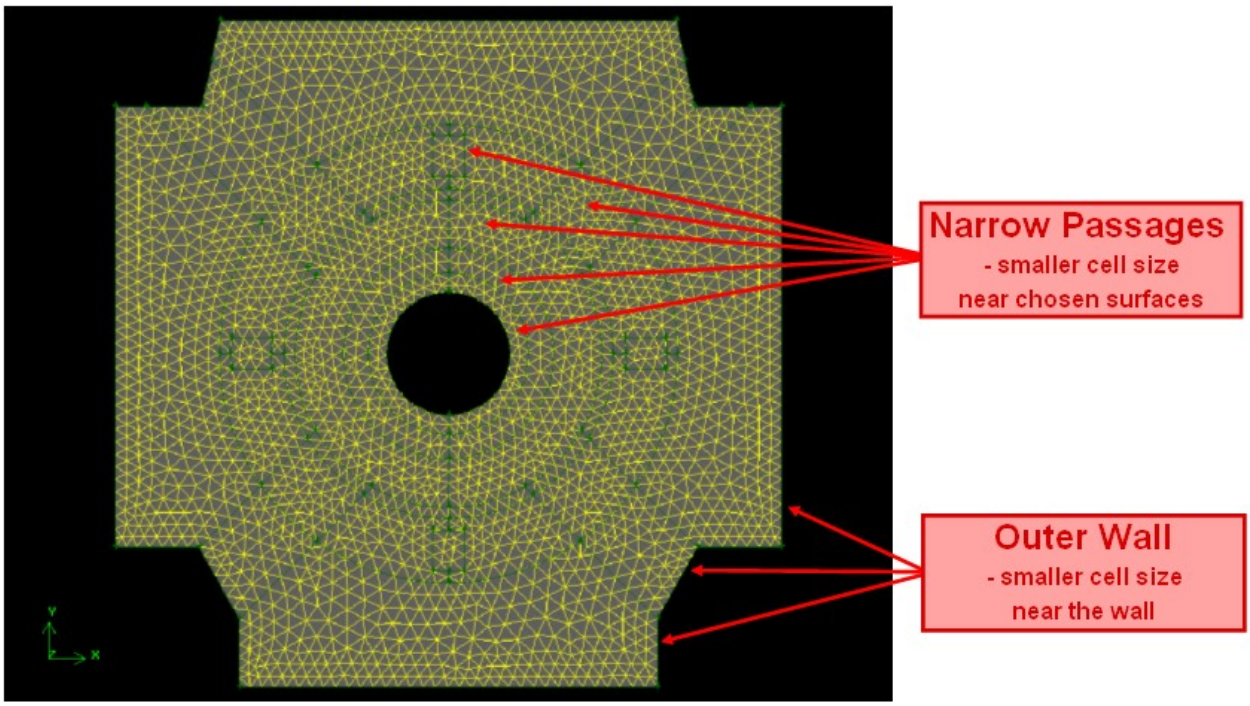

Figure 46: Front view of the mesh of section C in model 2

4.2 Simulations

Each of the mesh models of the DC-motor generated from Gambit was imported to FLUENT. In this chapter the simulation process, from the initial setting of the simulations to the actual simulation and the final results, will be described.

4.2.1 Boundary Conditions and Settings

Since the task for this thesis was delimited to a relative examination of the mesh and the mesh size influence on the result the settings for the simulations were of less importance. All values for the boundaries were roughly set and no strong effort was made to find the exact values. This was a necessary decision to make since the work had to be limited down. The boundary conditions were identical for all the simulations and they are presented in Figure 47.

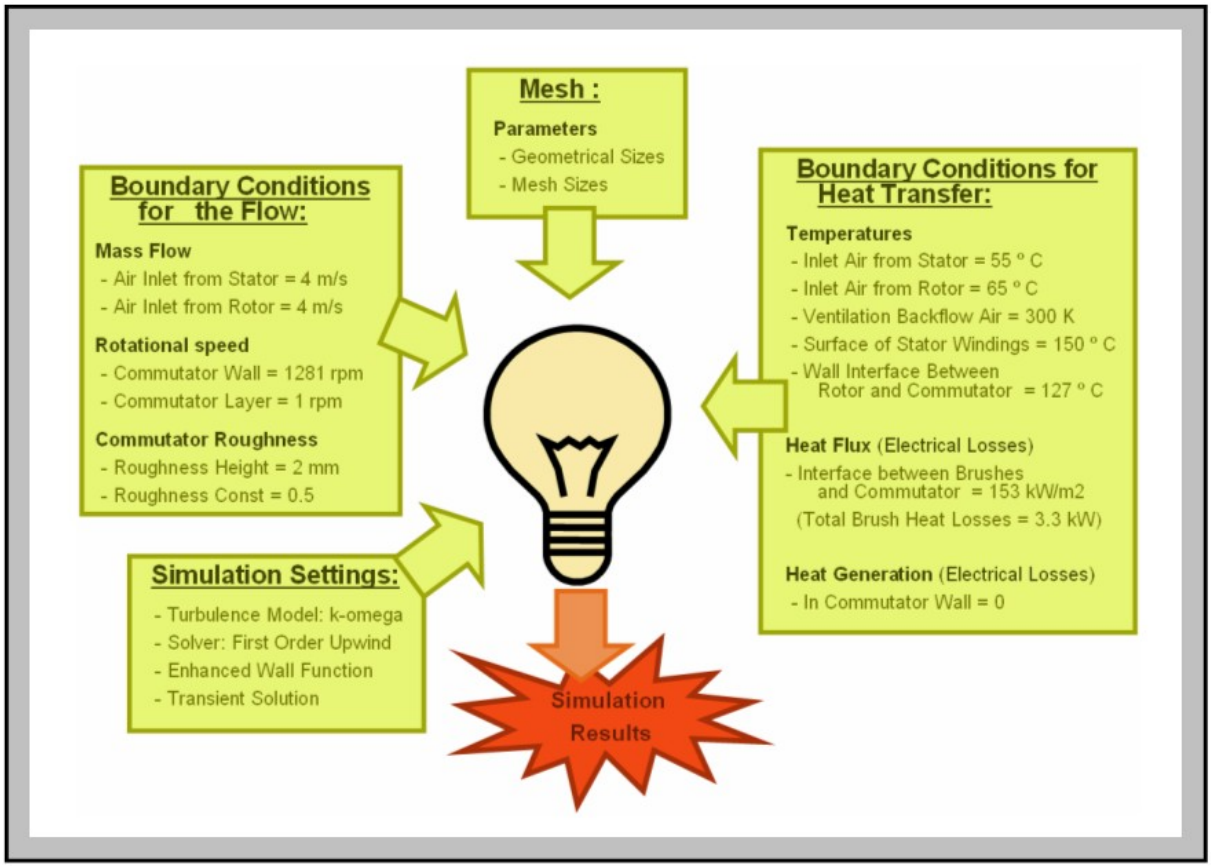

Figure 47: The simulation setup of the model

Temperatures and velocities for the inlet air coming from the rotor and from the stator were set. A temperature was also given for the inflow through the ventilation opening since there is a backflow of air there. Some delimiting surfaces of the model such as the surface of the different stator windings were set to a fixed temperature. This was also done to the solid interface between the rotor and the Commutator where the heat is transferred to the copper layer on the Commutator. One rotational speed was set for the surface of the Commutator that

is corresponding to the rotational case simulated. The solid copper layer under the Commutator surface was initially set to rotate at the same speed, but since it was creating a lot of convergence problems this rotation speed had to be lowered down. We know out of experience that mesh cells rotating with a high speed make the governing equations difficult to converge, since the movement adds an extra difficulty level to the problem. The rotating speed of the solid was set high enough to yield a reasonable axisymmetry of the temperature on the Commutator surface which would in fact have been the case if the volume speed was not corrected. By doing so we are hoping to prevent the speed correction to interfere with the results. Perhaps in the future we will increase it with a factor of 10 to create a larger safety margin.

All the electrical losses in the Commutator and the brushes are given as heat flux entering the model from the surface interfaces between the brushes and the Commutator and continue in to the copper layer of the Commutator. All other boundary surfaces in the model, except for the above mentioned with fixed temperature, are adiabatic. Some of the adiabatic surfaces are the motor casing walls, the insulated rotor surface, the interface between the copper layer and the insulation layer, the gear brush and the brushes. There is no heat generation anywhere in the model, since all heat is entering through fixed surface temperatures and heat fluxes at the active surfaces.

There are tracks carved onto the surface of the Commutator that are going from side to side in axial direction. Those tracks have an influence on the flow and the heat transfer from the surface and should be considered in the simulation. But since the depths of the tracks are so small it is not possible to include them in the geometry. If doing so there would either be a problem with the mesh discretisation or else the mesh size in that area would need to be very small, which on the other hand would result in an unacceptably long simulation time. An alternative to modelling the tracks was to create a smooth surface and instead use some constants in FLUENT to define the roughness of the surface, and through this way consider the roughness effect on simulation. The two constants used for that in FLUENT are stated as roughness height and roughness constants and they refer to a surface with evenly distributed pin fins. Unfortunately, since the Commutator surface is more similar to straight rectangular fins than pin fins, there would be a certain error in the simulation results which needs to be corrected. Probably the pin fins would give a higher heat transfer from the surface than the rectangular fins, since the total cooling surface would be larger than. Though for the time being this error was neglected and the two constants were given an approximate value, because the work had to be limited down.

The turbulence model used for the simulation is the k-omega model, because it is mostly convenient to use in this case. In the k-omega model you can use a function that prevents you from doing a separate computation in the mesh cells near the wall and at the same time it is possible to enable the function for wall roughness on the same surfaces. This is not possible for the k-epsilon model, where you only can enable one of those functions at a time. Reynold's stress model was also excluded even though it is the theoretically most accurate turbulence model, since it would give an unrealistically large processing time and cause converging problems according to earlier experiences with similar simulations. It was necessary to use a near wall function to make the mesh model less sensitive to the near to wall effects. The fluid flow is acting differently within the boundary layer near a surface from when it is flowing freely because of the shear stresses it is submitted to. Without this near wall function the y+ value of the mesh near the solid surface would have had to be examined manually, to make sure that the boundary layer is not containing more than one layer of mesh

cells. In places where this condition is not fulfilled it would have been necessary to adjust the size of the mesh cells to get a prober y+ value. This iterative procedure is a very tedious and difficult and was avoided through the use of the near wall function.

For the numerical computation a pressure based solver was used with the 1st order implicit method. A steady state solution was preferred, but since we couldn't get a converged steady state solution transient solutions had to be found.

4.2.2 Sensitivity Analysis

The influence of the mesh size for the model was studied in a sensitivity analysis. For this purpose five different mesh models were generated, all with different mesh sizes. The mesh models have different combination of mesh sizes in the outer main region of the model as well as in the boundary layer directly above the Commutator surface, further described in chapter 4.1.3.2. Those five meshes were simulated with the same case setup to find out if the simulation results would differ between them. Based on this analysis a mesh size should then be chosen as the standard mesh for the model.

For the final result the heat transfer, the fluid flow and the turbulence of the flow was needed to be considered by solving the following equations: the energy balance equation, the continuity equation, the momentum equation in 3 directions and the two turbulence equations in the k-omega model. In the first test simulation all those equations were activated to search for a steady state solution, which would have been the most convenient way. Unfortunately the equations in this simulation could not converge, more specifically the continuity equation. The reason for that was that the flow was oscillating and no steady state solution could be made. Therefore the simulation would have to be set as transient. A transient solution is usually more accurate but it takes more time to get a result since the time variation also has to be taken into consideration. A time span of one second was assumed to be sufficient enough to include the whole oscillation process, and throughout this simulated second the simulation file was saved into a separate file at regular intervals. Another problem encountered during the simulation process was that the actual simulation was too time consuming when all the equations where activated at the same time. This occurred because of the fact that the heat equation needs long time to stabilise and can be simulated with large time steps, while the fluid motion is stabilising quicker but needs small time steps. When simulating the fluid motion and the heat transfer at the same time a long simulation time with small time steps would have been required. To get around this problem the heat equation was firstly deactivated and set to be solved in a later stage of the simulation process.

The simulation process for the sensitivity analysis will be described in detail bellow, according to the schedule in Figure 48.

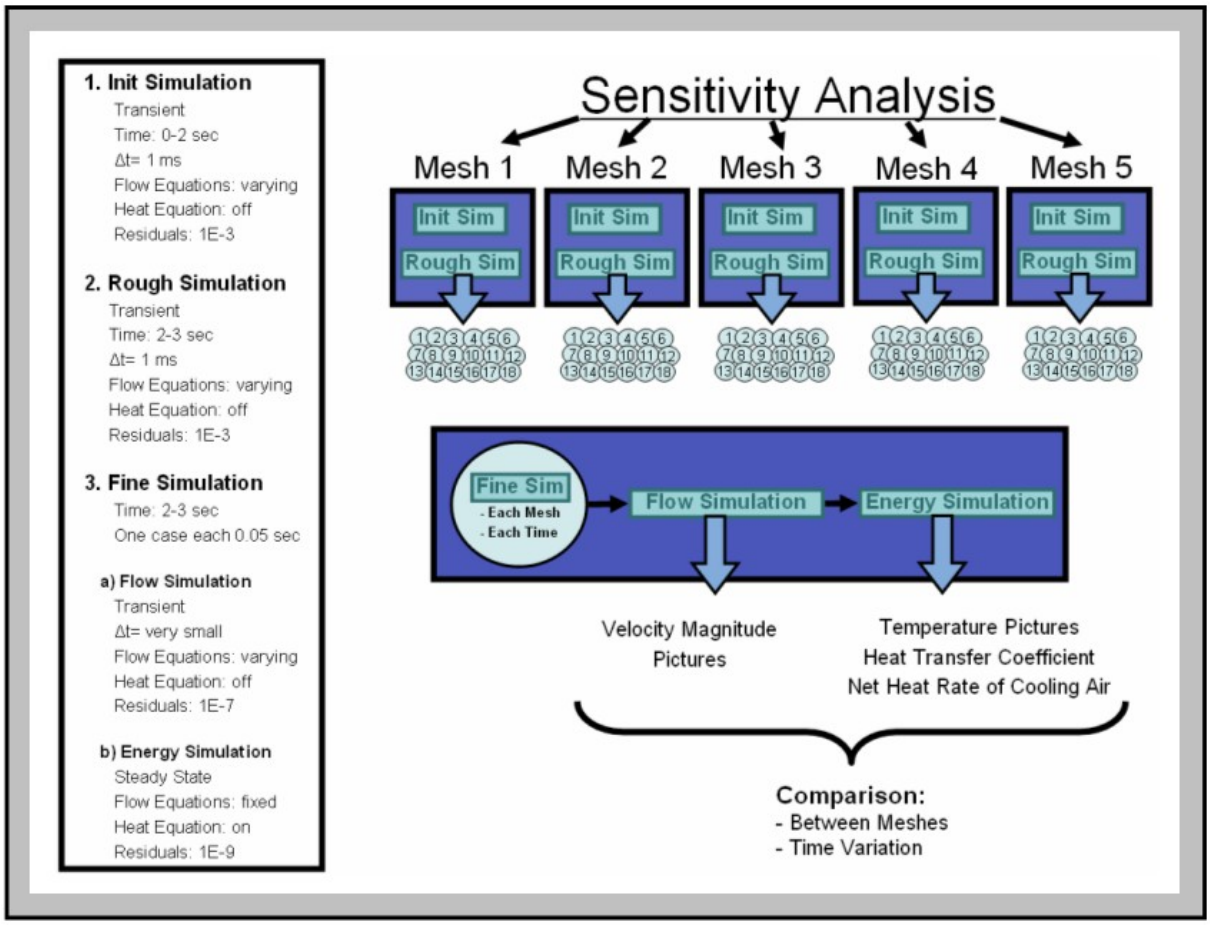

Figure 48: The simulation process during the sensitivity analysis of the mesh size effect

1. Firstly an initial simulation was made for all the mesh cases. The time span for this simulation was set to 2 seconds which was assumed to be long enough for the flow to stabilize. Further the time steps where around one millisecond and the residuals of all the equations were set to 1E-3. During this simulation the heat equation was deactivated.

2. In the rough simulation the simulation was set to run one more second with the same conditions as in the initial simulation. During this second the simulation file was saved into a separate file each 0.05 second and finally 18 different simulation files had been generated for each mesh model. Along with the file generation there were also a lot of pictures saved, showing the velocity magnitude of the air flow. In total there where about 150 pictures for each mesh model, taken at different times during the simulated second, and they were later put together to form a movie.

3a. In the fine flow simulation each of the generated files, totally 5*18 cases, had to be simulated separately. The original solutions were refined through increasing the residuals to 1E-7 for all the governing equations. A transient flow was still simulated but only one time step was taken and this time step was made as small as possible, with the heat equation still inactivated. This was made to insure that the flow field is conservative and therefore free of heat sources and sinks inside the volume.

3b. The simulation files from the fine flow simulation was further adjusted in a final simulation stage, the fine energy simulation. All the governing equations for the flow were

fixated at their present values, while the heat equation was activated and thereby became the only equation to be solved. Since the flow was fixated a steady state solution could be found.

From the created files of the fine simulation all the simulation results were extracted. Pictures showing the velocity magnitude and the temperature of the fluid were taken at all time steps, for all mesh models. Further the heat transfer coefficient at the Commutator surface, given as the area weighted average, was collected from all the files. The heat transfer coefficient in a discrete surface node is defined between the temperature on the surface node and a free stream temperature above its boundary layer. Also the overall heat transfer rate to the flow from the boundary, here referred to as the net heat rate, was collected. Those two simulation data would give us the means to measure the heat transfer in the model. All the pictures and the simulation data from the different mesh models were then compared to each other between the meshes. From this comparison it was possible to see how much the simulation result differs depending on the mesh size. Generally speaking, if the difference of the mesh size is found to be negligible a coarser mesh would be preferred since it requires less simulation time.

The time dependence of the simulation results was finally examined. This was done by comparing the variation of the net heat rate and the heat transfer coefficient within each mesh. A visual examination of the flow pattern was also done based on the velocity movies made from the extracted pictures at the rough simulation.

4.2.3 Simulation Results

The sensitivity analysis in the chapter above gave us the means to analyze what influence the mesh size has on the simulation results. In this chapter the results from the mesh models with different mesh sizes will be gathered together and compared. Later this will be useful when a decision has to be made about which mesh size that would be most suitable for future use of the general model. The difference in mesh between the generated mesh models is the size of mesh near the Commutator surface here referred to as inner mesh, and the mesh size in the rest of the model referred to as the outer mesh. By varying those two factors five different mesh models were generated. During the simulations of those models one simulation was interrupted, namely mesh model nr1, because the simulation was found to be too slow to be of any further use. The simulations of the other mesh models were all completed after running during a certain simulation time.

A rough presentation of the simulation results will be done here bellow and the comparison of the different mesh models will be summarised. The compared data can also be seen in Table 1. Later in the following chapters 4.2.3.1 and 4.2.3.2 the results and the method for calculating them will be described more in detail.

Table 1: Comparison of simulation results when using different sizes of mesh.

	Mesh 1* Fine Outer Mesh Normal Inner Mesh	Mesh 2 Normal Outer Mesh Normal Inner Mesh	Mesh 3 Coarse Outer Mesh Normal Inner Mesh	Mesh 4 Fine Outer Mesh Fine Inner Mesh	Mesh 5 Normal Outer Mesh Fine Inner Mesh
Number of Mesh Cells	1.005 million	0.781 million	0.658 million	1.530 million	1.234 million
Simulation Time for 1 Sec	-	12 h	10 h	2 days 15 h	1 day 21 h
Heat Transfer Coef. Av. Deviation from Mesh 2	-	-	0.0 %	1.4 %	1.2 %
Net Heat Rate Av. Deviation from Mesh 2	-	-	1.0 %	2.6 %	3.2 %
Heat Transfer Coef. Max Fluctuation Within 1 sec	-	0.18 %	0.04 %	0.13 %	0.27 %
Net Heat Rate Max Fluctuation Within 1 sec	-	0.93 %	1.61 %	0.80 %	3.49 %

Mesh Var.

Time Var.

* Simulation of Mesh nr1 was stopped because it was running too slow

The first thing compared between the mesh models was the total amount of mesh cells. Mesh nr 4 has the largest amount of cells, namely 1.5 million, which is rather obvious since it both has a fine inner and outer mesh. Next to come is mesh nr 5 with 1.2 million cells, as a result of having a normal outer mesh and a fine inner mesh. This is also corresponding to the simulation time, where mesh nr 4 needed the longest time closely followed by mesh nr 5. Mesh nr 2 and 3 have less mesh cells, under 1 million, and therefore a simulation time of just 10-12 hours each was enough. The mesh models are differentiated by their different sizes of the inner mesh, which is the mesh near the Commutator surface, and the outer mesh which refers to the whole mesh when the inner mesh is excluded. The inner mesh has two sizes, one called normal and one fine. As for the outer mesh it has three different sizes: the fine mesh, the normal mesh and the coarse mesh. All those sizes have a direct effect on the total number of mesh cells in the model. The y+ for the different models is found to be around 50-150, which is within the accepted interval for the use of the near wall function in the k-omega turbulence model [6]. The value of the y+ above the Commutator surface is plotted for mesh model 2 and 3, which can be found in figure 80 and 81 at the appendix. A common value of y+ lies around 70-80.

The heat transfer mainly focused on in this analysis occurs between the Commutator surface and the cooling air. By comparing the corresponding heat transfer coefficient from the different models it would be possible to see how sensitive the heat transfer through the boundary layer is to the mesh size in this area. A relative comparison was made between mesh nr 2, with normal inner and outer mesh size, and the other meshes. The deviation of the heat transfer coefficient was within 1% from mesh nr2. In a similar way the increase of heat in the cooling air, here referred to as the net heat rate, was compared. By comparing the net heat rate the influence of the mesh size for the whole model could be studied. Also here the deviation was found to be low compared to mesh nr 2, only 3% at most. From the study of the net heat rate and the heat transfer coefficient it was concluded that the choice of mesh size, within the examined interval, was of less importance since the deviation between the simulation data was low. Another way to compare the simulation results from the different mesh models is through a visual comparison which is done in chapter 4.2.3.2.

The other phenomenon that was examined was the fluctuation of the simulation results with time and how big influence the mesh size would have on it. This would tell us how sensitive the mesh is to the transient effects. When looking at the average heat transfer coefficient it is found that the time has negligible influence on the result since the time fluctuation for all the meshes is less than 0.5%. The time dependence is also low according to the fluctuation of net heat rate in the cooling air, especially for mesh nr 2 and 4 that has a fluctuation lower than 1 % of its middle value. For mesh nr 3 and 5 the fluctuation is slightly higher but still within an acceptable range. The time effects can also be visually examined through the simulation movies, which have been put together from the collected pictures taken at different simulation time. Those movies are further described in chapter 4.2.3.2.

4.2.3.1 Figures

Two heat transfer qualities were used for measuring the simulation differences between the mesh models, namely the heat transfer coefficient at the Commutator surface and the net heat rate of the cooling air. In this chapter the values of those qualities will be presented and compared for different mesh sizes and time steps. The average heat transfer coefficient is calculated in FLUENT through an area-weighted integral at the whole Commutator surface. This coefficient was monitored through the whole simulation of one operating second, by saving its value after each time step of 0.05 seconds. In the same way the value of the net heat rate for the cooling air was monitored as well. The net heat rate was also calculated in FLUENT from the difference of heat content in the inlet and the outlet cooling air. The measured values of heat transfer coefficient and the net heat rate are presented in Figure 49 and Figure 50 bellow.

When examining the heat transfer coefficient the most outstanding notation is that the values for mesh 2 and mesh 3, as well as for mesh 4 and mesh 5, are going together through the whole simulated time. After a closer look it is also noted that the mesh near the Commutator surface, here called the inner mesh, has the same size within those pairs. In mesh model nr 2 and 3 the inner mesh size is normal and in mesh model nr 4 and 5 the mesh size is fine. The above mentioned similarity could therefore be explained as a consequence of the strong influence the conditions in the boundary layer has on the heat transfer. This proves that the heat transfer from the Commutator surface is sensitive to the mesh size in that area. Though when looking at the percental deviation of the heat transfer coefficient between the different meshes, see Table 2, the difference is small enough to be neglected.

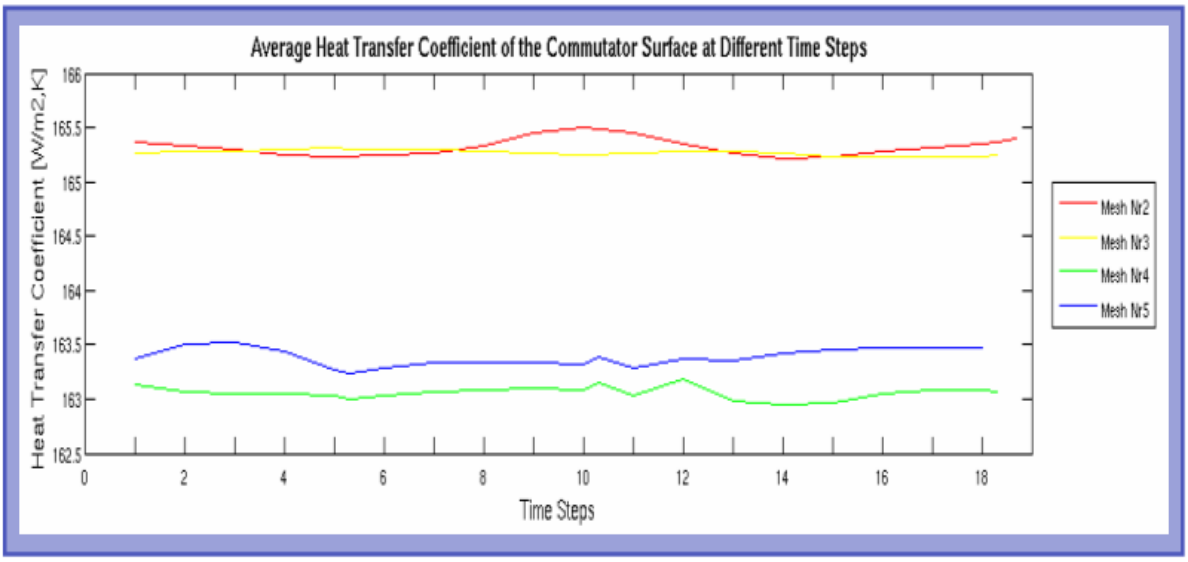

Figure 49: The time fluctuation of the heat transfer coefficient [W/m2,K] at the Commutator surface, where each time step is 0.05 seconds and the total time span is 1 second. It should be noted that mesh nr 2 and 3 has a normal inner mesh, while mesh nr 4 and 5 has a fine inner mesh.

In Table 2 the deviation of the heat transfer coefficient is presented using mesh nr 2 as a reference. The percental deviation of the heat transfer coefficient in mesh 3-5 is calculated from the actual difference in value between the examined mesh and mesh 2, divided by heat transfer coefficient in mesh 2. This comparison is done separately for each time step. The maximum percental deviation from mesh 2 is thereafter shown in a separate column and finally the calculated average deviation is given.

Table 2: The deviation of the heat transfer coefficient [W/m2,K] at discrete time steps compared to mesh nr 2, with 0.05 seconds between each time step

Time Step	1	2	3	4	5	6	7	8	9	10	11	12	13	14	15	16	17	18	Max	Ave-rage
Deviation in % of Mesh nr3	0.1	0.0	0.0	0.0	0.0	0.0	0.0	0.0	0.1	0.2	0.1	0.0	0.0	0.0	0.0	0.0	0.1	0.1	**0.2**	**0.0**
Deviation in % of Mesh nr4	1.3	1.4	1.4	1.3	1.3	1.3	1.3	1.4	1.4	1.5	1.5	1.3	1.4	1.4	1.4	1.3	1.4	1.4	**1.5**	**1.4**
Deviation in % of Mesh nr5	1.2	1.1	1.1	1.1	1.2	1.2	1.2	1.2	1.3	1.3	1.3	1.2	1.1	1.1	1.1	1.1	1.1	1.1	**1.3**	**1.2**

In Figure 50 the net heat rate of the cooling air is shown, monitored over one second of simulation. A diverging behaviour can be seen at the first four time steps of mesh nr 5. The reason for this is probably that air flow was not stabilized yet from the initialization. A similar tendency can be seen at the first five time steps in mesh 3. The only similarity between mesh 3 and mesh 5 compared to the two other meshes is that they both have a higher degree of the mesh size in the inner mesh than the outer mesh. Mesh nr 3 has a normal inner mesh but a coarse outer mesh, while mesh nr 5 has a fine inner mesh but a normal outer mesh. A possible explanation for this delay in stabilisation could be of numerical reasons. The big size differences between nearby placed cells of the inner mesh and the outer mesh can cause increased numerical instability and thereby extend the initiation time for reaching stability.

Another thing noted is that the net heat rate in mesh 2 and mesh 3 are, as well as in mesh 4 and mesh 5, are closely connected to each other in pairs in a similar way as for the heat transfer coefficient previously discussed. Some kind of connection can therefore be assumed between the heat transfer coefficient and net heat rate within each model. This is very likely also seen from a theoretical aspect since the heat transfer from the Commutator surface has a direct effect on the heat increase of the cooling air flowing above it.

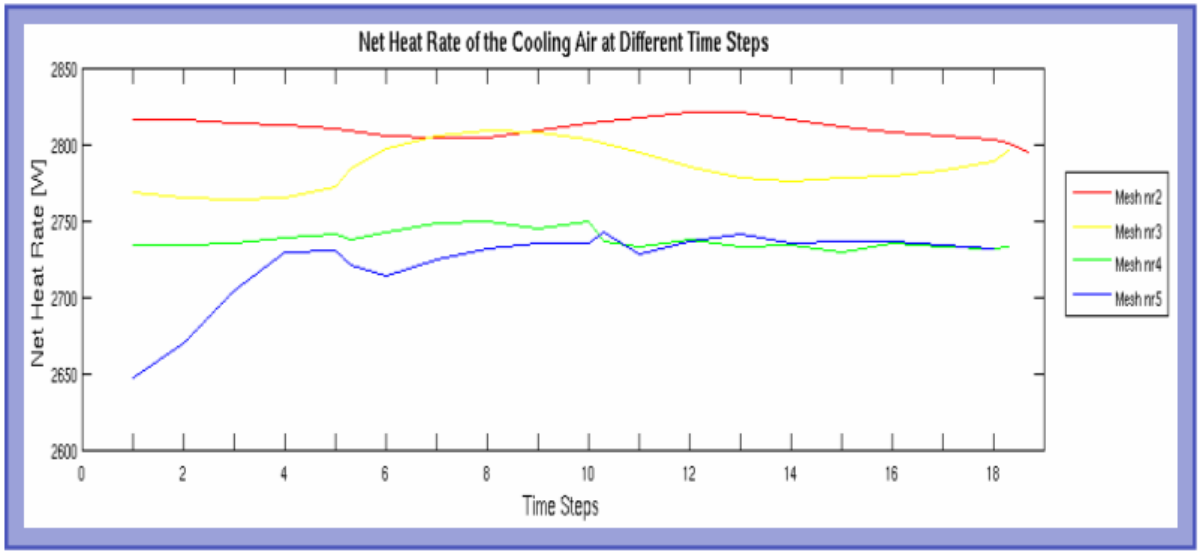

Figure 50: The time fluctuation of the net heat rate [W] for the cooling air, where each time step is 0.05 seconds and the total time span is 1 second

In Table 3 the deviation of net heat rate is presented using mesh nr 2 as a reference. Similarly done as in Table 2 the percental deviation of the net heat rate in mesh 3-5 is calculated from the actual difference in value between the examined mesh and mesh 2, divided by the net heat rate in mesh 2. This comparison is done separately for each time step. The maximum percental deviation from mesh 2 is thereafter shown in a separate column and finally the calculated average deviation is given.

Table 3: The deviation of the net heat rate [W] at discrete time steps compared to mesh nr2, with 0.05 seconds between each time step. Note that the data from the two first time steps of mesh 5 is extensively higher than in the following time steps and could be regarded as initiate instability.

Time Step	1	2	3	4	5	6	7	8	9	10	11	12	13	14	15	16	17	18	Max	Ave-rage
Deviation in % of Mesh nr3	1.7	1.8	1.8	1.7	1.3	0.3	0.0	0.2	0.1	0.4	0.8	1.3	1.5	1.4	1.2	1.0	0.8	0.5	**1.8**	**1.0**
Deviation in % of Mesh nr4	2.9	2.9	2.8	2.6	2.5	2.3	2.2	2.0	2.1	2.3	3.0	2.9	3.1	2.9	2.9	2.6	2.6	2.5	**3.1**	**2,6**
Deviation in % of Mesh nr5	6.0	5.2	3.9	3.0	2.8	3.3	2.8	2.6	2.5	2.8	3.1	3.0	2.8	2.9	2.7	2.6	2.5	2.6	**6.0**	**3.2**

The time fluctuation within each mesh is clearly visualised in Figure 51 and Figure 52 and the lowest and highest data for each mesh are collected in Table 4 and Table 5.

In Figure 51 the distribution of the heat transfer coefficient is plotted separately for all the meshes. The stretched length of each column shows how big the variation of the heat transfer coefficient is within the mesh during the simulation time of one operating second. In Table 4 the lowest and the highest value of the heat transfer coefficient is shown for each mesh.

Additionally the maximal percental fluctuation is calculated, by comparing the total distribution interval to the middle value of the interval. From the presented values of percental fluctuation it can be concluded that the time influence on the heat transfer coefficient is rather low for all the meshes. In other words the mesh size doesn't seam to have a significant effect on the distribution interval of the heat transfer coefficient. In the last column of Table 4 the total distribution interval for all the meshes are summarized and the total percental difference is calculated to be 1.5%, which is decided to be acceptable.

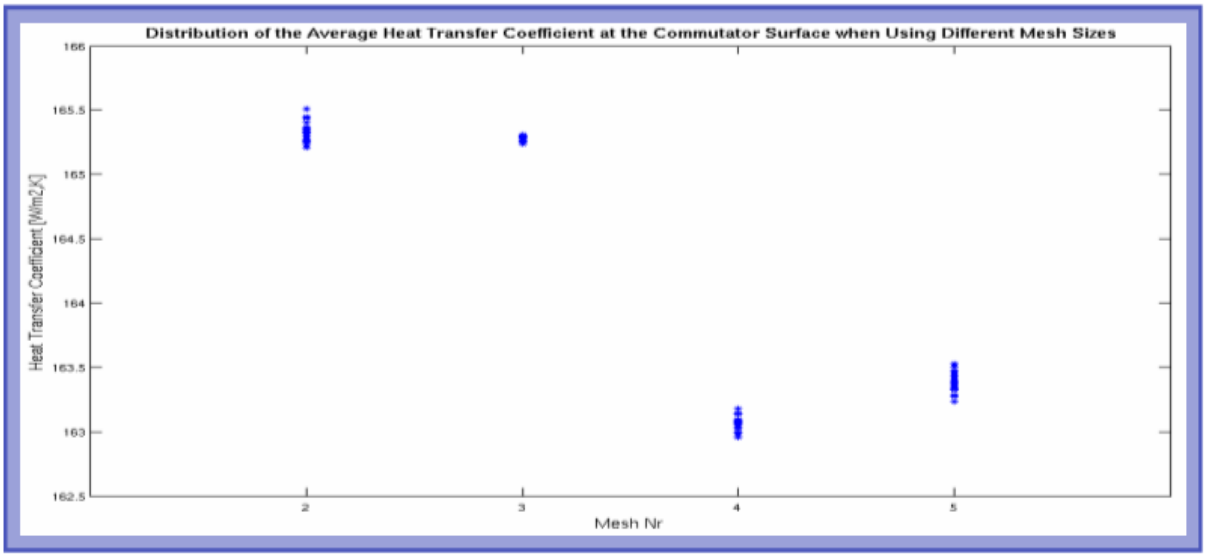

Figure 51: The distribution of the average heat transfer coefficient [W/m2,K] at the Commutator surface during 1 second, when different mesh sizes are used

Table 4: The variation of the heat transfer coefficient [W/m2,K] within each mesh during 1 simulated second, according to figure 51

	Mesh nr2	Mesh nr3	Mesh nr4	Mesh nr5	Total
Heat Transfer Coeff. Min [W/m2,K]	165,2	165,2	163,0	163,1	163,0
Heat Transfer Coeff. Max [W/m2,K]	165,5	165,3	163,2	163,5	165,5
Total Interval Compared to Middle Value [%]	0,18	0,04	0,13	0,27	**1,52**

In Figure 52 the distribution of the net heat rate is plotted separately for all meshes, in the same way as previously for the heat transfer coefficient. The stretched length of each column shows how big the variation of the net heat rate is within the mesh during the simulation time of one operating second. In Table 5 the lowest and the highest value of the net heat rate is shown for each mesh and the percental fluctuation within the mesh compared to the middle value is also given. The total percental variation of the net heat rate is also calculated and it is found to be rather high, more than 6%. One explanation to that could be the previously described assumption that mesh nr 5, where the deviation occurs, has not yet got stabilized values at the beginning of the simulated time. If this misleading initialization effect would be removed the total distribution interval would be lower and probably within the acceptable range. It can also be seen from the above figures that the global net heat rate is more time dependent than the local heat transfer coefficient. One attempt to explain this is by assuming that the oscillating flow would create a pulsating movement out through the ventilation which would directly affect the net heat rate of the system to oscillate as well. The heat transfer coefficient on the other hand would be less sensitive to this pulsating movement because the high turbulence in the flow that causes rather good mixing in any case.

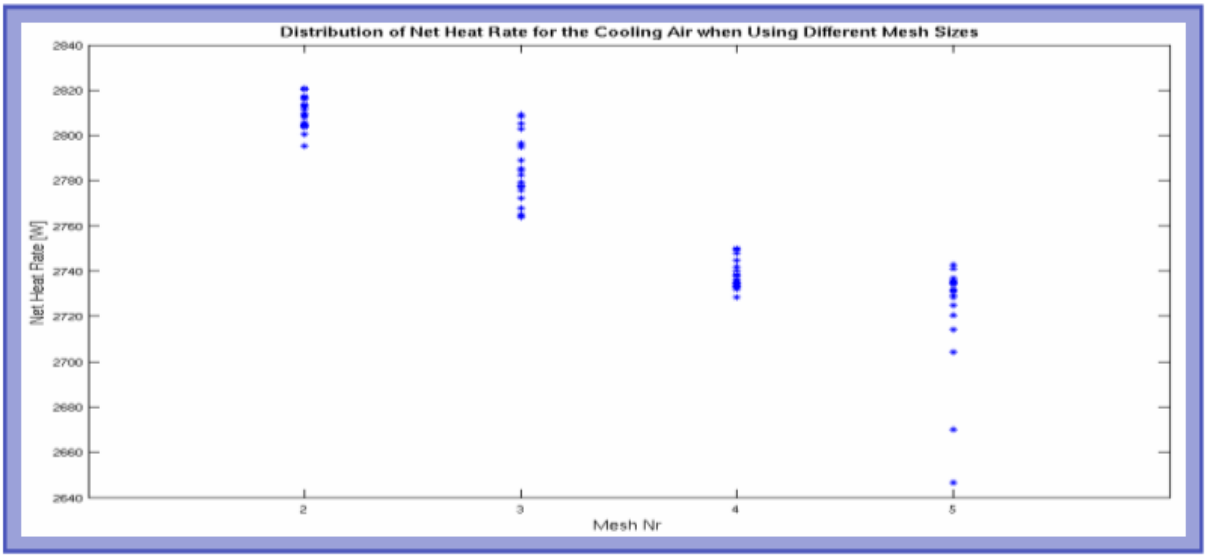

Figure 52: The distribution of net heat rate [W] for the cooling air during 1 second, when different mesh sizes are used

Table 5: The variation of net heat rate [W] within each mesh during 1 simulated second, according to figure 52

	Mesh nr2	Mesh nr3	Mesh nr4	Mesh nr5	Total
Net Heat Rate Min [W/m2,K]	2795	2764	2728	2647	2647
Net Heat Rate Max [W/m2,K]	2821	2809	2750	2741	2821
Total Interval Compared to Middle Value [%]	0,93	1,61	0,80	3,49	**6,36**

4.2.3.2 Pictures

Visual comparisons of the simulation results were used as a method to analyse the mesh size effect, besides the above described comparison of simulation data. The results that were visualized were mainly the velocity magnitude and the temperature of the cooling air pictured at the radial cross section through the middle of the Commutator. The pictures were taken for all meshes and at a particular simulation time and presented together next to each other to simplify the comparison, see Figure 53 and Figure 54.

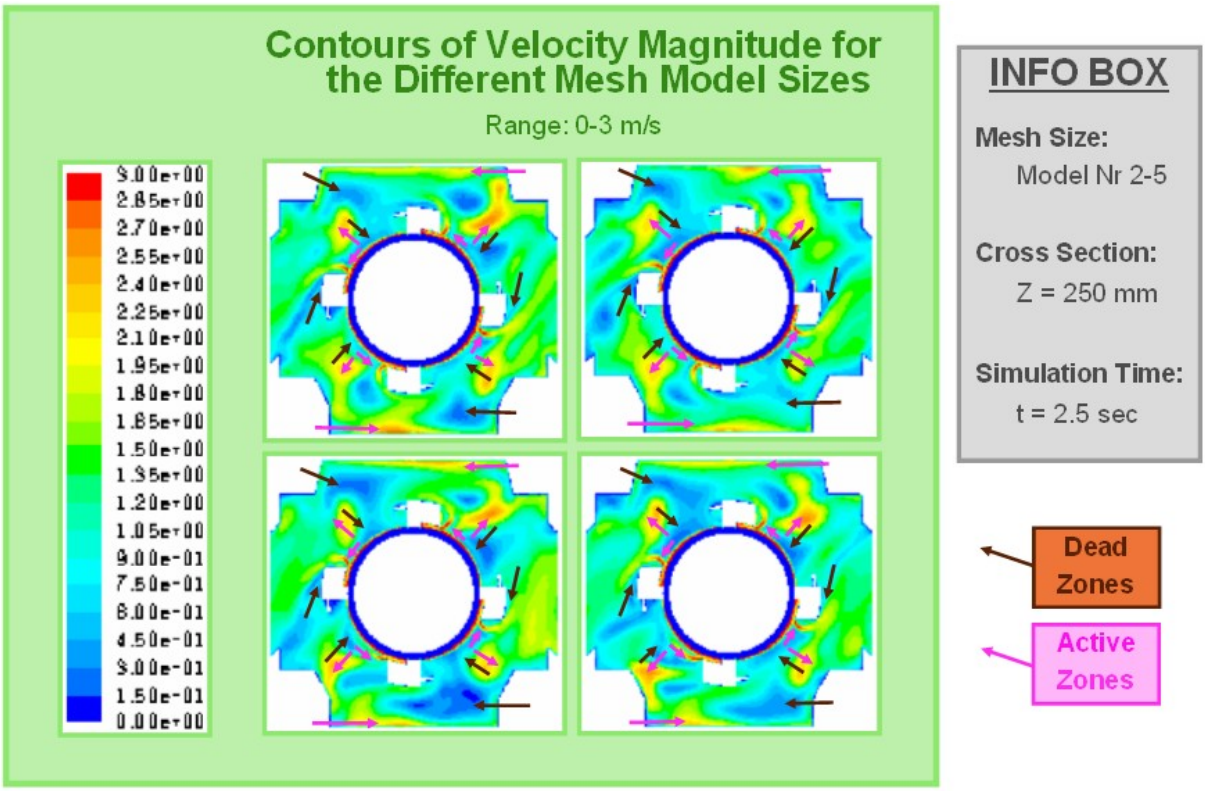

Figure 53: Comparison of the velocity magnitude for the different mesh models. The picture is taken at the radial cross section in the middle of the Commutator

In Figure 53 the contours of velocity magnitude are pictured for the different meshes. The blue areas are spots where the air is hardly moving, so called dead zones. Dead zones occur either in the wake behind a blocking object or in the eye of a vortex formation. The zones coloured yellow and red have a high flow activity, probably due to a high axial velocity. Those dead zones and active zones are used as marking points when looking for similarities in the flow pattern between the meshes. It can clearly be seen that the zones pointed out with arrows are existing in all the meshes somewhere in about the same position but with a slightly difference in size. The difference in size and position can partly be a result of a continuous variation in time.

One pattern noticed are the dead zones appearing over the velocity boundary layer of the Commutator, between the brushes. Those could be explained as vortex circulation driven by

the high speed of the Commutator surface, but the axial flow needs to be taken into consideration as well. Dead zones are also appearing at two corners of the motor casing, one at the bottom and one at the top, where the flow is partially screened off from the ventilation opening. Other dead zones are found after the brushes in the rotating direction and they can be considered as wake formations behind the brushes.

The highest velocity occurs at the boundary layer above the Commutator surface, caused by the shear stress from the moving surface. When this flow reaches the stationary brushes it changes direction and thereafter dissipates into the surroundings. Four other active zones found in the cross section are situated between the brushes and centred between the Commutator wall and the outer wall. The air passing through those spots is forming axial channels between the brush arms. Along the bottom and top of the casing wall the velocity of the air is found to be high as well. An axial air stream flowing along the wall is causing this as well.

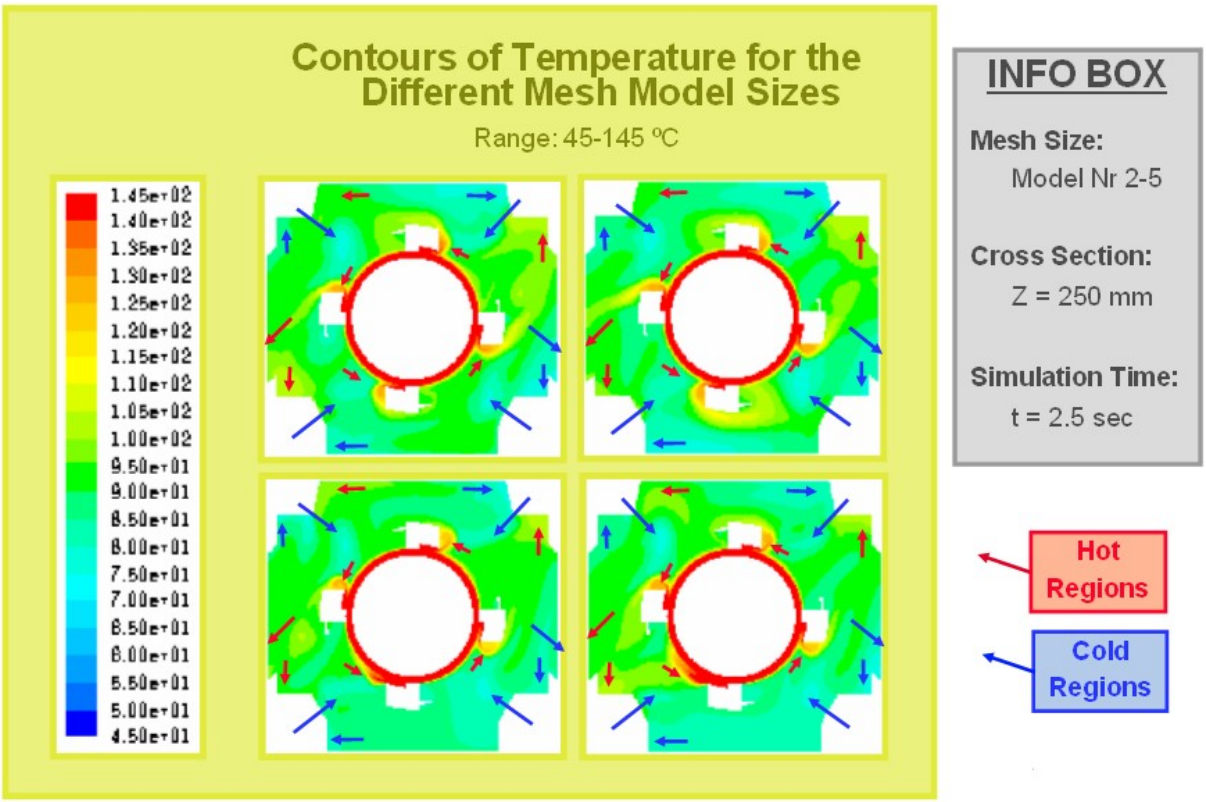

Figure 54: Comparison of the temperature for the different mesh models. The picture is taken at the radial cross section in the middle of the Commutator.

In Figure 54 the air temperature at the chosen cross section is shown for the different mesh models. The hot regions and the cold regions, marked with red and blue arrows respectively, are compared between the meshes to examine if the mesh size has an influence on the simulated temperature. As for the velocity comparison, the regions pointed out by the arrows exist in all the mesh models, but they are slightly different in size and position.

From the pictures it can be seen that the air temperature is at its highest near the Commutator surface. A thin temperature boundary layer is formed between the hot surface and the cooling air, which further up is disrupted by the stationary brushes and forced to change flow direction. At the ventilation opening on the left side a stream of heated up air is flowing out of the machine. Though on the lower left part of the ventilation opening there is a cold region and this is caused by a backflow of air that is sucked into the machine. Further it is noted that the regions at the corners of the motor casing either are uniformly hot or cold. The cold regions are suspected to be axial air flow channels that are taking a short cut passage next to the casing wall without interacting with the hotter regions. The hot corner regions are probably appearing due to gatherings of stagnated air. Cold spots are also found in the region between the brushes and are probably also axial flow channels of cold air.

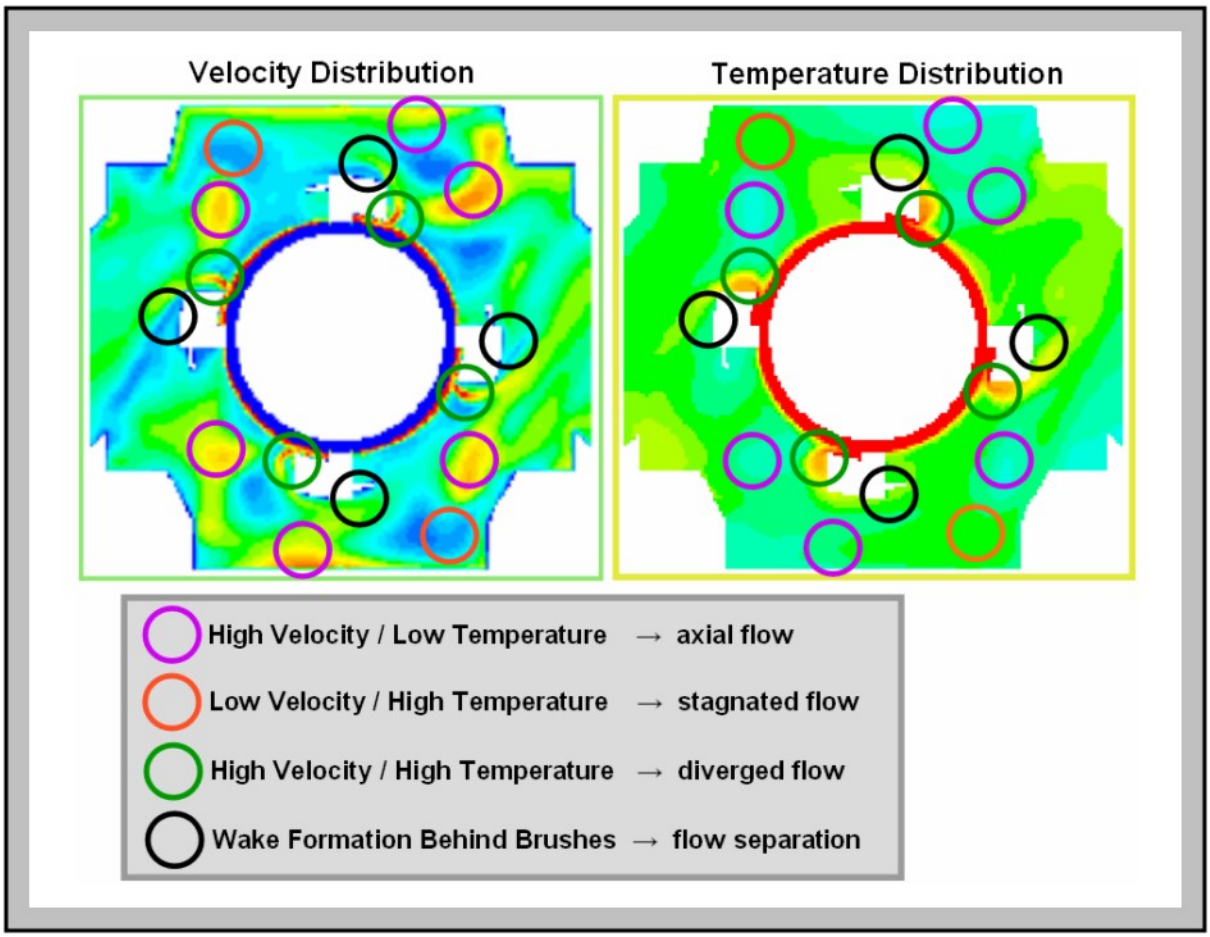

Figure 55: A comparison made between the simulated velocity and temperature in the air for mesh 2. The pictures are showing the radial cross section in the middle of the Commutator at the simulation time 2.5 seconds.

Out of curiosity the two simulated values, the velocity magnitude and the temperature, were then compared to each other and an attempt was made to find possible connections between them. For this study the simulation pictures from mesh 2 at the simulated time 2.5 seconds were used.

The first thing noted was that some spots with high air velocity had a correspondingly low temperature. Judging from the formation of the spots the air seems to be travelling in the axial direction. It can be assumed that this axial air flow comes directly from the air inlet between the stator windings and therefore is colder. This cold air forms a straight channel through the machine and if it finds a short cut to the ventilation opening this phenomena will cause loss of cooling. Further more there are other spots with lower air velocity but higher temperature and they appear most visible in the shielded corners of the casing. In those areas the air seams to have stagnated more or less which gives the temperature enough time to get evenly distributed. It would be desirable to lead this hot air directly out through the ventilation to prevent it from heating up the surrounding air. Other phenomenons that are studied are the velocity and temperature boundary layers close to the Commutator surface. They are generated from the velocity and temperature difference between the moving, heated up surface and the free stream of cooling air. When the boundary layers reach a brush they will be disrupted and the flow will be forced to change direction. During this divergence the flow will experience loss of speed from the friction that will be transferred into heat. Therefore is the hot spot in front of the brushes larger than the area of high velocity. Finally, it can be seen that the high speed flow over the brushes separates from the brush surface at a certain point and continues out to the free stream. In the area after the flow separation a so called wake is formed, where stagnation of flow and drop of pressure occurs.

The time fluctuation of the velocity magnitude was also studied for each mesh. For this study the velocity movies, created during the simulation process of the sensitivity analysis, were used. About 150 velocity pictures were taken during one operating second, between second 2 and 3, and they were put together to form the movie. An oscillation of the flow is slightly visible for the eye. It can be noted as a slow movement back and forward of the hot areas and the cold areas, and a repeated growing and shrinking of them. The oscillation of the flow is corresponding between the different models and the differences are considered small enough to be neglected. The four different flow simulation movies will follow this report as separate attachment files.

The final picture (Figure 56) is showing the temperature variation in the solid at the copper layer on the Commutator. It is noted that there is a temperature variation of about 7 K in the solid. In the real machine this temperature difference would never occur due to the high rotational speed of the solid. In the simulation though, the solid is set to rotate slower than the surface to avoid numerical problems, and the temperature is therefore not distributed evenly enough. This problem can be avoided by increasing the rotational speed of the solid. An increase of the rotational speed from 1 rpm to 10 rpm should probably be enough for achieving that. Hopefully the rotational speed would still be low enough to not cause any numerical problems, and thereby cause convergence problem for the governing equations.

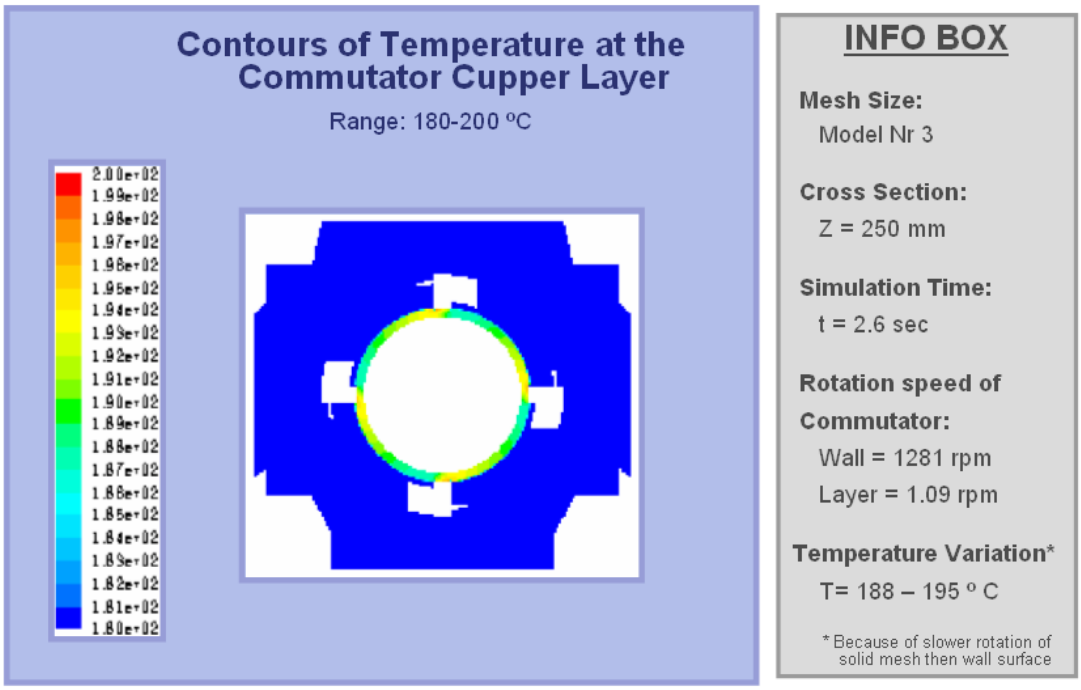

Figure 56: A plot of the solid temperature of the copper layer on the Commutator. The picture is taken at the radial cross section in the middle of the Commutator. Note that the surface of the Commutator, here called the “Wall”, and the solid copper layer of the Commutator, here called the ”Layer”, don’t have the same rotational speed. The speed of the solid volume is decreased to prevent convergence problems in the governing equations.

4.3 Conclusions for the 3D Model

From the simulations of the 3D model it is possible to get a more detailed understanding of the airflow that goes through the DC-motor. The three-dimensional flow effects can be further studied in FLUENT or in another post processing software program, within this thesis though this is just briefly studied. Some flow effects are noted such as a short-cutting flow, which is cold air that runs from the inlet at the stator windings and directly to the ventilation openings, and the stagnated flow, which is hot air that gets stuck at the corners of the bearing shield wall. To improve the cooling of the machine the short-cutting flow needs to be redirected towards the hot surfaces and prevented from flowing out from the machine, while the stagnated flow should be led out by increasing the circulation at those hot spots of the fluid. A more detailed study needs to be done of those flows later on before certain geometrical changes can be suggested for an improved cooling.

The simulation of the mesh model nr 1, with mesh near the Commutator called the inner mesh considered as normal sized and the rest of the mesh called the outer mesh considered as fine sized, was not functioning smoothly. Therefore it was concluded that it is of no use to refine the mesh for the main model if the mesh near the Commutator is not made finer as well. Probably the size of the mesh near the Commutator surface is of more importance for the simulation than the mesh in the rest of the model, since it contains a boundary layer of both the velocity and the temperature that will influence the rest of the model.

Further it can be said that the mesh of the model is very robust for simulations and no numerical problems are occurring. All the mesh sizes that were studied of the model are sufficiently fine to dissolve geometry modifications. The weakest point of the model is instead the turbulence modelling which is usually the case when doing flow simulations. One of the uncertainty factors of the turbulence modelling is that it might be not accurate enough to use the k-omega turbulence model, since no other models have been tested and compared with it. Neither has the simulation results been validated with actual experiments on a real machine. Furthermore, the roughness of the Commutator surface was very roughly set and since the rotating surface is a very significant turbulence factor the simulation results will not be reliable until this is investigated further through experimental validation.

Another thing that is problematic with the 3D-model is the long simulation time to get the final simulation results. The simulation time is important because the license of the software used for the simulation is very expensive and also because it complicates the process of making a comprehensive simulation study where a lot of simulations are needed. The simulation time for 1 simulated second is 12-63 hours, depending on which mesh size that is used, and this slowness is mainly due to the complexity of the geometry and the flow. On top of that the high turbulence and the unsteadiness of the flow cause a fluctuation of the simulation results in time and therefore a convergence of a steady state solution is disturbed. A transient solution has to be reached instead and this is further increasing the simulation time according to former experiences with other simulations. When simulating transient flow the time steps have to be made small enough to resolve the oscillating flow, but meanwhile the whole simulation span has to be long enough for the heat conduction in the solid to stabilize. If those two phenomena would be simulated at the same time the total time needed for the simulation would be unacceptably long. So therefore it was necessary to divide the whole simulation process into two steps, first a transient simulation where the heat transfer was neglected and thereafter a steady state simulation of the heat transfer with the flow fixed at its

current position. This way the simulation could be made within reasonable time and the result would be accurate enough since the heat transfer in the model is not likely to influence the fluid motion noticeably. Free convection is only considered in cases where forced convection does not exist or is very low and the simulated flow is far from this condition. The reliability of this assumption is further confirmed by the fact that the fluctuation of the net heat rate of the air between different time steps is rather low. A high fluctuation would have indicated that something could have been wrong with the made assumption.

In the sensitivity analysis made to evaluate the mesh size effect, the average heat transfer coefficient of the Commutator surface as well as the net heat rate of the cooling air within the boundaries, are used for the comparison. The deviation of the data between the different mesh models is small enough (below 3%) and from this we can draw the conclusion that the mesh size effect is negligible. Additionally, the data fluctuation within each mesh was examined and it was also low (below 3%) and based on those results the transient effect of the simulations could be neglected at further simulations. Those assumptions are further confirmed visually from the velocity and temperature pictures compared between the different mesh models as well as from the velocity movies picturing the fluid oscillation in each mesh model. Mesh model nr 2, with a so called normal mesh size near the Commutator surface and also a normal mesh size in the rest of the model, was chosen as the mesh model that should be used at further studies. The reasons for choosing mesh nr 2 is because of its quick simulation time (12h for 1 simulated second), its low fluctuation of data with time (< 1%) and its negligible deviation of data compared to the finer meshes (1-3%).

5) Future Work

The task of improving the cooling system of the DC-motor could be approached from different directions. One way is to use the simulation results for the cooling air only as guidance and from there try to find appropriate modifications that supposedly could lead the airflow in the wanted direction. The resulting flow generated from the new design could then be measured experimentally and evaluated by examining its cooling effectiveness.

Another alternative is to use a more systematic way to search for appropriate geometry modifications. By trying out a couple of ideas firstly through modification of the existing model and then simulating the flow, the most promising idea could be selected for an experimental validation. This way a lot of expensive and time consuming experiments on a real machine could be avoided. On the other hand the modification of the model geometry could also be troublesome since the geometry of the old model needs to be adjusted. Though, on the other hand, if the model would be frequently used as a tool the user would become more familiar with it and eventually the time for modifying the geometry would be speeded up.

In any case the simulation results from the original model need to be validated with experiments on the real DC-motor to check if the turbulence modelling and some assumed boundary conditions such as the roughness of the Commutator surface are correctly made. All the modified models would perhaps not be validated, but the relative effect on the flow could also give us valuable hints as well.

5.1 Overview Plan

The ideal way for the process of developing the cooling system would be to run model simulations parallel to experiments on a real machine. Since the simulation process probably would be quicker than the experiment setup a lot of geometry modifications could be simulated while an experiment was running. For each of the modified geometry models a parameter study needs to be done where the input parameters are varied within a reasonable range to check if the simulated results would be continuous as well. The mesh size would need to be refined where the simulation results are unstable. When the parameters seem stable for a certain simulation geometry model an equation will be formed for it. Those equations together with the values of the experimental validation should be compared with each other and the optimal case should be chosen as guidance for modifications on the real machine. After this is done the process can be continued starting at the beginning again with an absolute calibration through the experimental validation while the relative calibration using the simulation model would be redone again, but for different geometry modifications. This idea is also shown in the schedule of figure 57.

This is of cause a purely theoretical approach and this process could encounter problems that would make it troublesome to continue. If so the purely practical solution, to just try everything experimentally would do as well.

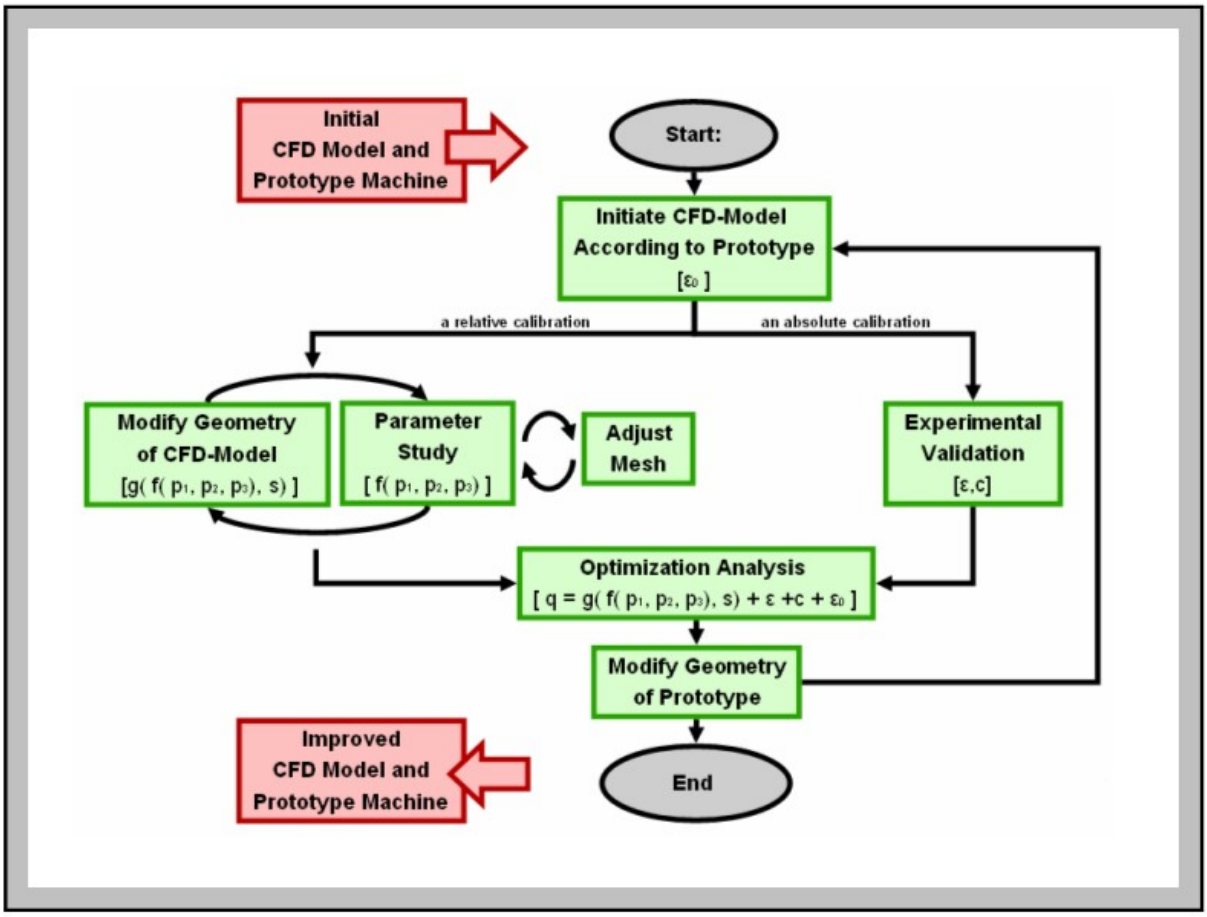

Figure 57: A theoretical schedule over the geometry modification process

5.2 Ideas for improving the cooling

There are a lot of different ideas of how to increase the heat transfer in the DC-motor by doing some modifications on it. Some of them are based on trying to redirect the flow in a certain way that is expected to be favourable. One example of that is to put air guides in front of the rotor air inlet to lead the cold airflow smoothly up to the Commutator surface. Another is to put cylindrical walls around the stator inlet airflow to prevent the cold air from shortcutting directly out through the ventilation opening.

By increasing the turbulence of the air near the Commutator surface the heat transfer would increase as well. This could be done by placing baffles above and along the Commutator surface. The increased turbulence and heat transfer would unfortunately also lead to a higher pressure drop and if too many obstacles are placed out they would stop the flow instead of mixing it up. Or perhaps by increasing the Commutator surface by giving it larger “fins” would be a good idea since this would both increase the surface of the heat transfer and at the same time cause turbulent mixing.

Something could be done to the inlet air from the stator windings. For example it could be directed with a nozzle that also could increase its velocity. Or if all the air is found to be

heated up already when entering the Commutator area a separate airflow could be taken from the fan and bypassed directly to the Commutator.

A final idea could perhaps be to consider the rotation as a source of turbulence and let the fan speed be controlled by the actual need of cooling air at different rotations and operating points of the machine.

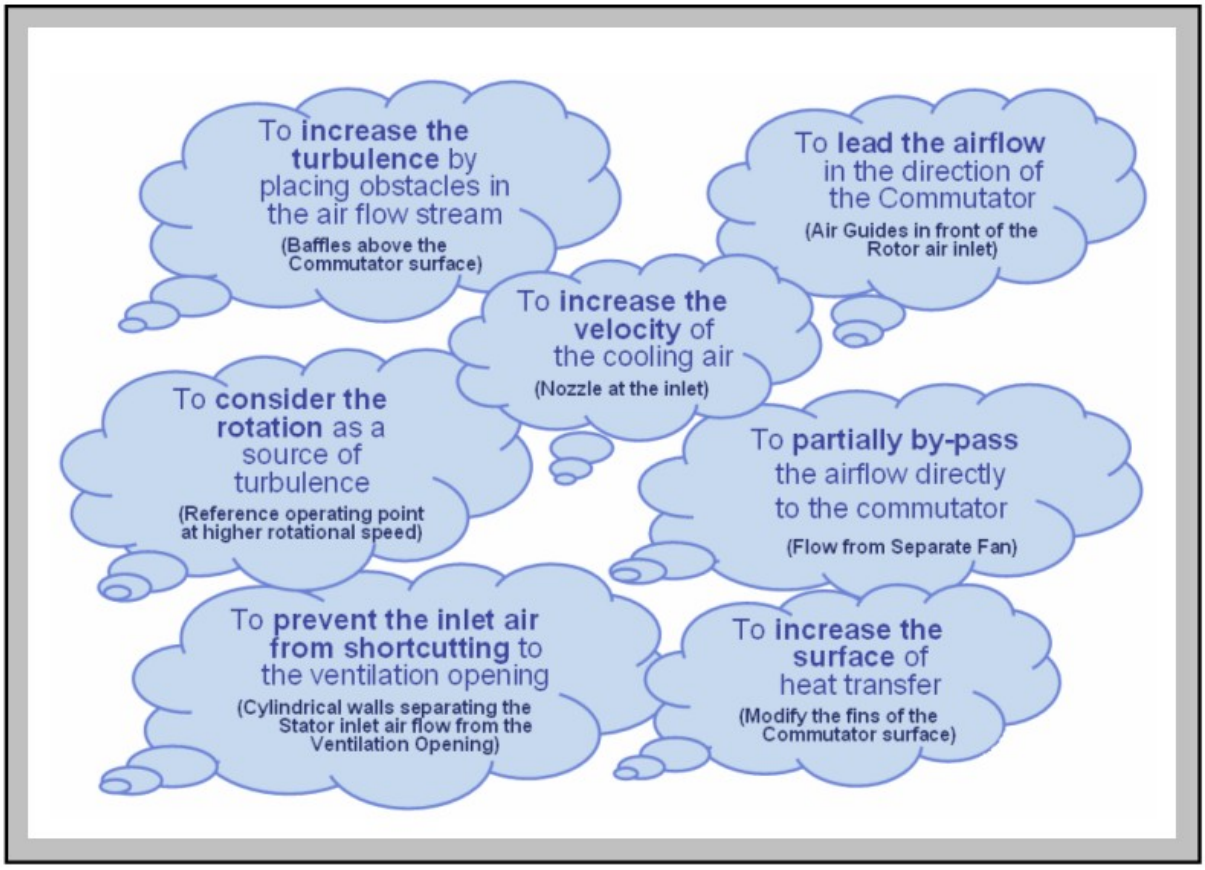

Figure 58: Ideas for improved cooling and heat transfer

References

[1] Teknografiska Institutet, Elektriska Maskiner, ISBN 91-7172-237-8, 1980

[2] Versteeg, An introduction to Computational Fluid Dynamics, ISBN 0-582-21884-5, John Wiley & Sons Inc, 1995

[3] Incropera, Fundamentals of Heat and Mass Transfer, ISBN 0-471-38650-2, John Wiley & Sons Inc, 2002

[4] Wikipedia, DC-motor
http://en.wikipedia.org/wiki/DC_motor

[5] Solarbotics, DC-motor
http://www.solarbotics.net/starting/200111_dcmotor/200111_dcmotor2.html

[6] CFD online
www.cfd-online.com/Wiki/Near-wall_treatment_for_k-omega_models

Other:

FLUENT 6 User's Guide
www.fluentusers.com

The general knowledge of the people at ABB Corporate Research and ABB Machines

Appendix

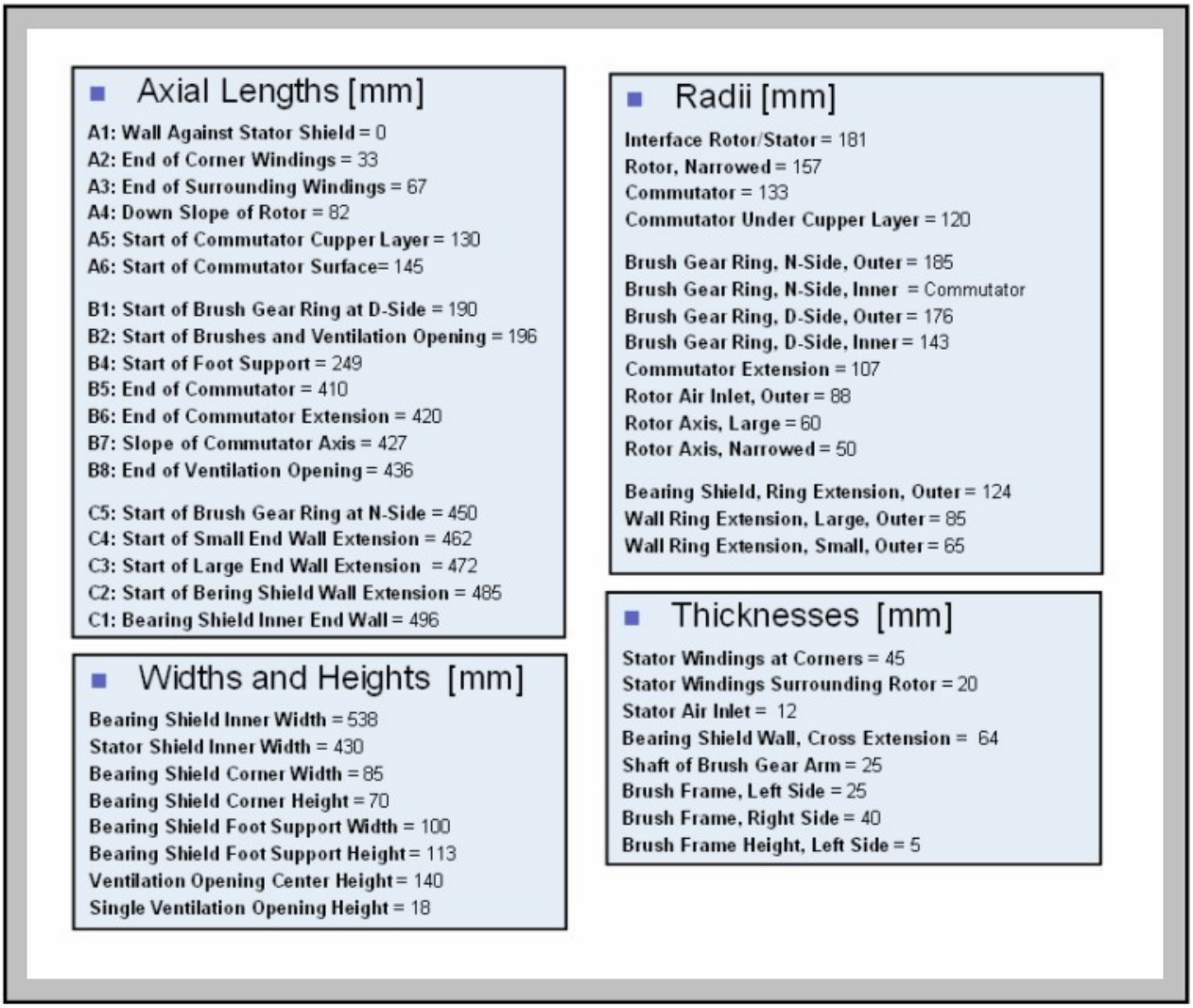

Figure 59: The geometry parameters for the model and their set values

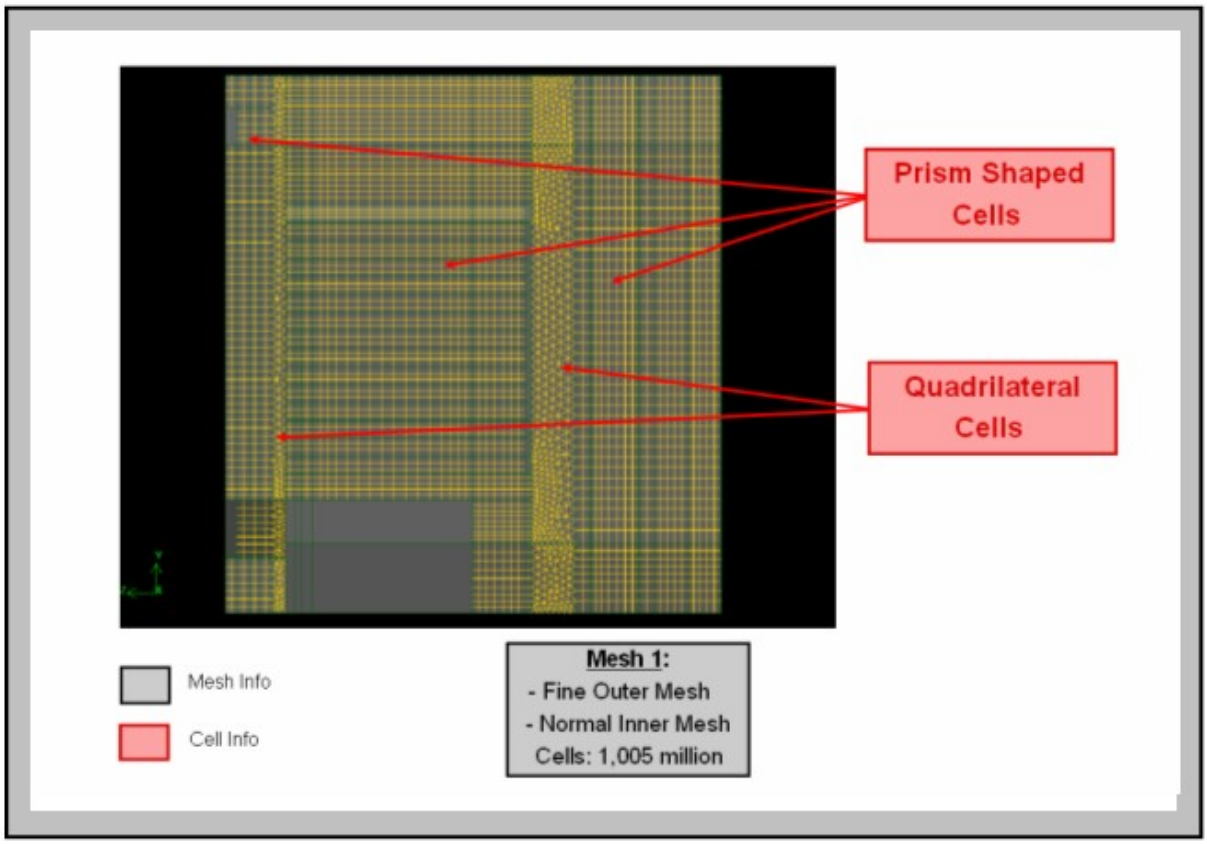

Figure 60: Side view of mesh model 1

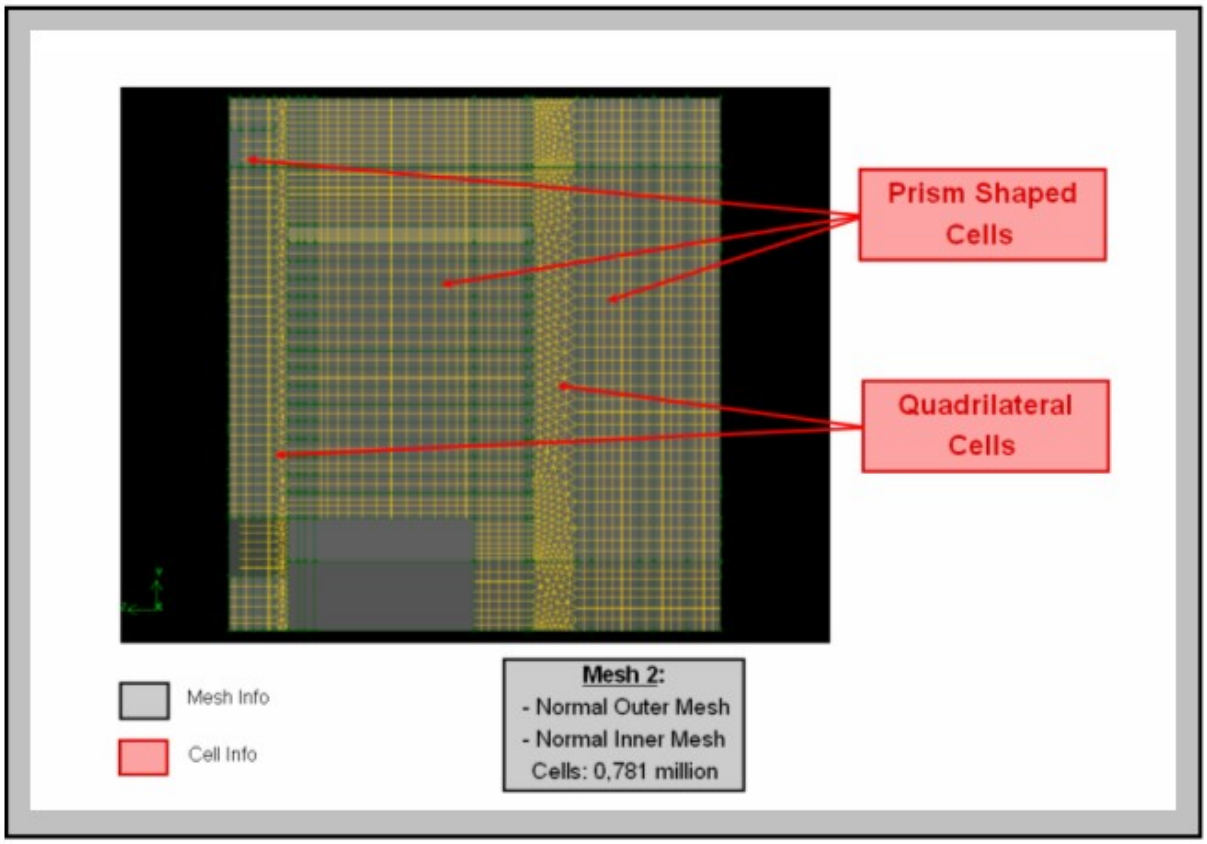

Figure 61: Side view of mesh model 2

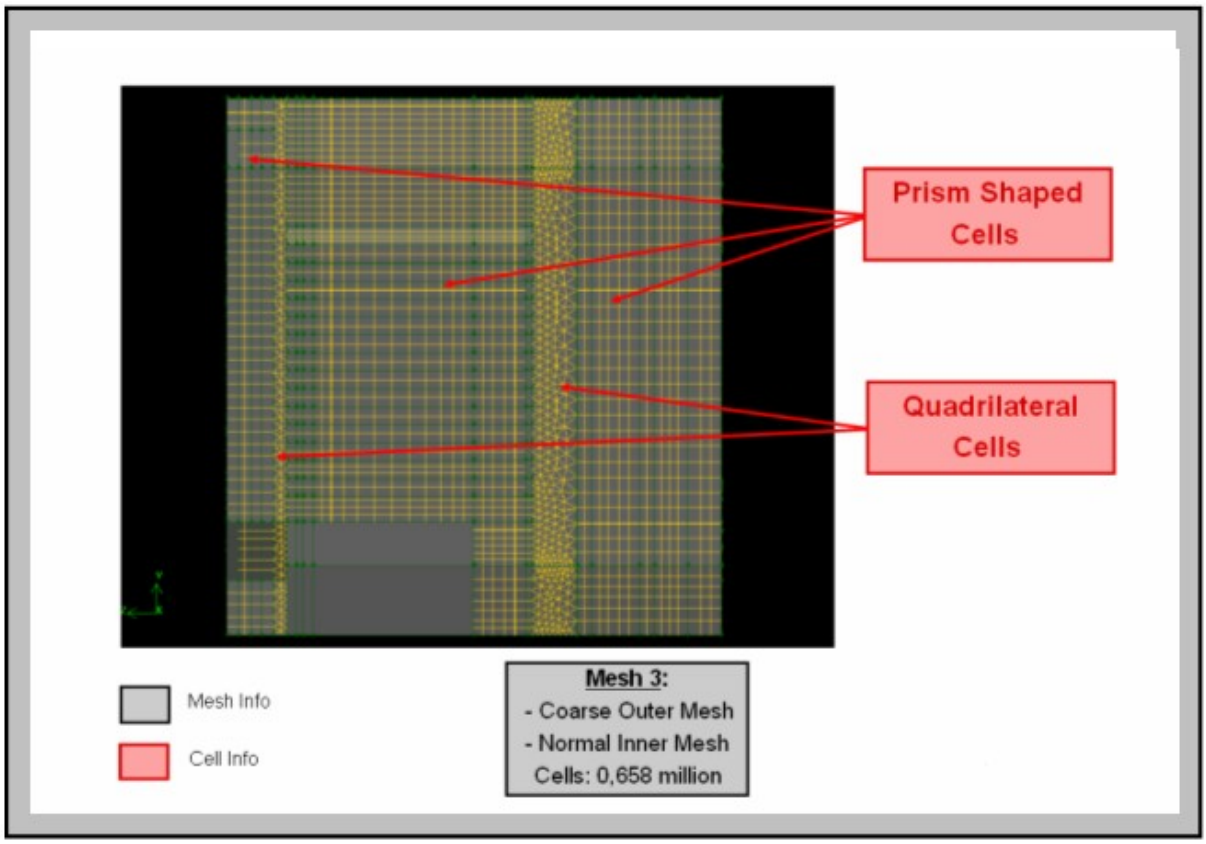

Figure 62: Side view of mesh model 3

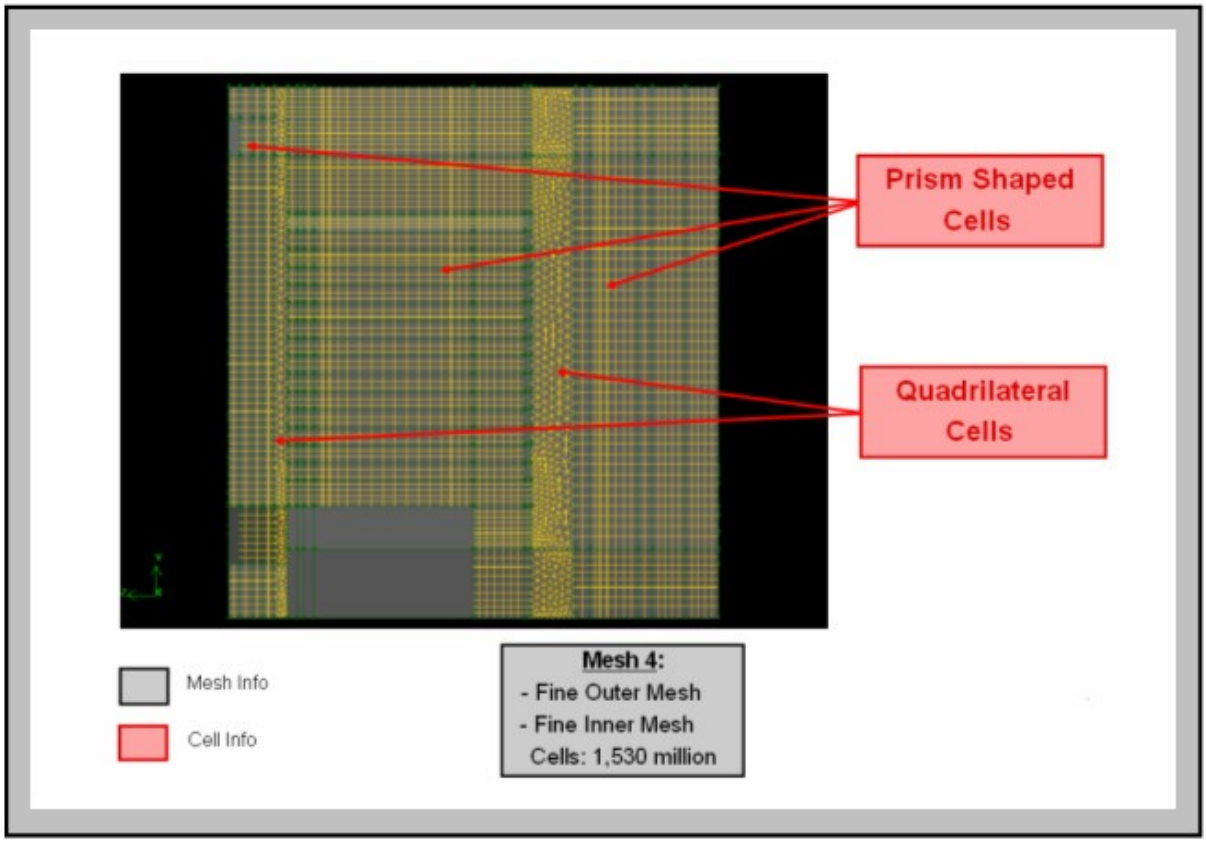

Figure 63: Side view of mesh model 4

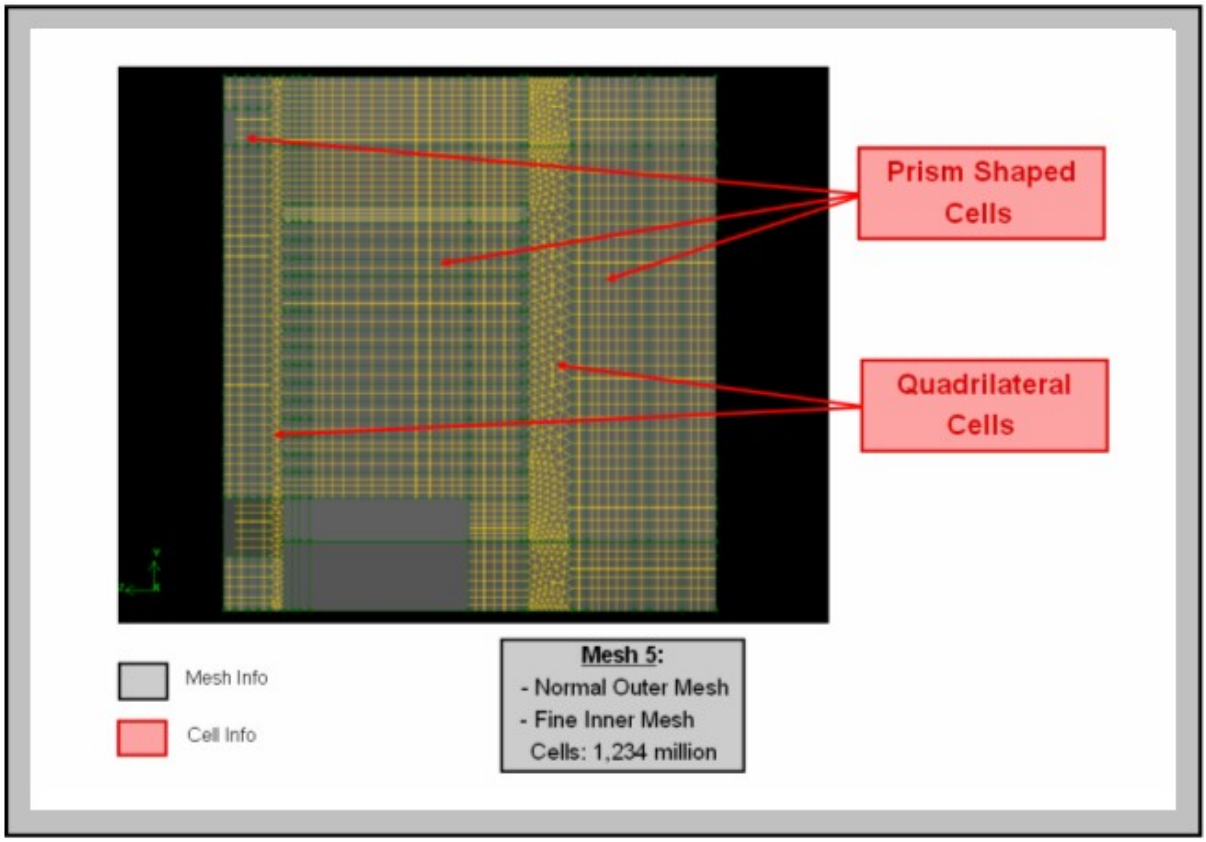

Figure 64: Side view of mesh model 5

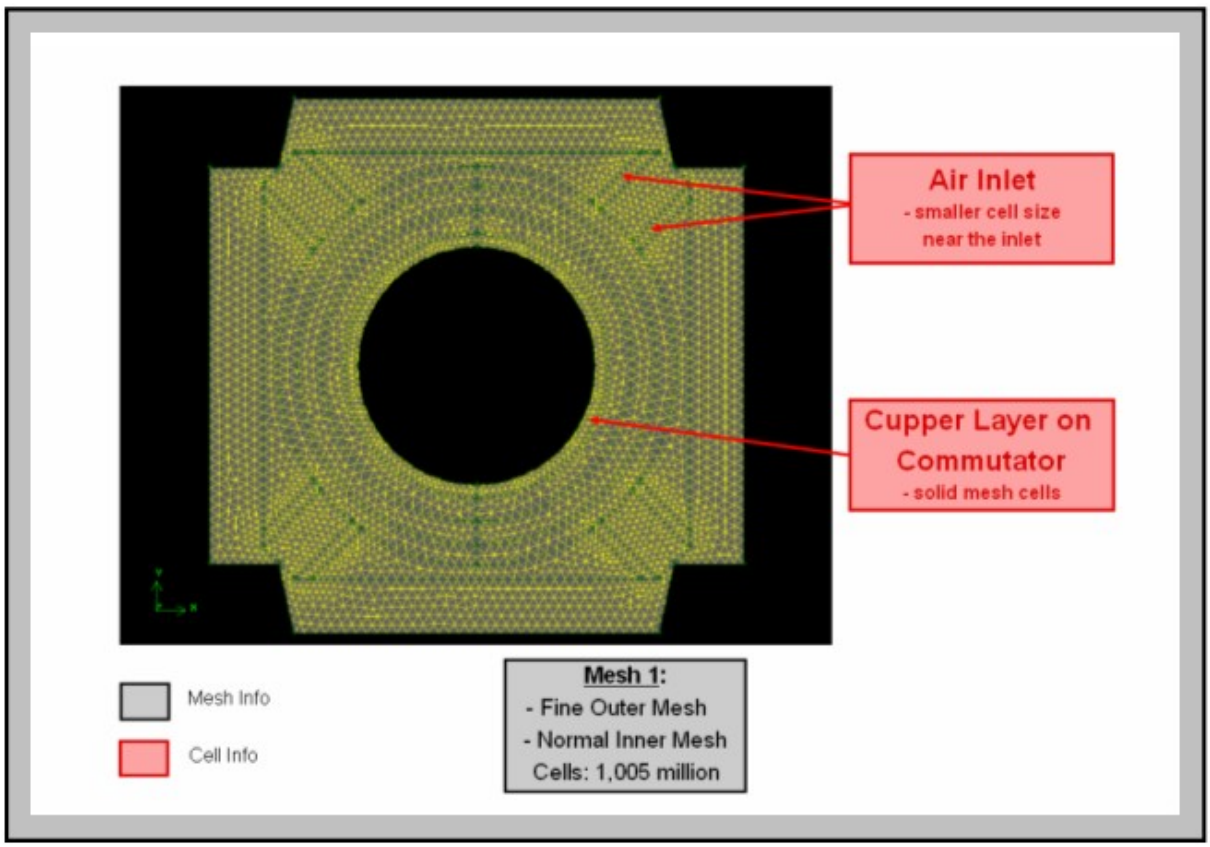

Figure 65: Front view of section A in mesh model 1

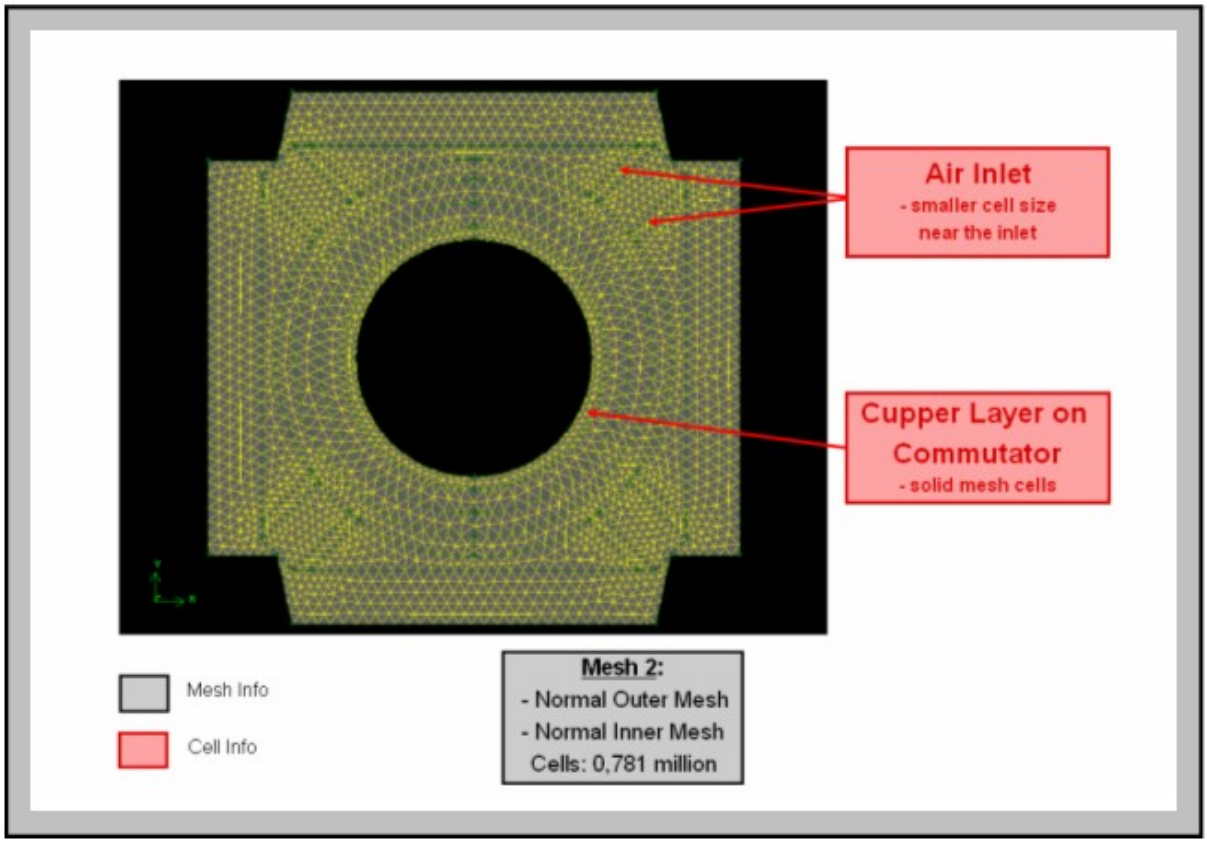

Figure 66: Front view of section A in mesh model 2

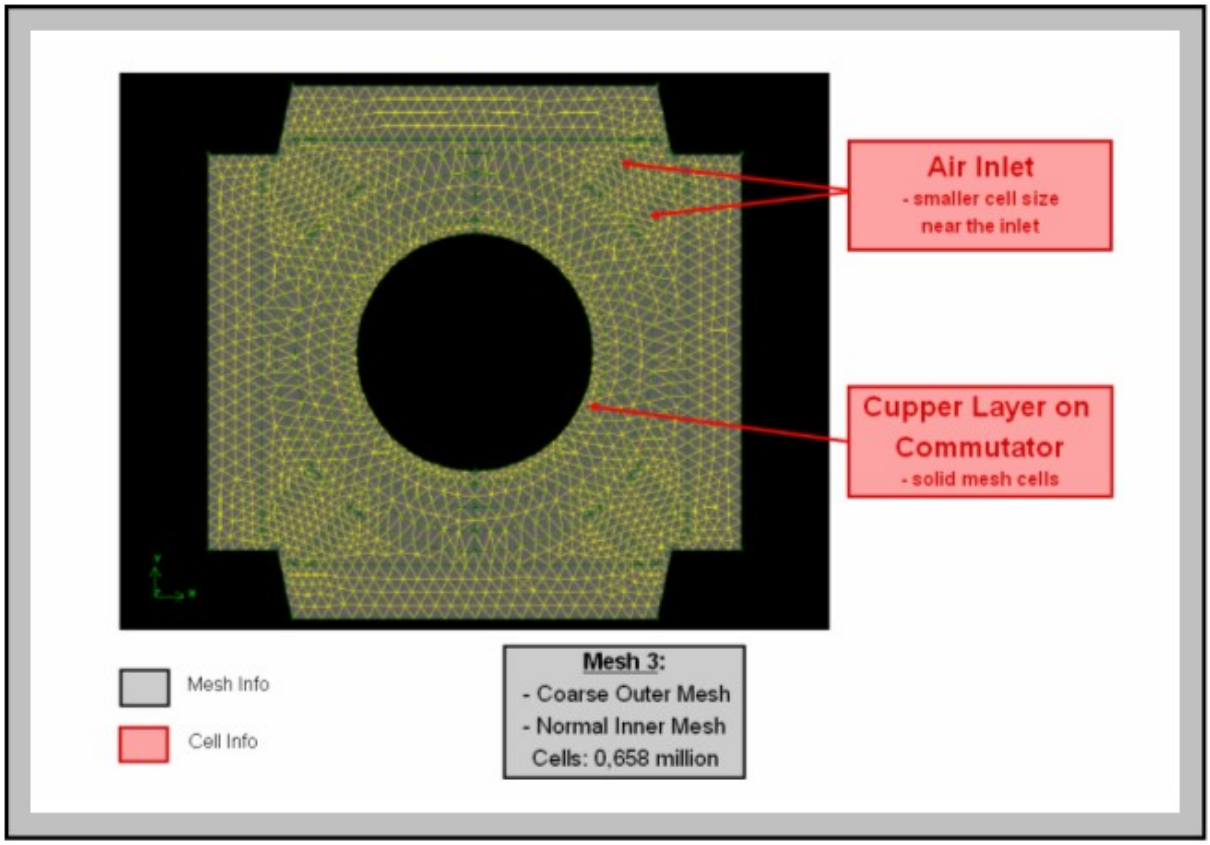

Figure 67: Front view of section A in mesh model 3

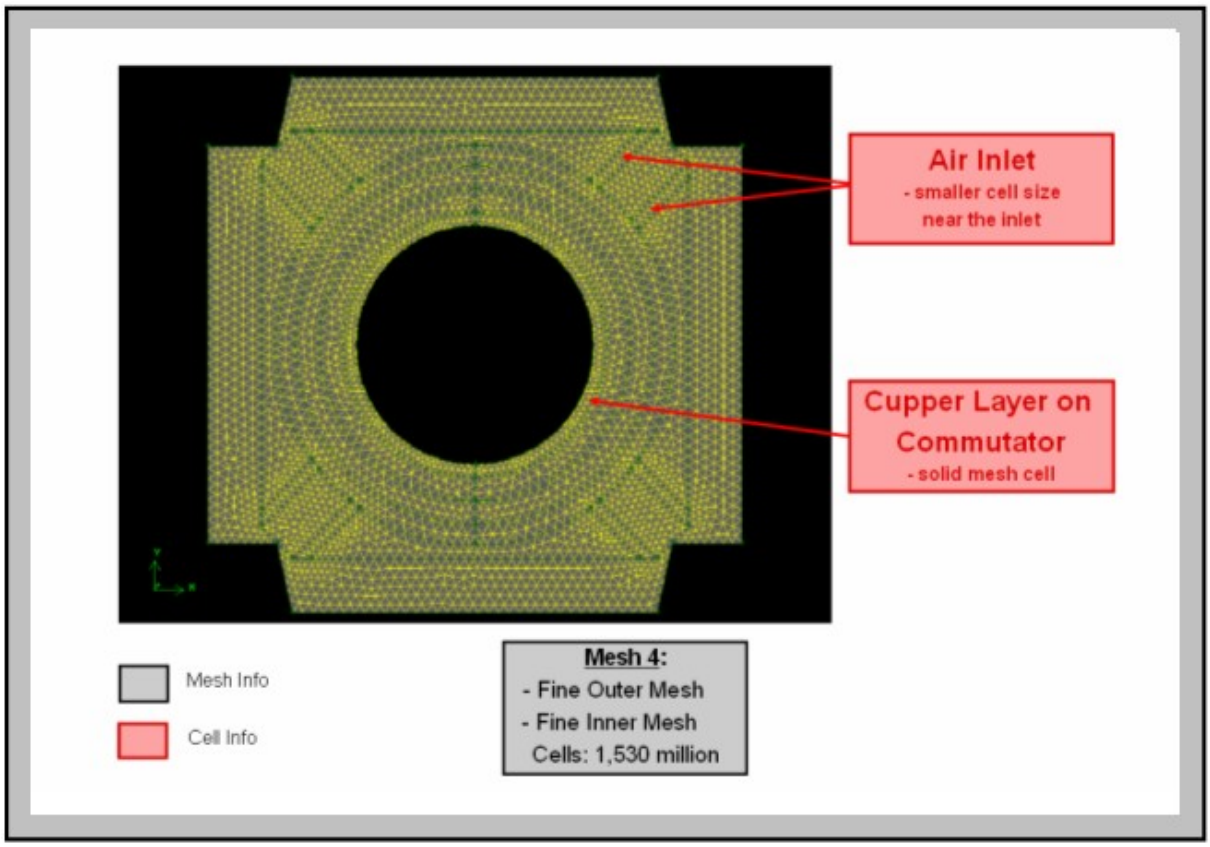

Figure 68: Front view of section A in mesh model 4

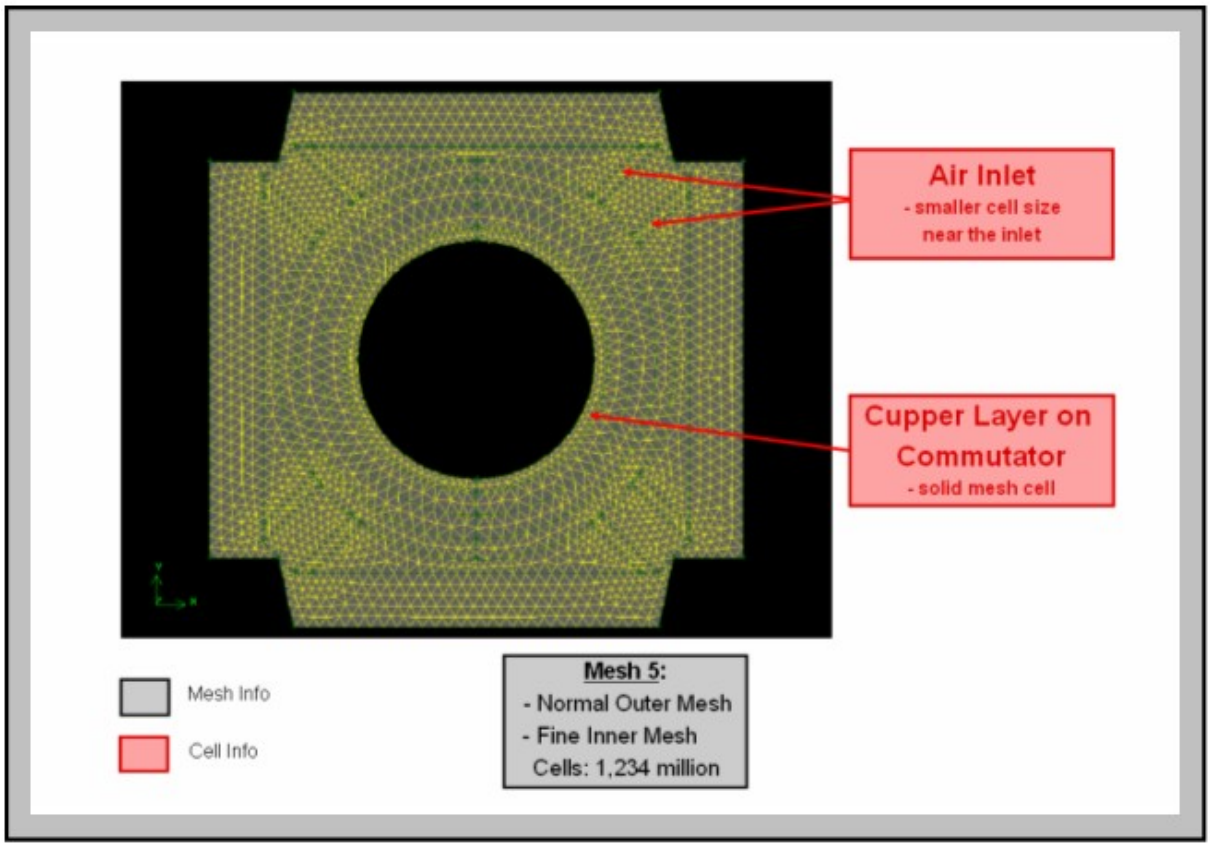

Figure 69: Front view of section A in mesh model 5

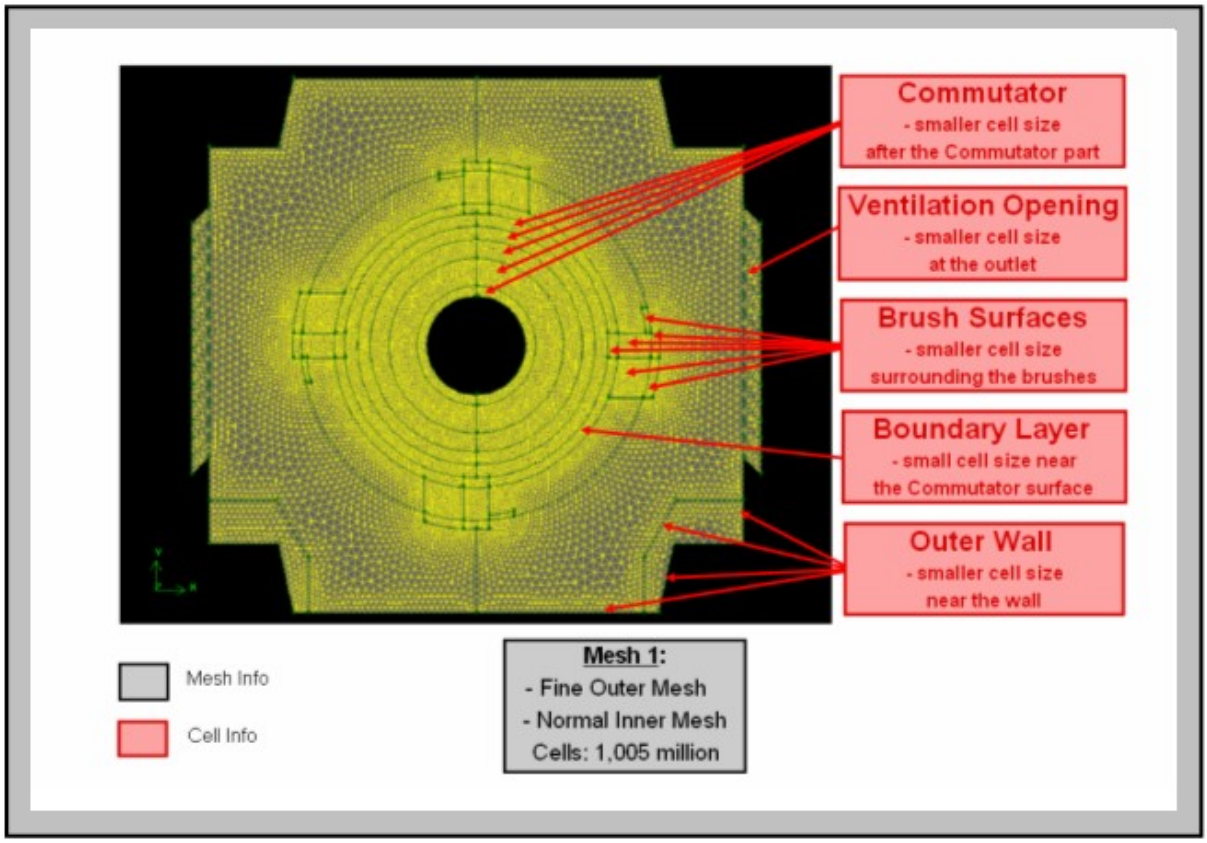

Figure 70: Front view of section B in mesh model 1

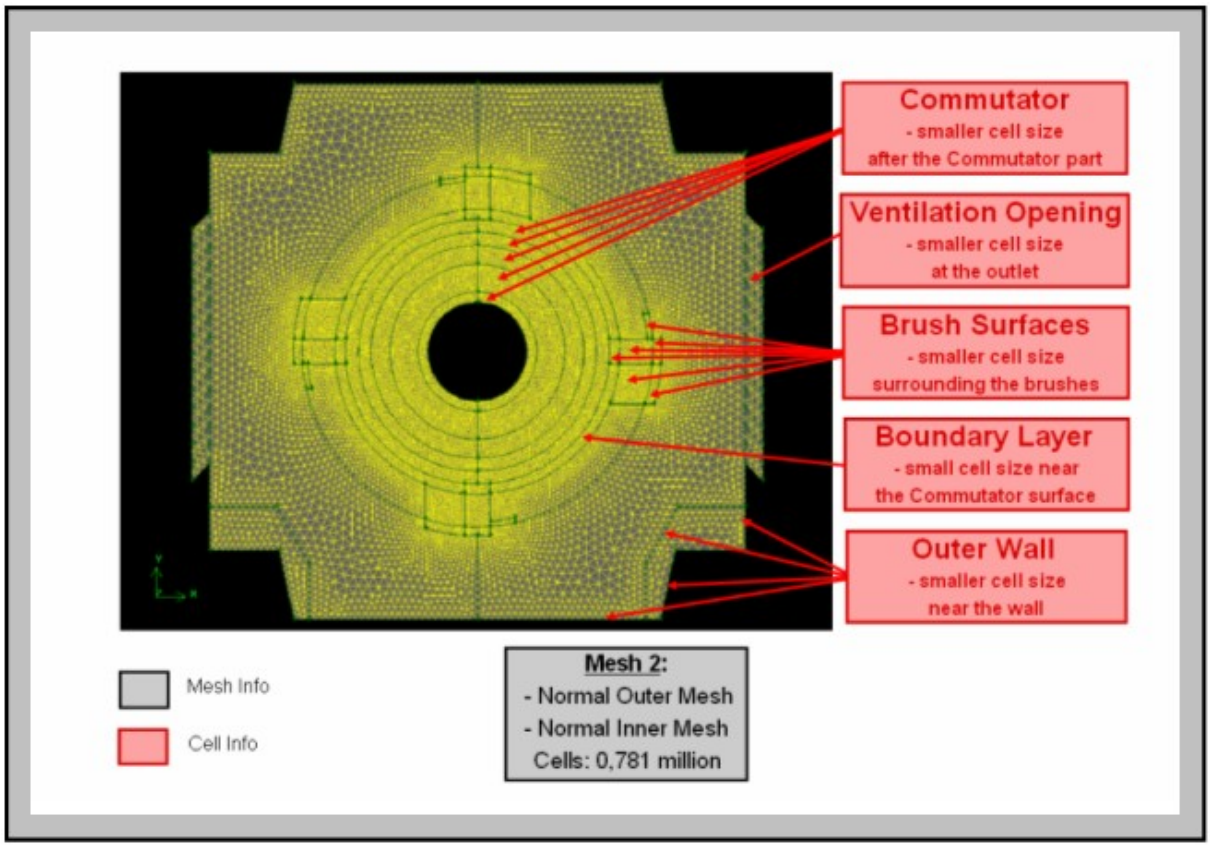

Figure 71: Front view of section B in mesh model 2

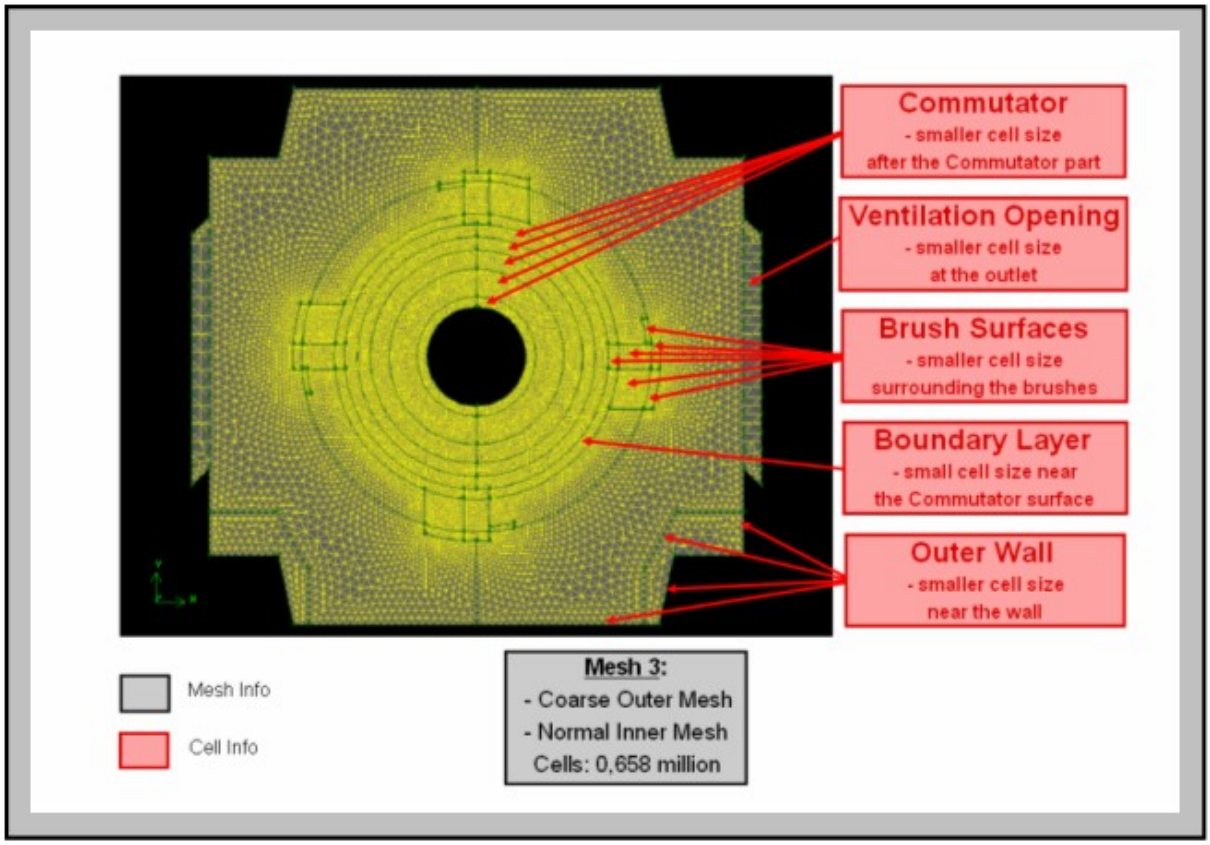

Figure 72: Front view of section B in mesh model 3

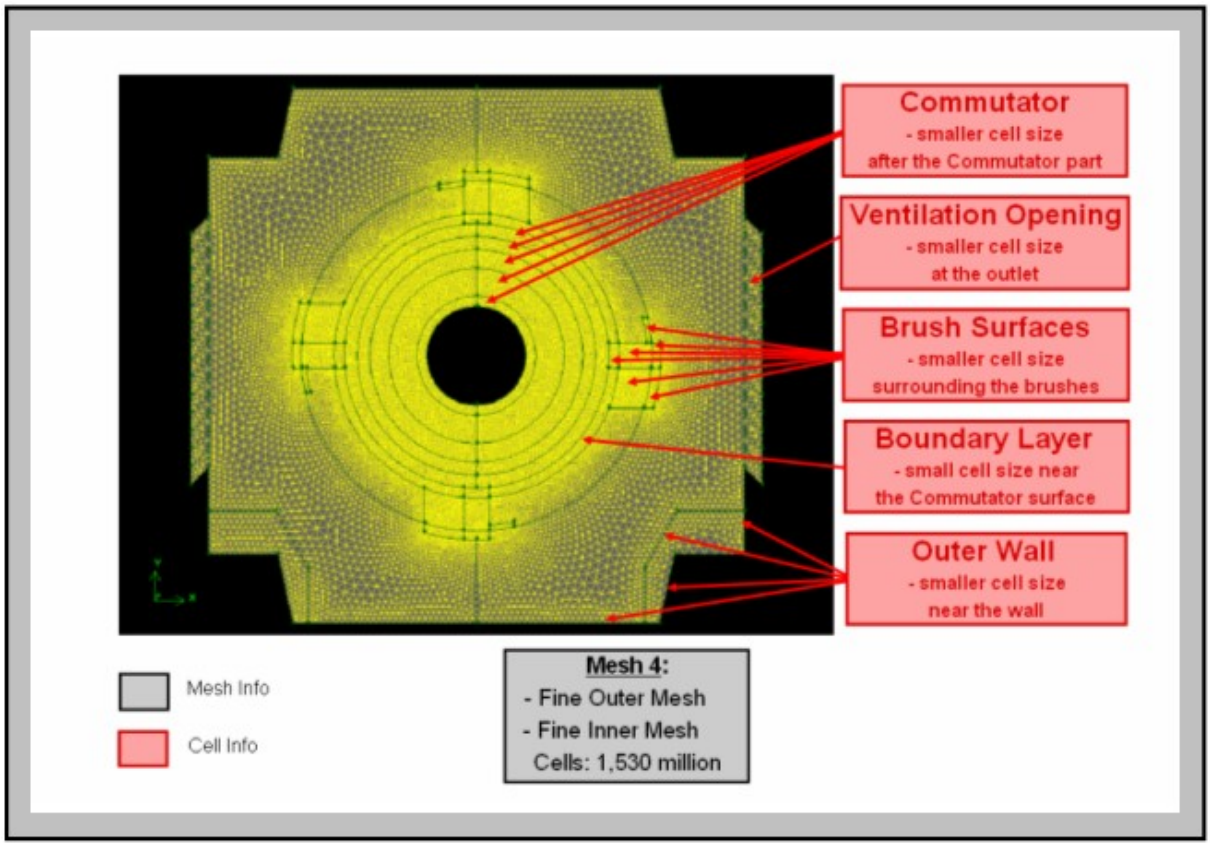

Figure 73: Front view of section B in mesh model 4

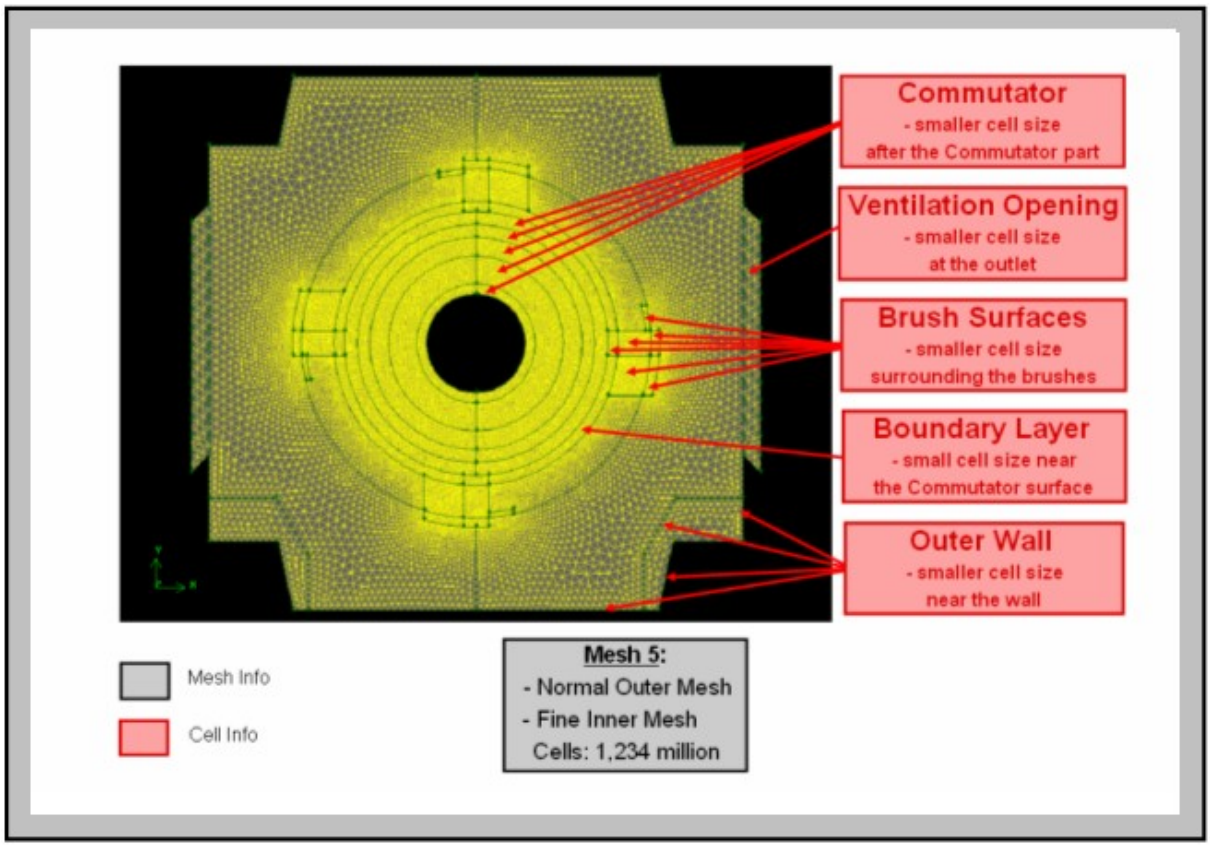

Figure 74: Front view of section B in mesh model 5

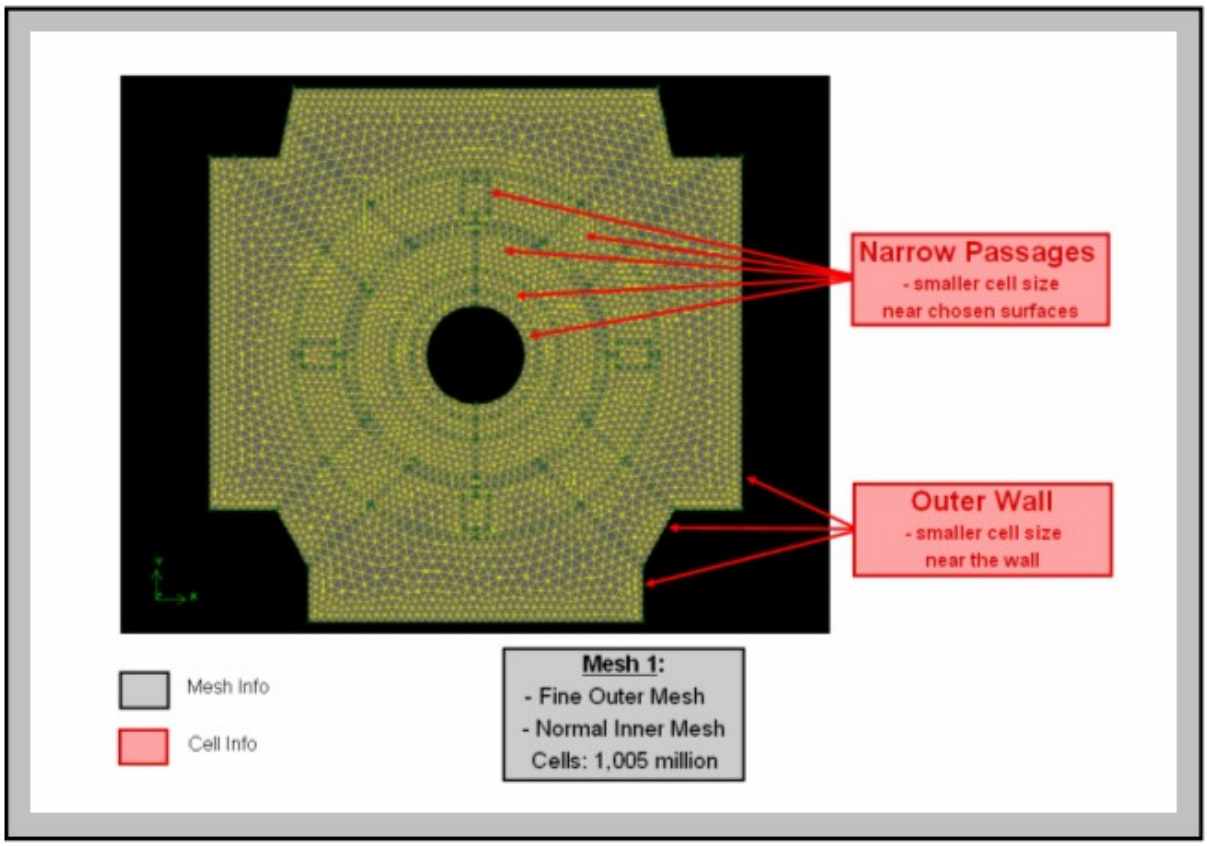

Figure 75: Front view of section C in mesh model 1

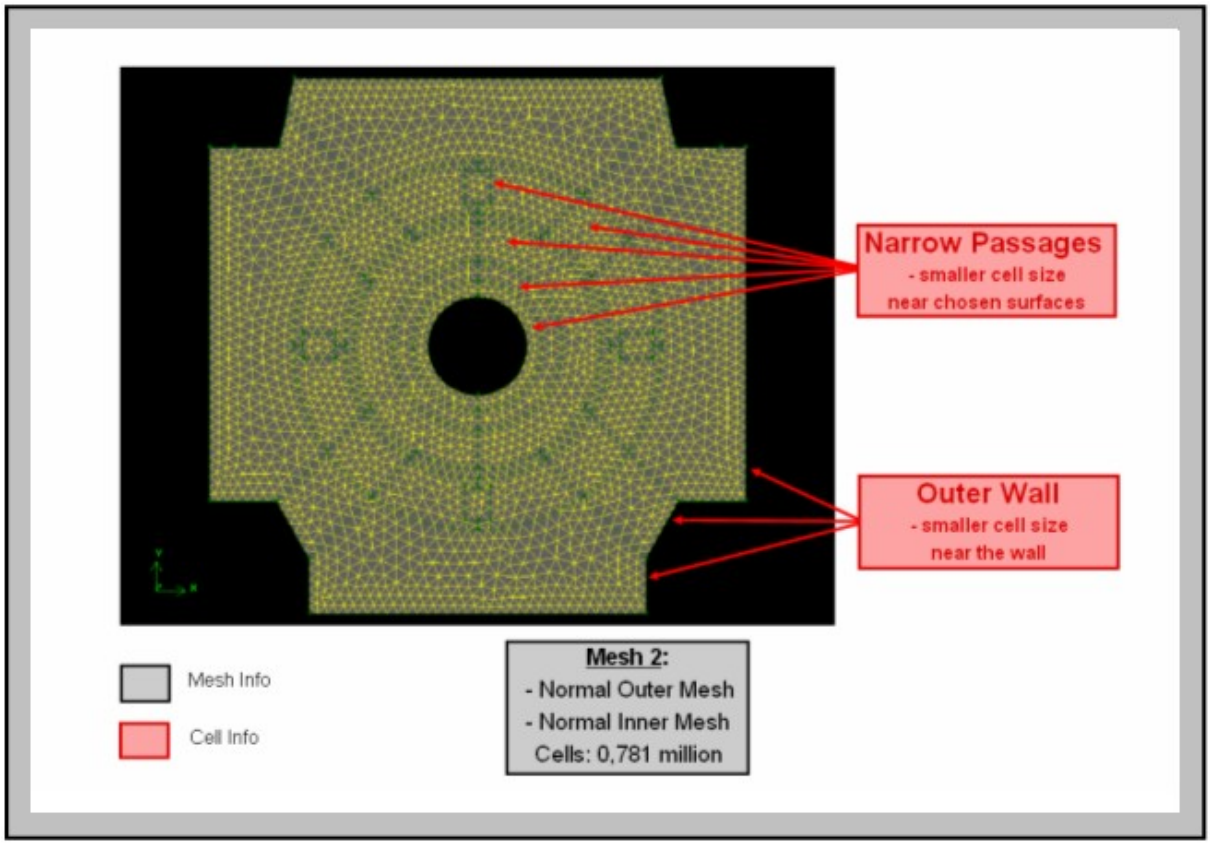

Figure 76: Front view of section C in mesh model 2

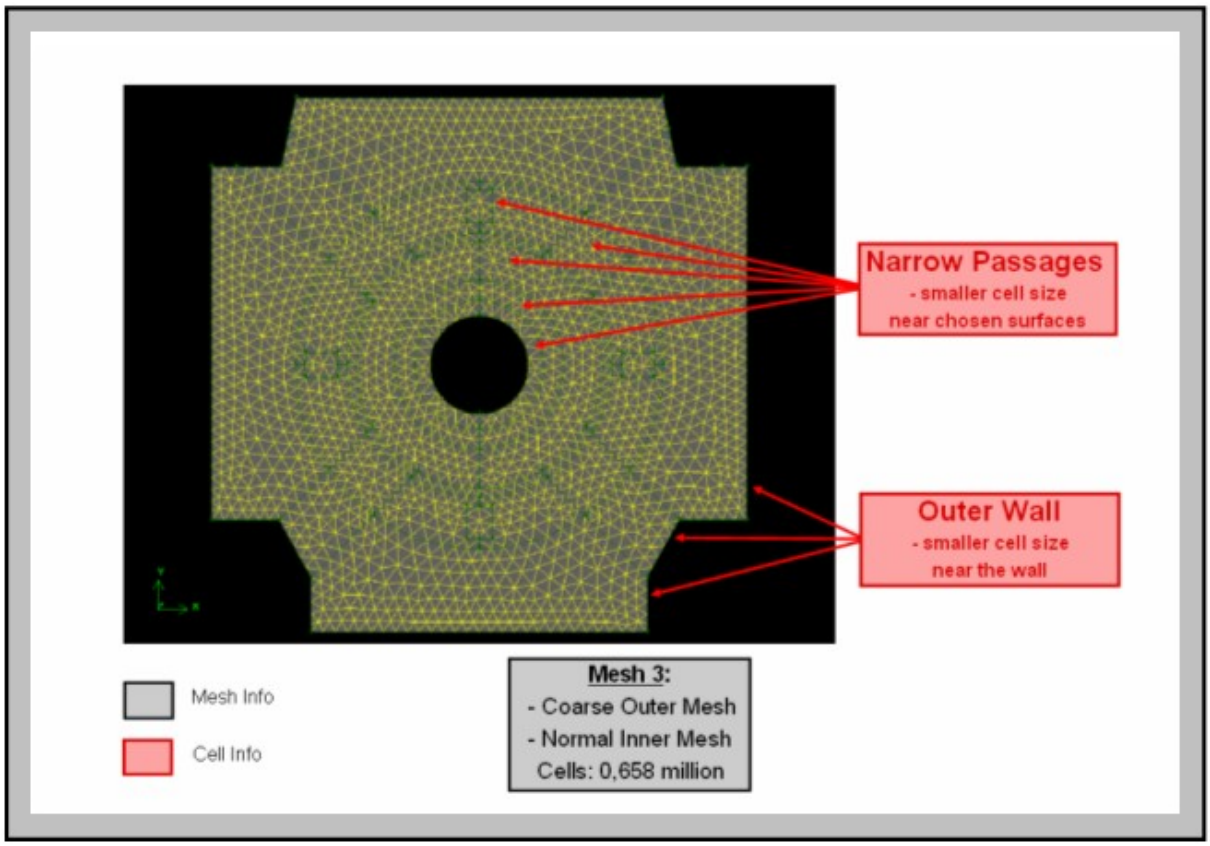

Figure 77: Front view of section C in mesh model 3

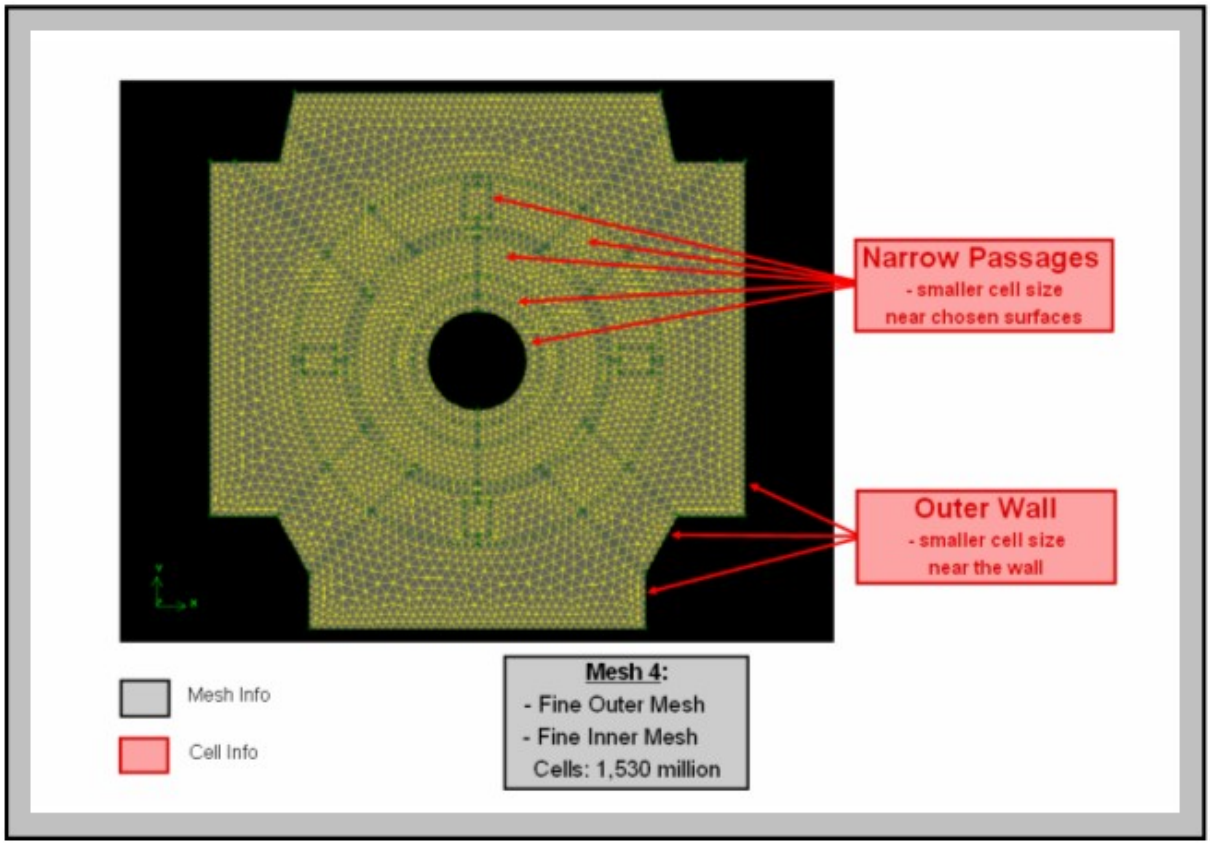

Figure 78: Front view of section C in mesh model 4

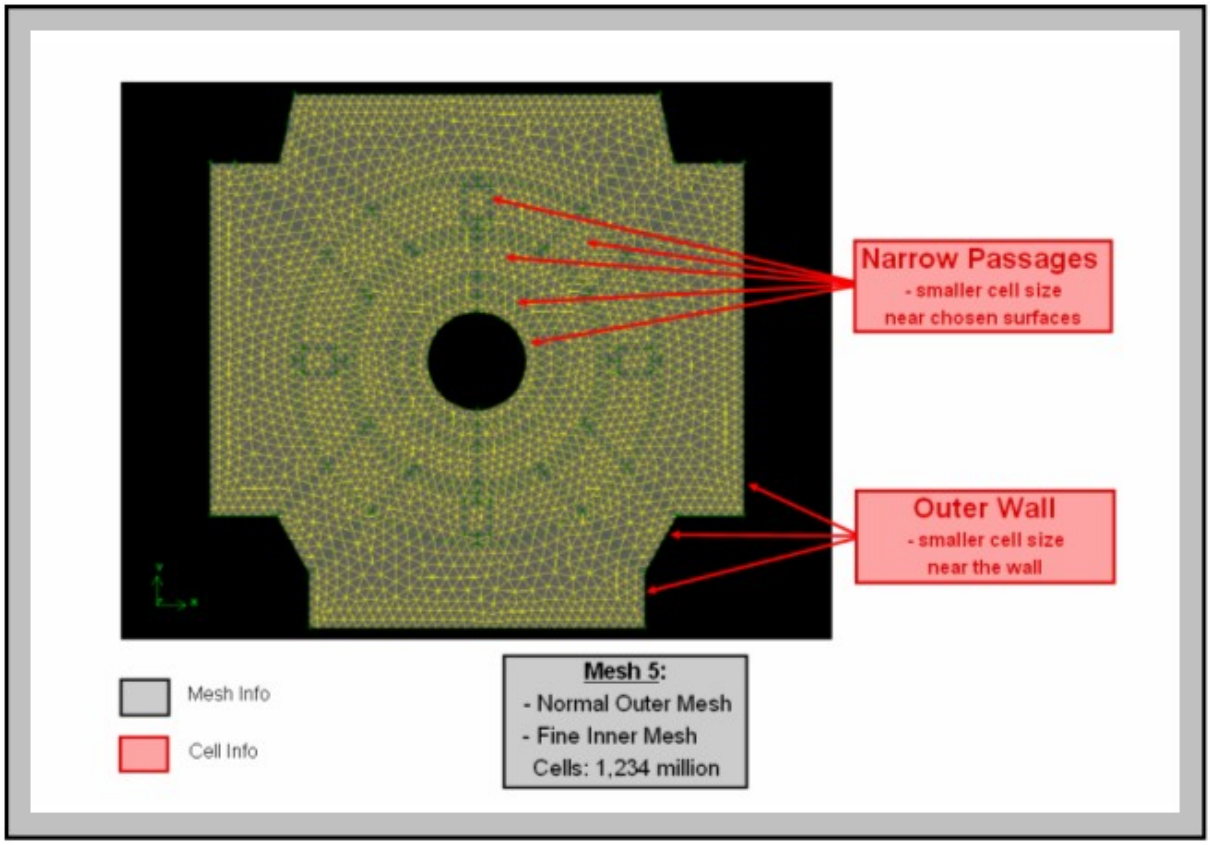

Figure 79: Front view of section C in mesh model 5

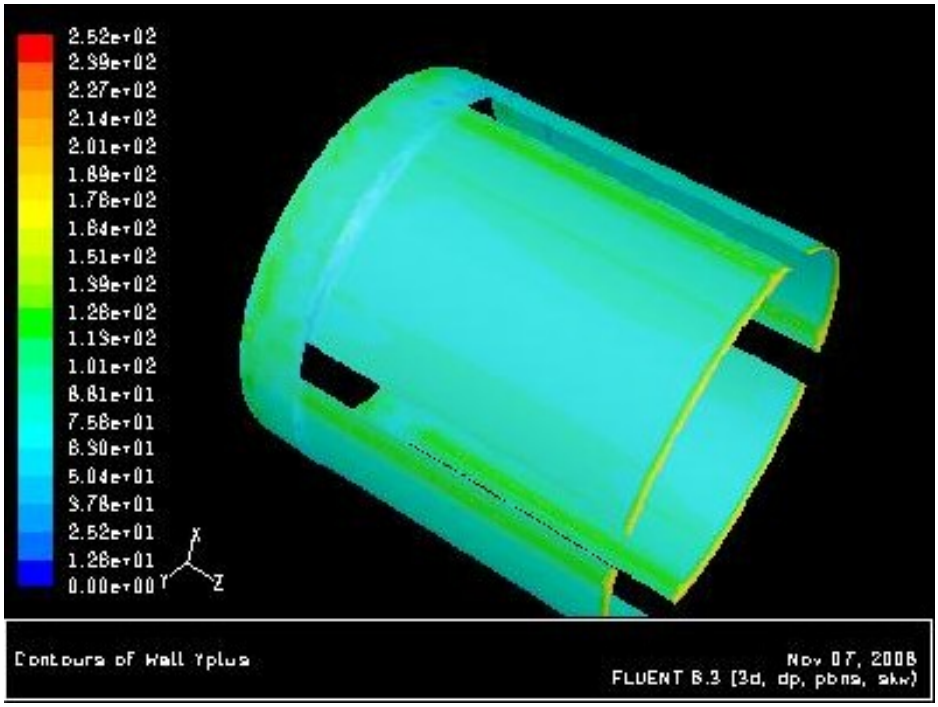

Figure 80: A side view plot of the y+ value over the Commutator surface, for mesh model nr 2. The most common y+ value is around 70-80.

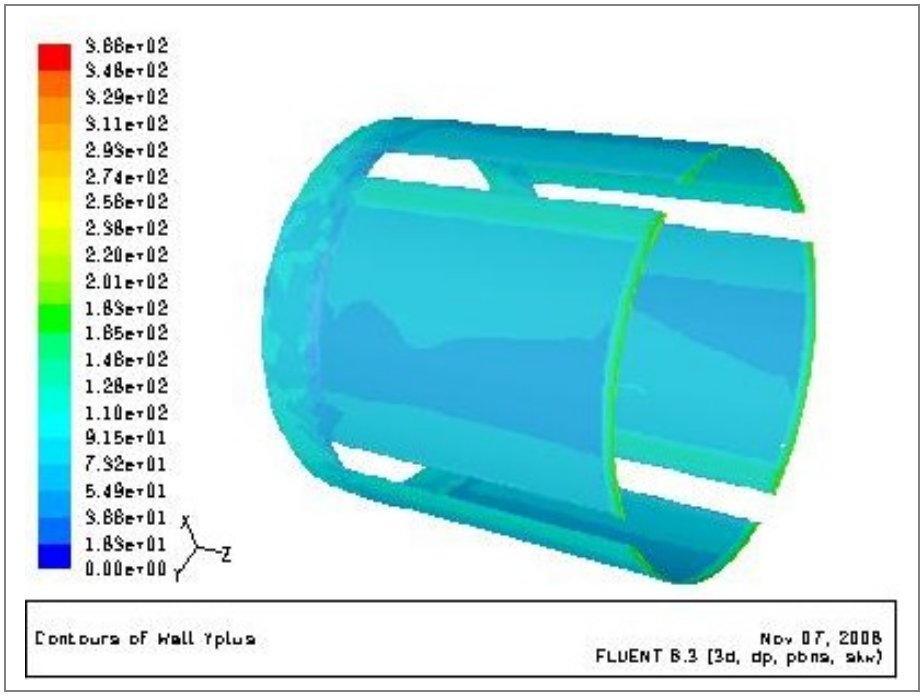

Figure 81: A side view plot of the y+ value over the Commutator surface, for mesh model nr 3. The most common y+ value is around 70-80.